Spring 2020

Development of novel materials and processes for direct conversion of CO_2 flue gas to chemicals and fuels

Ahmed Al-mamoori

Department: Chemical and Biochemical Engineering

DEVELOPMENT OF NOVEL MATERIALS AND PROCESSES FOR DIRECT CONVERSION OF CO_2 FLUE GAS TO CHEMICALS AND FUELS

by

AHMED ADNAN ATSHAN AL-MAMOORI

A DISSERTATION

Presented to the Graduate Faculty of the

MISSOURI UNIVERSITY OF SCIENCE AND TECHNOLOGY

In Partial Fulfillment of the Requirements for the Degree

DOCTOR OF PHILOSOPHY

in

CHEMICAL ENGINEERING

2020

Approved by:

Fateme Rezaei, Advisor
Ali Rownaghi
Joseph Smith
Xinhau Liang
Mark Fitch

PUBLICATION DISSERTATION OPTION

This dissertation consists of the following five articles, formatted in the style used by the Missouri University of Science and Technology:

Paper I, found on pages 3–53, has been published in *Energy Technology*

Paper II, found on pages 54–78, has been published in *Industrial & Engineering Chemistry Research.*

Paper III, found on pages 79–111, has been published in *Sustainable Chemistry & Engineering Journal*.

Paper IV, found on pages 112–140, has been published in *energy&fuels*.

Paper V, found on pages 141–169, is intended for submission to *ACS Catal*.

ABSTRACT

This research focused on addressing the pressing issues of greenhouse gas emissions that greatly contribute to climate change. Specifically, the focus was given to the reduction of anthropogenic CO_2 emission and its subsequent conversion to commodity chemicals and fuels. In the first part of the research, a series of novel high temperature CO_2 adsorbents including double salts (K-Ca and Na-Ca) and metal-doped calcium oxide (Fe_x@CaO and Ga_x@CaO) was developed and evaluated. Both sets of materials exhibited high CO_2 capacity, fast kinetics, and long-term stability. In particular, at 650 °C, the doped adsorbents comprising of 10 wt% Fe@CaO and 10 wt% Ga@CaO exhibited the highest adsorption capacities of 13.7 and 14.2 mmol/g, respectively, which were at least 2-folds higher than that of the bare CaO. the bare material.

In the second part of the research, an integrated capture-utilization process was designed, developed, and optimized to directly convert CO_2 flue gas into syngas and ethylene. In particular, capture performance and catalytic activity of several dual-function materials (DFMs) were investigated for dry reforming of ethane (DRE) to syngas and oxidative dehydrogenation of ethane (ODHE) to ethylene under various process conditions. The DFMs investigated for DRE consisted of K-Ca, Na-Ca, Na-Mg, and K-Mg double salts mixed with Ni@γ-Al_2O_3, while for ODHE, a series of physically-mixed double salts (or CaO) with Cr@H-ZSM-5 were used. The results reported herein propose a novel integrated process for capture and utilization of waste CO_2 into commodity chemicals and fuels in a sustainable manner.

ACKNOWLEDGMENTS

I would like to thank my research guide, Dr. Fateme Rezaei for her support and guidance in helping me to finalize the research and in conducting the research throughout my PhD journey at Missouri University of Science and Technology. With out her advice, my research would not have been completed.

I gratefully acknowledge HCED/Iraq and Al-nahrain university/Iraq for their financial support.

I also would like to thank Dr. Ali for allowing me to use the instruments to conduct my research work. Many thanks to my committee members for guiding me.

I want to thank department chairs (Dr.M. Al-dahhan and Dr.J. Smith) for their dedicated work, labmates, and colleages.

To my parents who raised me up and they reached me to the level where Iam right now. Specifically, to my dad in memory, I wish he would stay to this day and be proud of me. He was always encouraging me and pushing me forward to acomplish this mission.

To my mom who prayed for me and was patient during the whole time of my graduate school. To my wife and kids who help and endure me to achiev this mission. To my brother, sisters, and friends who help me a lot.

TABLE OF CONTENTS

LIST OF ILLUSTRATIONS

PAPER I Page

PAPER II

PAPER III

PAPER IV

LIST OF TABLES

PAPER V

NOMENCLATURE

Symbol	Description
γ-Al_2O_3	gamma alumina
α-Cr_2O_3	alpha chromia

1. INTRODUCTION

Greenhouse gas emissions have greatly contributed into climate change issue. In 2015 intergovermental panel on climate change (IPCC) has agreed to keep the average temperature rise below 2 ºC by 2100. This necessitates significant efforts to reduce emissions resulting from anthropogenic actions. Also, increase the world population lead to increase the energy demand so new energy is required to meet this demand. Carbon capture and storage (CCS) is expected to contribute appreciably to the reduction of CO_2 emissions to the atmosphere. However, the high cost related to the storage infrastructure, CO_2 transportation and compression could limit this process. Carbon capture and utilization is another potential solution that can address those issues, as treated CO_2 as raw materials to produce good commodity like fuel and chemicals instead of considering it as waste.

The goal of this investigation is to develop materials and processes for integrated CO_2 capture and utilization into syngas and ethylene. First, high temperature adsorbents for CO_2 capture were developed. Then the developed materials were treated physically or chemically with catalyst/support to produce dual function materials (DFMs) that has the capability to capture CO_2 first and subsequently converted into syngas or ethylene. Those processes were conducted isothermally or semi-isothermally to eliminate the adsorbent regeneration that requires high temperature and thus a lot of energy is required. Also, conducting the process in single-unit bed (adsorber/reactor) reduce the capital cost. Overall, combined CO_2 capture and utilization is a promising solution for addressing

climate issue due to the cost-effective approach and sustainable energy with less environmental footprint.

The overall objective of this reseach is to engineer novel materials and processes for combined CO_2 capture and utilization. The specific objectives are as follows:

1. Develop double salts adsorbents based CaO at high temperature.
2. Develop metal based CaO adsorbents at high temperature
3. Develop and optimize dual function materials (DFMs) for integrated CO_2 capture and utilization into syngas through dry reforming of ethane.
4. Develop dual function materials (DFMs) for integrated CO_2 capture and utilization into ethylene through oxidative dehydrogenation of ethane.

PAPER

I. CARBON CAPTURE AND UTILIZATION UPDATE

Ahmed Al-Mamoori, Anirudh Krishnamurthy, Ali A. Rownaghi, Fateme Rezaei*

Department of Chemical & Biochemical Engineering, Missouri University of Science and Technology, 1101 N State Street, Rolla, MO, 65409, United States

ABSTRACT

In recent years carbon capture and utilization (CCU) has been proposed as a potential technological solution to the problems of greenhouse gas emissions and ever growing energy demand. To combat climate change and ocean acidification, as a result of anthropogenic CO_2 emissions, efforts have already been put forth to capture and sequester CO_2 from large point sources especially power plants, however, utilizing CO_2 as a feedstock to make valuable chemicals, materials, and transportation fuels is potentially more desirable and provides a better and a long-term solution than sequestration. The products of CO_2 utilization can supplement or replace chemical feedstocks in the fine chemical, pharmaceutical, and polymer industries. In this review, we first provide an overview of the current status of CO_2 capture technologies and their associated challenges and opportunities with respect to efficiency and economy followed by an overview of various carbon utilization approaches. The current status of combined CO_2 capture and utilization, as a novel efficient and cost-effective approach, is also briefly discussed. We summarize the main challenges associated with design, development, and large scale

deployment of CO_2 capture and utilization processes in order to provide a perspective and roadmap for development of new technologies and opportunities for accelerating their scale-up in the near future.

1. INTRODUCTION AND MOTIVATION

It is widely accepted that fossil fuels remain the main source of energy at least for the next 50 years and the CO_2 emissions derived from such energy sources contribute greatly to global climate change.[1] This will require deployment of advanced low carbon fossil energy technologies in the short-term. The December 2015 U.N. Climate Change Conference in Paris has agreed on a long-term goal of keeping average warming below 2 °C that could be accomplished by considering two long-term emission goals: first, a peaking of emissions as soon as possible and then, a goal of net greenhouse gas neutrality (expressed as a balance between anthropogenic emissions by sources and removals by sinks) in the second half of this century.[2] Therefore it is imperative to reduce such anthropogenic emissions.

On the other hand, with the increase in world populations, demand for energy supply is expected to increase significantly over the next decades and thus new and renewable energy sources are required to meet this demand. The captured CO_2 can be treated as a valuable feedstock for production of many value-added chemicals and fuels, thus providing a solution to both emission control and energy supply challenges.[3]

The concepts of CO_2 capture, utilization, and sequestration (CCUS) are commonly used in the context of carbon management and climate change. The CCS refers to

technologies that focus on selective removal of CO_2 from gas streams, its compression to a supercritical condition, and finally its transportation and sequestration in geologic formations including depleted oil and gas reservoirs or oceans.[4] Despite promises for mitigating large volumes of CO_2 and despite extensive government incentives and regulatory drivers, high cost of CCS has largely impacted its large-scale deployment. The high cost of CCS comes primarily from capture and compression which accounts for 75% of the total cost of CCS. According to International Energy Agency(IEA) report published in 2013,[5] CCS will greatly contribute to emissions reduction from all applicable processes in power generation and industrial applications (e.g. cement, iron and steel, oil refining, pulp and paper and biofuels sectors) through implementing 3,000 CCS projects around the world, with over 7,000 Mt CO_2 annually stored in the process.

As a more attractive alternative, CCU technologies have received a large deal of attention recently for turning the captured CO_2, as a renewable carbon feedstock, into valuable products instead of permanently sequestering it. In fact, CCU treats captured CO_2 as a renewable resource to complement or alternate the conventional petrochemical feedstocks.[6] Moreover, the long-term effects of sequestration is not a concern for this approach. Despite significant advantages offered by CCU in comparison to CCS, converting CO_2 and utilizing it in chemical reactions is very challenging mainly due to the thermodynamically stable nature of CO_2 molecule itself.

The purpose of this paper is to review the most recent developments in the field of carbon capture and utilization while providing an overview of current challenges and future opportunities in the context of carbon management. Detailed description of various capture and utilization technologies falls outside the scope of this review and the interested reader

is referred to previously published reviews that, in addition to providing a detailed description, address life cycle analysis, risk assessments, and industrial ecology considerations of the CCU technologies.[7–11].

2. CO_2 CAPTURE OPTIONS – CHALLENGES AND OPPORTUNITIES

CO_2 capture technologies are either related to direct CO_2 removal from flue gas streams (referred to as postcombustion) or development of advanced low carbon-intensive combustion systems (referred to as precombustion) that include integrated gasification combined cycle (IGCC), as well as oxyfuel combustion that employs pure oxygen to reduce the carbon intensity of power generation.[12] Techno-economic analyses have indicated that the current CO_2 capture technologies are energy-intensive and result in significant decrease in combustion efficiency as well as electricity price increase. The choice of capture technology differs widely across industries, depending on the source of CO_2 and industrial processes generating CO_2. Capturing CO_2 from different sources have different energy penalties, for example, some industries such as ethanol production plants produce high concentration CO_2 streams while thermal power plants produce CO_2 at a very low concentrations, requiring much higher energy to recover.[13] The latter however, is the largest source which is a conundrum in the industry.

Typically, power plants alone account for ~45% of the worldwide CO_2 emissions, thus offering significant opportunities for CCU or CCS options as main sources of captured CO_2.[14] Industrial deployment of postcombustion CO_2 capture technologies will offer a larger economic impact on the reduction of capture cost than the other options. However,

in the best scenario, for a new power plant equipped with the current postcombustion capture technologies, the cost of capture is estimated to be about $56/ton, incurring an energy penalty of 62% to the power plant.[11] Carbon capture has already been commercialized in chemical production and natural gas industry. Recently in 2014, SaskPower has demonstrated postcombustion CO_2 capture from coal-fired flue gas on an industrial scale in Boundary Dam 110 MW Power Station.[15] Shown in Figure 1, are various capture routes that have been investigated in industry and academia within the past few decades and will be discussed in the next section.

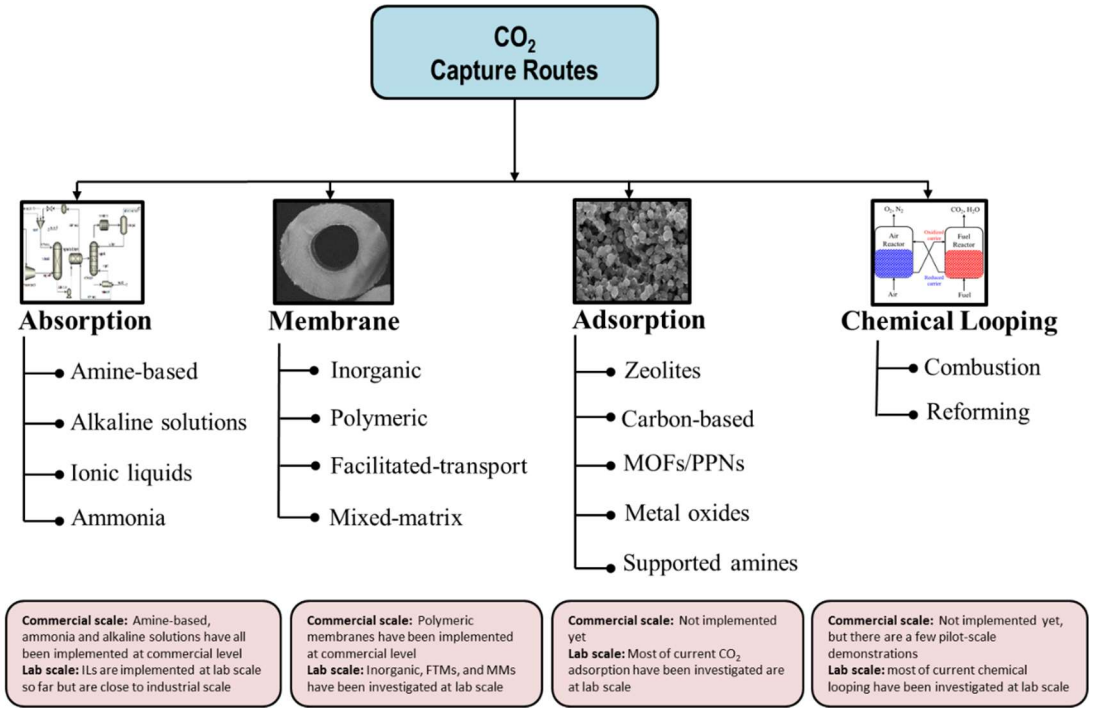

Figure 1. Various carbon capture technologies and the corresponding materials being investigated currently.

2.1. ABSORPTION-BASED CO_2 CAPTURE

The most mature separation method in the oil and chemical industries involves absorption by chemical or physical solvents.[3] This technology has been used intensively for both postcombustion (with chemical solvents) and precombustion capture (with physical solvents). Chemical absorption by aqueous ammonia, amine-based solvents such as monoethanolamine (MEA), diethanolamine (DEA), and N-methyldie-thanolamine (MDEA), and alkaline solvents such as $Ca(OH)_2$ and NaOH, is the most common method for postcombustion capture in various industries including cement, iron and steel, power plants, and oil refineries.[16–19] The well-established commercial physical absorption technologies for precombustion CO_2 capture include Selexol, Rectisol, Purisol, and Fluor. Recently, ionic liquids (ILs) have been identified as suitable alternatives to the conventional physical solvents used in the above processes as a result of their inherent properties such as low volatility, low vapor pressure, high thermal stability at elevated temperatures, and low regeneration energy requirement.[20–22] However, their low working capacity is a main obstacle toward their widespread use in CO_2 capture.

Although absorption is a mature and well-established separation method which results in high capture efficiency, the energy penalty incurred is very high mainly due to the high energy requirements for solvent regeneration option.[3] Although the heat integration can reduce the need for energy in some industries like power plants, other industries such as cement or iron and steel cannot provide such heat integration. Besides, other known operational limitations such as corrosion, and large volume of water makeup represent a significant barrier. Typically, chemical absorption relies upon thermal swing regeneration and thus optimal selection of solvents with an optimum combination of

thermal and physical properties is of paramount importance in developing energy-efficient absorption-based CO_2 capture. For instance, piperazine (PZ) and PZ derivatives have been suggested as alternatives to conventional chemical solvents based on their superior performance such as fast reaction kinetics, low chemical reactivity, and low regeneration energy.[23] Another opportunity is to enhance working capacity of ILs through incorporation of functional groups (such as perfluoroalkyl groups, amine and amino acid groups or carboxylate anions) that could eventually pave the way toward their utilization as solvents for CO_2 absorption.[24] The trade-off between heat of reaction and kinetics is another important consideration. Typically, for chemical absorption, employing solvents with a high heat of absorption (> 60 kJ/mol) could reduce energy consumption while utilizing thermally stable solvents with low regeneration energy requirements can greatly improve the thermodynamic efficiency of the separation process.[4] Poisoning by impurities present in flue gas or other effluent streams is another challenge reducing the stability of chemical solvents, thus tolerance to impurities in addition to resistance to solvent oxidation and vapor losses should be considered as key performance metrics in developing novel aqueous solvents for CO_2 absorption. Increasing the concentration of amines in aqueous solutions could help increase the capture capacity of amine solutions as well.

In addition to advancement in materials development and optimal selection of solvents with better energy performance, process improvements are of equal importance for scaling up next- generation of absorption technologies. In that regard, next generation absorption processes with optimized process configuration and intensification that provide heat integration strategies such as interheated strippers (for effectively recovering heat from the stripper overhead) and intercooled absorbers (for providing more reversible

absorber operation with greater rich and lean loading), could offer a competitive CO_2 capture solution.

2.2. CO_2 CAPTURE BY MEMBRANE SEPARATION

Generally, the use of membranes for gas separation applications can offer an energy-efficient and more environmentally friendly approach than other separation methods. Furthermore, membrane-based CO_2 separation is usually operated under continuous, steady-state conditions and a pressure difference across the membrane drives the permeation process. Membrane's material, configuration, morphology, and composition as well operating conditions are all key factors that dictate its gas separation performance to a great extent. Membrane separation for the removal of CO_2 from power plants flue gas streams has been the subject of many studies.[25–28] Application of membrane technology for postcombustion CO_2 capture is very challenging mainly due to the low pressure of flue gas streams. In contract, membranes are more suitable for high pressure precombustion processes such as IGCC. Notably, compared to other capture routes, multi-stage operation and streams recycling are often perceived as challenges which making the operation difficult and complex.

Various porous inorganic membranes typically composed of zeolites, MOFs, carbon molecular sieves (CMS), ceramics, and a few oxides (alumina, titania, zirconia) have been extensively studied for CO_2 capture from flue gas or other effluent streams. Although inorganic membranes can withstand high temperatures and often have mechanical stability, simply their high costs still hamper their commercialization. Inorganic membranes have not been demonstrated on a large scale yet and in fact, they are

still far from scale-up. The main challenges associated with their large scale utilization stem from their fabrication routes which are very expensive and their long-term stability and reliability.

Conversely, polymeric membranes that can be easily formulated in hollow fiber modules have shown tremendous interests for large scale industrial applications. In addition, inorganic membranes cannot reach the high packing density offered by polymeric membranes, as in the case of polymeric composite hollow fiber membranes assembled in the modules, reaching up to 10,000 m^2 of filtration area in 1 m^3 of reactor at low production cost, crack-free thin membranes, and large-scale production.[29–32] However, polymeric composite membranes have relatively low separation performance compared to inorganic membranes. For example, CO_2 capture by current polymeric membranes still suffer from several drawbacks such as low CO_2/N_2 selectivity and permeability for postcombustion processes, the trade-off limitation between permeability and selectivity, swelling, aging, sensitivity to impurities, and mechanical stability especially for high pressure operations. For polymeric membranes to be cost effective for postcombustion CO_2 capture, a minimal CO_2/N_2 selectivity of 200 is required while maintaining relatively high permeance.[33] High permeability eliminates the need for a high membrane area needed for an acceptable separation rate, thus reducing the capital cost of the separation process. One way to address the challenges inherent with traditional polymeric membranes is to utilize polymers of intrinsic microporosity (PIMs) that contain large free pores within the polymer matrix thus allowing for higher CO_2 flux. Polymeric membranes have been commercialized for CO_2 capture in natural gas sweetening. MTR has implemented a pilot-scale membrane-based

process for postcombustion CO_2 capture from flue gas coming from a 880 MW pulverized coal power plant with a capture rate of 90%.[34]

Facilitated transport membranes (FTMs) such as liquid membranes, ion-exchange membranes, and fixed carrier membranes have proven to be highly selective for CO_2, however, they are subject to poisoning by trace amount of acid gases NO_x and SO_x present in flue and suffering from long term stability.[35–37] Among various commercially available membrane types, hollow fiber membranes provide the highest surface-to-volume ratio, optimum geometry for high production rates and provide more compact modules compared to flat sheet or spiral wound units.[35] Composite hollow fiber membranes comprising a thin selective layer with a thickness lower than a micrometer supported on a highly porous polymeric substructure provide opportunities for advanced membrane development.[38]

Mixed matrix membranes (MMMs) formed by dispersing highly selective molecular sieve particles such as zeolites, carbon nanotubes, layered silicates, MOFs, etc. in polymer matrix are promising contactors that combine the scaling up and processing polymeric membranes with the advantages in separation performance of molecular sieving materials. In comparison to porous zeolites, MOFs as fillers exhibit better properties such as higher pore volume and lower density, better affinity to polymer chains, and easily tanning cavities in terms of size and shape by choosing appropriate ligands with different functionalities. The MMMs provide a solution to go beyond the known polymeric membranes upper-bound trade-off limit as well as the inherent obstacles associated with the inorganic membranes cost and processing.[39–45] However, they are still in their early stages of development and far from industrial deployment. Besides, their current fabrication process are costly and complex.

In the context of membrane CO_2 capture, the future opportunities should therefore focus on composite membranes that take advantage of both polymeric and inorganic constituents and are capable of surpassing the current best performing membranes. Strategies to improve the composite systems via alternate chemistries, re-engineering the material systems and processing techniques will provide critical insight into the barriers to engineering sophisticated composite systems for future membrane-based CO_2 separation.

2.3. ADSORPTION-BASED CO_2 CAPTURE

CO_2 capture over porous solid materials offers a promising approach in selectively removing CO_2 from gas streams in various industries. To date, a variety of adsorbents have been extensively evaluated for CO_2 capture from precombustion and postcombustion gas effluents. Generally, the adsorbents used are classified as either high-temperature or low-temperature materials. The primary classes of high-temperature materials include hydrotalcites, alkali or alkaline earth oxides like calcium oxides, alkali silicates and zirconates, as well as double salts, whereas low-temperature adsorbents cover conventional porous materials such as zeolites, carbon-based materials (e.g. activated carbon, carbon nanotube, carbon nanofiber, graphene), molecular sieves, as well as recent classes such as MOFs/PPNs/COFs.[46–51] The high-temperature adsorbents are all chemisorbents, while the low-temperature adsorbents are chiefly physisorbents.[52] Supported amines are among the low-temperature adsorbents, but they are chemisorbents, with strong interactions with CO_2.

The efficiency and economic of adsorption processes such as pressure/temperature swing adsorption (PSA/TSA) are largely dictated by characteristics of the adsorbents in addition to process design and operation factors.[53,54] Generally, for any gas separation

application, adsorbents are required to satisfy several criteria in order to be efficient for large-scale separation. These metrics include high working capacity and selectivity, low cost, low regeneration requirements, long-term stability, and fast kinetics.[52] In addition to adsorbents' physiochemical properties, cycle configuration, number of steps, cycle time, operating pressures or temperatures, number of beds, etc. are other important process parameters that need to be optimized for optimum capture efficiency.

In the context of adsorptive CO_2 capture, the majority of lab-scale studies often overlook the performance of adsorbents under practical conditions. For instance, competitive water adsorption, structural, mechanical, and chemical stability to moisture that often exists in gas effluents, or the stability in the presence of other pollutants such as SO_x, NO_x (especially for postcombustion process), and fly ash are often not investigated. Retaining working capacity over many adsorption-desorption cycles and thermal management are other important criteria that are often overlooked in the design or screening of the adsorbents. In addition, most of the current studies fail to consider the ultimate process performance metrics while developing new materials. Although conventional zeolite 13X material is still the best choice in terms of capture cost for postcombustion under dry flue gas conditions, in comparison to best MOFs like HKUST-1, and Mg-MOF-74,[60,61] its water co-adsorption is still problematic which requires a guard bed or a dehydration unit before the PSA or TSA units. The design of composite adsorbents (such as zeolite or MOF functionalized amines) could address the known problems of conventional adsorbents and enable a cost-effective and highly-efficient capture approach for postcombustion CO_2 capture.

Adsorption-based CO_2 capture by PSA has attracted a great deal of attention due to simple process, low energy required, and low cost.[55] However, low recovery for CO_2 is still challenging for this approach.[54] Generally, for postcombustion CO_2 capture, vacuum swing adsorption (VSA) and TSA are more appropriate than PSA whereas (mainly due to large pressure drops in flue gas application), PSA is more promising for precombustion process.[56–59] Adsorbent particles attrition is another common process operation issue. The use of structured adsorbents such as monoliths or hollow fibers can address both pressure drop and attrition problems while allowing for rapid operation of cycles. Rapid swing cycles can enhance process throughput, thus allowing for smaller adsorbent inventory and column size. TSA process for CO_2 capture is still far from large-scale implementation as a result of high energy requirement for adsorbent regeneration and long cooling step time. Novel approaches that offer heat management options such as hollow fiber adsorbents with a cooling medium flown in the bore side or monolithic structures with optimum thermal management could address these scale-up challenges.[43,62–64] Moreover, in terms of process design, modifications in the original design that include novel indirect heating techniques such as heating jacket, heat-exchanger, or coils, could be implemented to further reduce energy consumption and/or shorten the required cooling time in the TSA process.[56,65–68]

Although adsorption-based separation can address most of limitations of absorption processes, the current technologies developed/proposed so far, are not cost-effective at their current stage of development. Furthermore, no large-scale operation has been fully deployed yet.[69–71] The design, development, and evaluation of high-performance adsorbents should be tightly coupled with their practical performance evaluations and process considerations. Moreover, cycle design, configuration, and optimization of any

cyclic process should take into account the characteristics of the specific adsorbent to be eventually used.

2.4. CO_2 CAPTURE BY CHEMICAL LOOPING

Chemical looping processes such as combustion and reforming (CLC and CLR) are considered as potentially cost-effective CO_2 capture options with minimum energy losses in which both CO_2 and H_2O are inherently separated from flue gas.[72] They can also largely minimize NO_x formation during reaction. For precombustion CO_2 capture, the chemical looping can be combined with IGCC to produce syngas as a valuable by-product. These technologies use a metal oxide as an oxygen carrier to circulate oxygen between air and fuel reactors, thus, their large-scale applications are highly dependent upon the availability of suitable oxygen carriers. High oxidation/reduction activity, mechanical stability (in fluidized beds), resistance to agglomeration, high melting point (to withstand the reaction temperature and avoid agglomeration), long-term stability under repeated oxidation/reduction, as well as cost and environmental impacts are key characteristics of metal oxides (mainly transition metal oxides such as Fe, Cu, Co, Mo, Mn, Cr, Nb, V, Ce, and In oxides) for chemical looping processes.[72] Off these properties, reactivity in both oxidation and reduction cycles is the most important criterion that should be considered. Moreover, these oxides should be capable of completely combusting the fuel to achieve maximum combustion efficiency. Current oxygen carriers investigated so far, are not capable of fulfilling all of the above requirements at once.

Another challenge associated with chemical looping processes is high pressure operation required in order to achieve high overall efficiency, though high pressure may

be favorable for CCS applications. Recent energy analyses have indicated that calcium looping postcombustion process in particular, can incur an efficiency penalty of only 6-8%.[73–76] Such a low energy penalty stems from improvements in the original design of the two-bed (carbonator and calciner) Ca-looping process such as incorporating an extra heat recovery bed to exchange heat between the CO_2 stream and the solid particles entering the calciner. Currently, most of chemical looping technologies considered for power generation sector are at the lab or concept stage of development with a few pilot-scale studies currently under investigation[77–79] and it is projected that their full deployment will not take place before 2030.[80] The technical hurdles from materials development and process design should be overcome in order to improve the current state-of-the-art chemical looping technologies. In that regard, novel chemical looping processes based on composite metal oxides such as Ca/Cu that provide the possibility of coupling an endothermic and an exothermic reaction in the same solid matrix could result in higher capture efficiency and lower equipment cost.

2.5. DIRECT CAPTURE OF CO_2 FROM AIR

Direct removal of CO_2 from ambient air, referred to as direct air capture (DAC), has recently gained significant attention among researchers because it could minimize the problems associated with transporting large volumes of CO_2 from point source emitters to sites suitable for geological sequestration.[81–85] In addition, unlike conventional capture processes that target only large-point sources and can at best slow the rate of increase of the atmospheric CO_2 concentration, DAC, if widely adopted, can reduce the atmospheric CO_2 level. Although the concept is essentially similar to adsorption-based CO_2 capture,

due to ultradilute nature of CO_2 in air (~ 400 ppm), the DAC technology has daunting technological challenges. As a result of ultra-low concentration of CO_2, materials with strong binding affinities (sharp uptake at low partial pressures) and high CO_2/N_2 selectivity are required for this technology. Various aqueous hydroxides such as calcium hydroxide solution, NaOH and KOH solutions, as well as solid materials including alkali and alkali-supported carbonates, anionic-exchange resins, amine-functionalized metal oxides, and MOFs have been evaluated for DAC.[85] It should be pointed out here that not every high-performance material that works well for large-point source CO_2 capture would necessary perform at an acceptable level for DAC process, mainly due to the differences pointed above.

Recent thermodynamic analyses have indicated that the TSA process is thermodynamically more efficient than the PSA for DAC application as the heat of adsorption or adsorbate affinity increases at dilute CO_2 concentrations.[86] At this point, the estimated DAC cost is significantly higher than that of capture from large-point sources ($30-1000/ton and $30-100/ton, respectively). Such huge uncertainty in the design considerations and economic analysis of the DAC process must be addressed by clearly laying out the underlying assumptions. Moreover, to apply air capture on large scales, low cost and highly durable materials are required. Although still in the early stages of development, any DAC process must minimize the cost for its adoption and implementation in society. Using minimal amount of energy, ideally from a distributed renewable source such as solar thermal energy would be a potential pathway toward enhancement of the feasibility of DAC process.

2.6. CO_2 CAPTURE BY HYBRID PROCESSES

One of the promising approaches that offers a cost-effective capture path is through hybrid separations that combine two or more capture subsystems. The concept of hybrid processes in gas separation and reaction has been previously applied to several applications. Hybrid technologies take advantages of having two or more separations units in parallel or in series aiming at enhancing separation efficiency while at the same time decreasing the overall cost of separation. The feasibility of several hybrid concepts for CO_2 capture such as membrane-PSA and membrane-distillation have been investigated.[87–91] A promising hybrid system with potential energy savings has been recently developed by American Air Liquide by which sub-ambient temperature (−50 °C to −20 °C) CO_2 capture is carried out through a hybrid membrane-cryogenic distillation process.[92] This hybrid process aims at retrofitting existing pulverized coal-fired power plants and is sought to enhance both membrane module productivity and selectivity, thus reducing both energy and capital costs of the capture process. For this technology to be widely adopted at large scale, a good heat integration strategy is crucial since all the feed gas needs to be cooled to sub-ambient temperature.

For hybrid membrane-PSA systems, the idea is to use the high pressure membrane permeation stream in the pressurization and high-pressure adsorption steps of a typical PSA process. In addition, the membrane permeation could be incorporated into the blowdown step of the PSA cycle so that the operating pressure of the PSA can be used as the driving force for membrane permeation. Both these options can result in significant savings by eliminating the need for high duty pumps.

Another example of such integrated systems is hybrid pressure-temperature swing process (PTSA) that can be operated at moderate pressure and temperature, thus leading to lower capture energy cost.[93,94] For this configuration, the need for a high vacuum level that is typically required in PSA to achieve high CO_2 purity, or high temperature that is often essential in TSA to achieve high recovery could be dramatically avoided, thus leading to less expensive operation, faster cycles, and longer service life of the adsorbent.[93] The general idea for designing PTSA is to get an effective mass transfer during adsorption and heat transfer during desorption steps.[95]

Overall, based on the current status of state-of-the-art technologies hybrid processes that combine two or more capture routes should be considered as a novel approach for improving the separation efficiency and cost. However, it is imperative that the future of related research focuses on a complete understanding of these hybrid processes from perspectives of feasibility, process design considerations, choice of materials, environmental impact, and overall cost reductions by taking into account uncertainty factors.

2.7. SUMMARY

In summary, despite significant progress within the past few years, most of CO_2 capture technologies have still a long way to become commercially available in various industries. It appears that a bridge between materials scientists and engineers is crucial to fill the gap between materials characteristics and process performance. In other words, investigation of the relationship between materials properties and hybrid process parameters is crucial to build a unique and comprehensive strategy for the design of highly

efficient and cost-effective next-generation capture technologies that greatly contribute to CO_2 emission reductions. Table 1 provides a summary of the current challenges and future opportunities related to various CO_2 capture methods discussed in this section.

Table 1. CO_2 capture technologies and their associated challenges and opportunities.

Capture Technology	**Challenges**	**Opportunities**
Absorption	• Equipment corrosion • Amine degradation • High regeneration energy requirement • High overall energy penalty • Environmental impact	✓ Improvement in commercially available absorption technologies ✓ The use of ILs ✓ The use of advanced amines
Membrane	• Energy intensive for postcombustion application • High fabrication cost of novel membranes • Not suitable for high temperature applications • Trade-off between purity and recovery • Low selectivity	✓ Composite hollow fiber membranes ✓ MMMs ✓ Hybrid membrane-cryogenic processes
Adsorption	• Long-term stability to impurities and moisture • Thermal management • Pressure drop and adsorbent attrition	✓ Composite adsorbents ✓ Structured adsorbents ✓ Rapid swing cycles ✓ Hybrid membrane-PSA processes
Chemical Looping	• High pressure operation • Efficient and stable oxygen carrier materials	✓ Composite oxides as oxygen carriers ✓ Process design modifications
Direct Air Capture	• Ultradilute CO_2 content • Energy intensive • Development of durable materials	✓ DAC coupled with renewable energy sources ✓ Structured adsorbents
Hybrid Capture Processes	• Less studied • Enhancement of synergy and process optimization • Development of hybrid materials	✓ Membrane-distillation ✓ Membrane-PSA ✓ PTSA

3. CO_2 UTILIZATION OPTIONS – CHALLENGES AND OPPORTUNITIES

The utilization of CO_2 can be considered as a viable option for providing a renewable energy source for production of various valuable products. The process is required to be economically viable, safe, and eco-friendly environment.[96] The primary utilization route can be classified as enhanced oil/gas recovery, chemical conversion, mineralization, and desalination. Figure 2 shows various ways in which CO_2 is being utilized. It should also be noted that, U.S. department of energy (DOE) categorizes the CO_2 utilization technologies into four main research focus areas that CCS program supports: cement, polycarbonate plastics, mineralization, and enhanced hydrocarbon recovery.

CO_2 is typically formed as a byproduct during ammonia synthesis. Additionally, it is produced during synthesis of ethylene oxide in the oil refinery and during fermentation process.[24] As a raw material, CO_2 is commonly used in beverages industry, food conservation, urea production, water treatment, enhanced oil recovery, chemical production, and polymer synthesis with the current global usage of 232 Mt/year.[4,97] However, urrently, less than 1% of CO_2 emitted into the atmosphere is utilized as a raw material in the above industries.[98,99] Efforts should be put forth to utilize the already captured CO_2 into valuable commodities like transportation fuels or fine chemicals.

3.1. ENHANCED OIL/GAS RECOVERY

Enhanced oil/gas recovery (EOR/EGR) refers to a procedure in which a substance is injected to a reservoir to repressurize the rock formation and release any oil/gas that may

have been trapped in the formation. During CO_2-EOR process, the injected CO_2 mixes with the oil and releases it from its otherwise hard to recover rock formation.

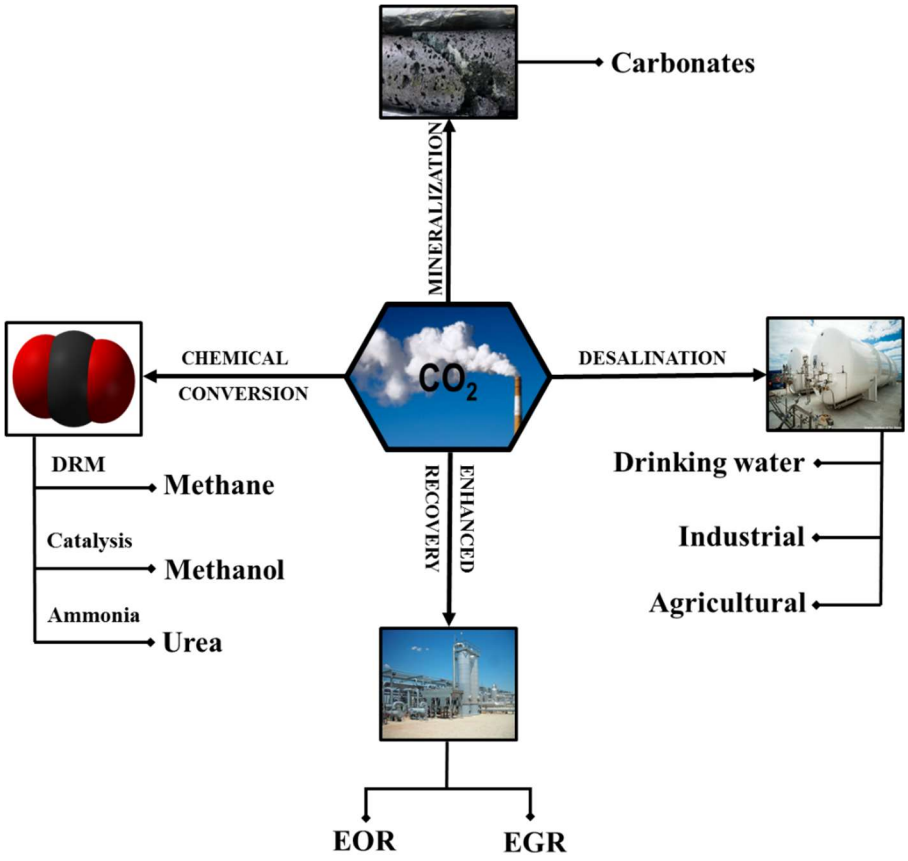

Figure 2. Various carbon utilization pathways.

This stream is then pumped to the surface and the CO_2 emerging with the oil is separated and re-supplied into the cycle to repeat the process. This process often yields more barrels per reservoir than the traditional oil recovery methods.[100,101] Basically, CO_2 flooding is one of the most common and efficient methods used in EOR as it mixes with the oil, expanding it and making it lighter and easier to recover.[102] Most CO_2-EOR systems use naturally occurring CO_2, but lately, research is focused on using CO_2 captured from

potentially hazardous gas streams, such as flue gas and other industrial gas effluents.[103] Two commonly used CO_2-EOR methods are continuous gas injection (CGI) and water alternating gas (WAG) with the later method yielding better oil recovery.[104] In the CO_2-EOR, the addition of an intermediate hydrocarbon such as propane can improve displacement efficiency and diffusion coefficient, thereby further increasing the recovery efficiency.[105] In general, the efficiency of the CO_2-EOR depends largely upon temperature and pressure of the reservoir involved.[106]

There are numerous challenges faced by the CO_2-EOR methods. For instance, due to heterogeneity of the rock formation between the wells, fluid properties and capillary pressure reduce the effectiveness of CO_2 flooding.[107] Furthermore, a large number of parameters such as fluid production rates, compensated neutron log (CNL), and production log are required for an efficient execution.[107] Despite these shortfalls, CO_2-EOR/EGR is drawing a significant deal of attention and is predicted to rise rapidly in the near future. Overall, CO_2-EOR/EGR is a promising approach in enhanced oil/gas recovery, with applications in most type of reservoirs. Despite this, currently, EOR contributes only to 3% of CO_2 utilization. While advances in this field have been retarded by the price of CO_2, it is steadily growing with numerous facilities having implemented this method in their reservoirs.[108–110]

3.2. CO_2 AS FEEDSTOCK FOR PRODUCTION OF FUELS AND CHEMICALS

CO_2 utilization is expected to overcome the known challenges associated with CCS such as high cost, public acceptance, and long-term uncertainty. Additionally, it makes CO_2 capture worthy and can be substituted partially for fossil fuels, as the main source of

energy.[111] It can open up new avenues for developing sustainable technologies that supplements the conventional fossil-based resources.

3.2.1. Fuels Production. CO_2 conversion into fuels is considered the best route in CO_2 utilization. Methane, methanol, syngas, alkanes, etc. can be produced by utilizing captured CO_2 as a feedstock. The fuel produced could be used in various sectors including fuel cell, power plant, transportation, etc.[4] There are tremendous pathways for producing fuels by CO_2 utilization. Since CO_2 is a thermodynamically stable molecule, its utilization requires the application of a large amount of heat and catalyst inventory to obtain high fuels yields.[98] In the context of fuels production from captured CO_2, hydrogenation process and dry methane reforming (DRM) are the two important pathways.[112]

CO_2 hydrogenation is very promising route for CO_2 utilization mainly because it offers the possibility of recycling CO_2, storing H_2, producing fuel, and solving the issue of electric energy storage.[99] DRM is also considered as one of the most important pathways for production of methanol and a variety of other liquid fuels by Fischer-Tropsch (FT) process.[113–115] In the hydrogenation of CO_2 into methane,[116] methanol,[117] carbon monoxide,[116] and formic acid,[118] the source of hydrogen from fossil fuel appears to be problematic as this can itself lead to increase in CO_2 emissions to the atmosphere. However, renewable energy (solar, wind, biomass) can be alternatives to fossil sources to mitigate additional CO_2 emissions during hydrogenation.[24] Recently, Audi motor company's "e-gas" in Germany has produced 1000 Mt/year of methane by CO_2 hydrogenation.[119]

For transportation, methane is not valuable as fuel because it has low volumetric gas density. Besides, its global warming potential (GWP) is 30.[98] Producing more methane

will not be profitable to CO_2 capture because of its availability (methane is plentiful in natural gas, shale gas, coal gas, and landfill gas). Rather, CO_2 hydrogenation to methanol appears to be a better pathway.[120] However, C-H bond activation over current catalysts (mainly Cu-based) for methanol production is very challenging and the current catalysts tested so far are not economically attractive.[121–123] Although methanol has many applications in paints, plastics, combustion engine, and organic solvents,[98] its production contributes to only 0.1% of CO_2 emissions reduced.[124] CO_2 conversion to CO from reverse water gas shift (RWGS) reaction is one of the most important routes for CO_2 utilization because CO is a raw material for methanol and hydrocarbon fuels synthesis through FT reaction.[123] Despite this, the endothermic nature of RWGS reaction and low conversion at moderate temperatures are the two main bottlenecks to deploying large-scale methanol production from CO_2 through FT process. Additionally, developing active catalysts that can accelerate the reaction kinetics and maximize the yield represents another significant barrier.

Recently, DRM has attracted significant research interest in utilizing CO_2 for syngas production.[125–127] Typically, the purity of syngas that is produced by DRM is higher than that of produced by partial oxidation and steam reforming.[128] In addition, the amount of unreacted methane in DRM process is only 2% which is less than that in steam reforming, thus making it possible to apply DRM at remote natural gas sites for production of liquid fuels that are easier for transportation than gaseous fuels.[114] Ni, Ni-cobalt, Ru, Ir, and Rh supported on silica, alumina, and lanthanum oxide have been evaluated extensively in the DRM reaction.[129] Despite significant advances in development of DRM catalysts with high activity and optimum stability, finding a suitable catalyst for this reaction still

remains a big hurdle specially at high operation temperature, since deactivation by coke formation is inevitable at high temperatures (> 700 °C).[130–134]

Oxidative dehydrogenation of light alkanes to alkenes (ODA) with CO_2 as a soft oxidant (instead of O2 that is typically used in dehydrogenation processes) is another attractive approach that can reduce the amount of coke formation and maintain the stability of the catalysts at elevated temperature.[135–139] Moreover, CO_2 enhances equilibrium conversion of oxidative dehydrogenation of light alkanes by removing hydrogen through RWGS reaction.[140] However, care must be taken in monitoring the temperature as excess heat would cause the olefins to undergo over-oxidation which yields carbon oxides resulting in low selectivity.[141] CO_2 also forms the redox cycle and produces active oxygen species. The role of CO_2 in ODA and the mechanism of this reaction is unclear and dependent on the nature of active sites, metal reducibility and its supporting material.[142] Despite initial high activity, the catalysts investigated so far suffer from low stability.

It is apparent from above discussion that the main hurdle in utilizing the captured CO_2 as a feedstock for production of synthetic fuels lies in design and development of novel catalysts that not only exhibit high catalytic activity under different reaction conditions but also resistant to coke formation and show long-term chemical and structural stability.

3.2.2. Chemicals Production. In addition to synthetic fuels, CO_2 can be used as feedstock to produce a large array of fine chemicals. The most important applications are urea (~160 Mt/year), inorganic carbonates (~60 Mt/year), polyurethane (~18 Mt/year), acrylic acid and acrylates (10 Mt/year), polycarbonates (4 Mt/year), and alkylene carbonates (a few kt/year).[4] Urea, as a major fertilizer, has the largest market for CO_2

utilization.[4,143] It is also widely used as feedstock in polymer synthesis, pharmaceuticals, fine chemicals, and inorganic chemicals such as melamine and urea resins.[144,145]

Organic carbonates such as acyclic (linear) carbonates (e.g. dimethyl carbonate (DMC), diallyl carbonate (DAC), diethyl carbonate (DEC), diphenyl carbonate (DPC)), cyclic carbonates (e.g. ethylene carbonate (EC), propylene carbonate (PC), cyclohexene carbonate (CC), styrene carbonate (SC)), polycarbonates (e.g. poly-(propylene carbonate), and bisphenol polycarbonate (BPA-PC)) that have many applications in pharmaceuticals, agrochemicals, polymers, lubricants, coating, and catalytic reactions, are another class of chemicals that could be produced from captured CO_2.[96,125] The challenges of this process arise from operation at high temperature and pressure and the need for high catalyst inventory. Moreover, the separation of the catalyst from the products is also another challenge in this process.[96,125] In the production of polycarbonates from the reaction of CO_2 with epoxide, the commercially available Al-based catalysts are widely used which are not environmentally friendly. In this regard, oxidative carboxylation route is an alternative with great potential to synthesize polycarbonates from CO_2 and olefins.[114] Polyurethane is another chemical produced by reaction of CO_2 and cyclic amines such as aziridines and azetidines or N-analogues of epoxides.[114,146]

Another important chemical that could be obtained through CO_2 utilization is formic acid. Hydrogenation of CO_2 into formic acid has recently attracted some interest mainly due to: (i) the mild reaction conditions, (ii) no formation of by-products, (iii) ability to store hydrogen in liquid form, and (iv) easily decomposing of formic acid into hydrogen and CO_2.[99,144]

Biological utilization of CO_2 offers another pathway for production of biodiesel and various biomass-derived commodity chemicals (used as food, silage, biogas, and fertilizer).[147] The advantages offered by this approach include higher growth rate, shorter growth cycle, no competition on the land with other plants, and production of different valuable by-products. However, the captured CO_2 should be purified prior to feed into photobioreactor to remove pollutants such as SO_x , NO_x, and heavy metals that are toxic to the growth of microalgae.[9]

In addition to EOR, utilizing CO_2 as a technological fluid without conversion to chemicals has found applications in many industries including air conditioning (as coolant), solvent, dry-washing, food reservation, and beverage.[4,97,99] generally, EOR consumes 50 Mt/y CO_2 while 8 Mt/y CO_2 is consumed in food and beverage industry.[148] Overall, although there is a great market in turning the captured CO_2 into chemicals and fuels, the proposed lab-scale technologies are still far from industrial commercialization. The reason for that is partly because the materials investigated so far are expensive to make yet not chemically stable, and partly because in most cases, CO_2 conversion rates and overall yield of the main products are low and thus do not meet the requirements for large-scale deployment. Moreover, there still exists limited understanding of reaction mechanisms involved in chemical transformation of CO_2. Evaluating the process requirements and considerations is also overlooked in this field.

3.3. NON-GEOLOGIC STORAGE OF CO_2 (MINERALIZATION)

Non-geologic storage or mineral carbonation of CO_2 results in the production of stable mineral carbonates by reacting CO_2 with metal oxides such as calcium and

magnesium oxides that are naturally abundant in the form of mineral silicates.[149] Carbonation of magnesium and calcium silicates through spontaneous reaction with atmospheric CO_2 at ambient conditions is a naturally occurring process (known as natural weathering) which is thermodynamically favored, however, it is very slow.[4] Artificial improvement of the carbonation kinetics can be achieved by injecting fluids with a higher concentration of CO_2 and increasing the temperature. Despite significant efforts devoted to accelerate this reaction, the slow kinetics is still the main drawback in scaling up the mineralization process.[4] Additionally, this process is energy-intensive since it requires extracting, processing, and transportation of the rocks, as well as high pressure (100-150 bar) and temperature (150-600 °C) to achieve carbonation efficiency higher than 80%.[149] Also, the duration of carbonation reaction is very long (6-24 h) and rocks should be mined (<37 μm). Large plant size, the need for additives to extract reactive species and separate (or dispose of) reaction products are other components of cost penalty.[150] In a sense, mineralization process may be viewed as a sequestration method because it aims at permanently fixing CO_2, but unlike CCS that suffers from leakage (geological storage of CO_2) the carbonates are stable and safe.[151] Also, the exothermic nature of the mineralization reaction along with the geothermal gradient (up to 20 °C/km) contribute to the reduction in energy consumption. Moreover, since pure CO_2 is not required for this process, flue gas can be used directly without removing impurities such as SO_x and NO_x.[152]

To address the operational and technological drawbacks associated with direct carbonation process, indirect carbonation (indirect storage) can be implemented in multiple reactors. In this method, high carbonation efficiency and purity can be obtained in the presence of additives under mild conditions and shorter time periods.[151,153] Another

advantage of this process is the production of diverse commodities such as magnesium/calcium carbonate, iron oxide, and silica that could compensate the process cost. However, since this process is complex, optimizing the operation conditions should be performed separately for each step.[4] In addition, the energy cost is still a main obstacle which prohibits its commercialization.[149,151] To reduce energy cost, other materials such as acetic acid, ammonium salts, and sodium hydroxide can be used instead of hydrochloric acid that is typically used in this process.[151,154] Accelerating the reaction kinetics through advanced materials is one way to improve the efficiency of the process.[153] Indirect mineral carbonation is considered to be the most useful process and it has the potential to be scaled up in the near future.[155] A near complete *in-situ* CO_2 mineralization in Basaltic rocks has been recently achieved under a two-year time frame.[156]

A possibility to upgrade alkali metal wastes into high commercial value-added products such as high-purity precipitated $CaCO_3$ through carbonization is a promising approach that should be the focus of future research in this field.[151–154,157] As an example, carbonation of Ca-carrying cementitious materials through reaction with CO_2 resulted in the development of high early stage strength for building materials applications, achieving CO_2 uptake of 7–12% in the process.[158] To date, only a few projects based on the utilization of inorganic wastes have moved to the commercial or small-scale demonstration phase. For example, retrofitting a cement plant in Texas by SkyMine® (Capitol Aggregates) to reduce its carbon emissions by 15% (83,000 t/year) through direct transformation of flue gas into marketable products, such as sodium bicarbonate, hydrochloric acid, and bleach is approaching the commercialization step. In another example, a pilot-scale demonstration

of mineral carbonation process based on utilization of coal fly ash to reduce CO_2 emissions has been installed at a 2120 MW coal-fired power plant in Point of Rocks, USA.[159].

3.4. DESALINATION AND WATER PRODUCTION

As another promising utilization approach, captured CO_2 could be used to remove total dissolved solids (TDS) and transform brine to water.[160–163] The resulting potable water could be utilized in places where there is a deficiency.[6] While most desalination plants do not employ CO_2 to perform desalination due to economic constraints, new technologies are being developed for the cheap and efficient utilization of CO_2 in this process. When sea water, mixed with ammonia (to weaken the salt molecules), is exposed to CO_2, the already weaker bonds start to form leading to removing the ions from the water phase.[163] The products formed, Na_2CO_2 and NH_4Cl, are heavy and thus can easily settle to the bottom of the tank. The latter can be recycled by thermal operations with calcium oxide or be used as feedstock for ammonia and chlorine synthesis. Hydrate forming method is another technique used for desalination which involves the formation of hydrates using CO_2 to separate the salts from water.[164,165] In this approach, CO_2 can be in either gas or liquid form. The CO_2 hydrates are either dumped into the ocean or transported elsewhere.[166] The ammonia-carbon dioxide forward osmosis process is yet another desalination technique that employs CO_2.[162] In this process, the driving force is osmotic pressure instead of hydraulic pressure in reverse osmosis and by using a 'draw' solution, the brine and fresh water are separated.

One problem commonly faced with the desalination processes is the brine waste that is generated in very large quantities during the process.[167] Additionally, high salt

concentrations, solvent chemical residue, and metal corrosion have the capacity to destabilize local ecosystem.[168] To overcome these problems, the use of three main units namely, carbonation, filtration, and recovery has been proposed for chloride and amine compounds.[169]

Desalination is unlikely to penetrate the market without any significant cost advantages. According to the recent DOE report published in 2013, the cost of potable water production with ~21 ppm TDS from 233,000 ppm brine using three stages of CO_2-based clathrate desalination is estimated to be $3.17/Kgal.[170] Depending on the source of brine the cost could vary significantly. The estimated desalination costs are currently higher than agricultural or municipal water costs, thus making CO_2-based desalination technology less attractive to address water market. In particular, given the high cost of providing agricultural quality water via CO_2-based desalination, it is highly unlikely that this technology could be adopted to supply agricultural water. Overall, although CO_2 remains an attractive option for desalination, the current cost of potable water produced by the CO_2 related technologies is far from being competitive.

3.5. SUMMARY

In summary, the future prospects of carbon utilization technologies are bright and there is a huge potential in various industries to market utilization of captured CO_2, as a renewable resource, instead of permanently sequestering it underground or in the oceans. It is expected that with future research and development on the key components of CO_2 utilization discussed above, the majority of proposed or emerging technologies related CO_2 utilization will continue to lower costs, making more of the fine chemicals, fuels, and water

markets addressable with sustainable CO_2-based processes. Adopting these emerging technologies depends to a great extent upon their cost-effectiveness.

Table 2. CO_2 utilization technologies and their associated challenges and opportunities.

Utilization Technology	**Challenges**	**Opportunities**
Chemical Conversion	• High operating conditions • Complexity of reaction pathways • Stability of catalysts to coke formation • Low conversion and product yield rates • Catalyst regeneration • Development of highly selective catalysts	✓ Dry reforming of methane ✓ Catalytic reduction to formic acid and its derivatives ✓ Noble metal doped transition metal catalysts ✓ Biological pathways to synthetic fuels ✓ Oxidative dehydrogenation
Enhanced Oil/Gas Recovery	• Transportation of CO_2 • Large number of parameters involved • Fluctuations in oil price	✓ Water alternating gas (WAG) system ✓ Compensated neutron log (CNL)
Mineralization	• Slow kinetics • High pressure and temperature operation • Expensive to implement	✓ Indirect carbonation ✓ Utilization of inorganic wastes
Desalination	• Equipment corrosion • Expensive operation • Large amount of brine waste	✓ Providing potable water to residential and municipal customers ✓ Possible implementation in various regions ✓ Modified Solvay process

To date, only a small fraction of CO_2 captured from gas effluents has been actually utilized in providing energy or producing other value added products. The estimated high cost along with their efficiency are the two key factors responsible for such a slow progress.

Table 2 provides a summary of the current challenges and future opportunities associated with various CO_2 utilization routes discussed in this section.

4. COMBINED CO_2 CAPTURE AND UTILIZATION

Combining capture and utilization offers an efficient strategy to minimize the high energy requirements for direct chemicals/fuels production from waste gas streams especially when the capture and utilization are carried out at the same temperature. Such process intensification will lead to smaller, cleaner, and more energy-efficient technologies. The concept of hybrid processes in gas separation and reaction has been previously applied to several applications. For instance, membrane-reactors (MRs) combine a membrane separation with a chemical reaction in one unit. MRs are capable of promoting a reaction process by selectively removing at least one of the products through the membrane from the reaction zone, making the equilibrium reaction shift to the product side.[171–173] Sorption enhanced reaction (SER) is a similar concept that combines adsorption and reaction in a single unit. SER has been widely applied to water gas shift (WGS) reaction for production of high purity hydrogen.[174–180] In this process, the *in-situ* capture of CO_2 allows the thermodynamically constrained WGS process to operate at higher temperatures (i.e., 350 °C) where reaction kinetics are more favorable.[179] Such novel concepts could be adopted for simultaneous CO2 capture and utilization in various industries. The schematic of proposed capture-utilization process is illustrated in Figure 3.

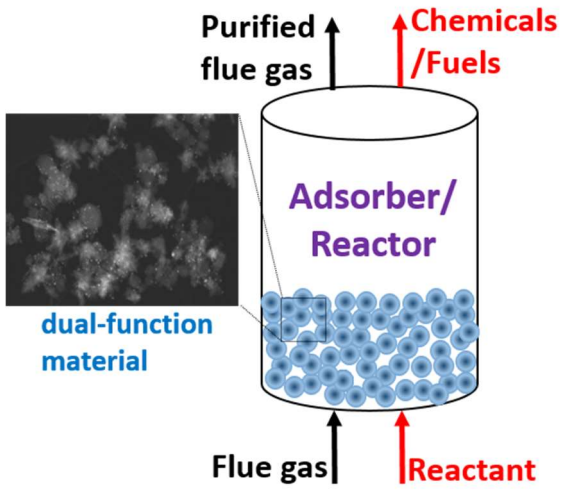

Figure 3. Schematic of proposed combined carbon capture-utilization process.

The concept of chemicals and fuels production directly from industrial flue gases over a dual-function material has been previously applied to the production of syngas (CO and H_2), a useful reactant for methanol synthesis.[181–183] In this process, called tri-reforming of methane, a synergetic combination of CO_2 reforming, steam reforming, and partial oxidation of methane occurs in a single reactor at 850 °C with supported nickel catalysts.[181–183] In another example, the *in-situ* capture and methanation of CO_2 has been studied over a dual-function material in the form of coated monolith to produce synthetic CH_4 using H_2 at 320 °C.[184–187] Hydrogenation of CO_2 is another example of combined capture and reduction that has been recently reported.[188] Simultaneous capture and mineralization of coal combustion flue gas CO_2 is another example of hybrid processes that has been demonstrated at a pilot scale in the US.[159]

Such integrated systems could provide a solution to both the energy and environmental problems currently encountered worldwide. However, creation of novel *in-situ* capture-conversion technologies requires advancements in both materials science and

process engineering. Given the different nature of adsorption and catalysis, the fundamental aspects of hybrid adsorbent/catalyst characteristics in conjunction with process considerations and operation conditions should be carefully studied to obtain a highly efficient and cost-effective technology. Also, for direct utilization of waste gas streams, the resistivity of materials (especially catalysts) to impurities may pose a challenge and efforts should be undertaken to ensure the reliability of the materials for a long service life.

5. OUTLOOK

In this short review, current challenges and future opportunities of carbon capture and utilization technologies were presented and discussed from perspectives of efficiency and cost. Indeed recent years have witnessed significant advancements in design and development of various CCU technologies with a few cases being deployed on an industrial scale. However, the majority of technology options being considered so far are still at the lab-scale stage of development. In both scenarios, commercial implementation of novel materials that outperform the current state-of-the-art materials in each respected technique will certainly decrease energy requirements of both capture and utilization processes. However, research and development on materials concepts should be coupled with process performance considerations to better evaluate their potential under real conditions. Having such holistic view of both materials and processes and a mutual communication between materials scientists and engineers will help accelerate scale-up of CCU technologies dramatically. In addition, small-scale evaluation of materials or processes should take into

account the large-scale implementation requirements in order to provide a realistic evaluation of the performance and to reduce the uncertainties in estimating the associated costs. Cost effectiveness is the ultimate factor determining the feasibility of the adoption of many emerging CCU technologies.

Long-term stability of the materials used in most CCU methods is an important consideration that not only impacts the system performance but also affects the economics of the process. In the context of utilization, in particular the production of fuels and chemicals, the use of renewable energy sources can bring down the total cost while providing a sustainable approach for production of value-added products. In most technologies, system integration and process intensification will enable a cost-effective approach to improve the separation and thermodynamic efficiency, however, the complexity of the operation and other related issues should be considered as well.

Hybrid processes that couple either CO_2 capture subsystems or offer a simultaneous capture and utilization approach should be the focus of future research as the thermodynamic analyses of such systems have highlighted their energy efficacy and cost-effectiveness (by reducing both capital and operating costs). Although the emerging hybrid systems appear to have many hallmarks of next-generation CCU technologies, more research (e.g. materials development, processes operation requirements) and development (synergistic assessment studies and process scale-up) are required for these emerging technologies to become commercially available in the near future. Any feasibility study should also include other considerations related to environmental impacts, risk assessment and life cycle analysis.

ACKNOWLEDGEMENT

Funding was provided in part by University of Missouri Research Board (UMRB).

REFERENCES

1. U.S. Energy Information Administration. Annual Energy Outlook. *DOE/EIA* **383,** 1–154 (2015).

2. http://www.c2es.org/international/negotiations/cop21-paris/summary.

3. Markewitz, P. *et al.* Worldwide innovations in the development of carbon capture technologies and the utilization of CO_2. *Energy Environ. Sci.* **5,** 7281–7305 (2012).

4. Boot-Handford, M. E. *et al.* Carbon capture and storage update. *Energy Environ. Sci.* **7,** 130–189 (2014).

5. Agency, I. E. Technology roadmap - Carbon capture and Storage. *IEA Rep.* 1–59 (2013). doi:10.1007/SpringerReference_7300

6. Styring, P., Jansen, D., de Coninck, H., Reith, H. & Armstrong, K. *Carbon Capture and Utilisation in the green economy*. *Centre for Low Carbon Futures* (2011).

7. Cuéllar-Franca, R. M. & Azapagic, A. Carbon capture, storage and utilisation technologies: A critical analysis and comparison of their life cycle environmental impacts. *J. CO_2 Util.* **9,** 82–102 (2015).

8. von der Assen, N., Voll, P., Peters, M. & Bardow, A. Life cycle assessment of CO_2 capture and utilization: a tutorial review. *Chem. Soc. Rev.* **43,** 7982–7994 (2014).

9. Meylan, F. D., Moreau, V. & Erkman, S. CO_2 utilization in the perspective of industrial ecology, an overview. *J. CO_2 Util.* **12,** 101–108 (2015).

10. Yuan, Z., Eden, M. R. & Gani, R. Toward the Development and Deployment of Large-Scale Carbon Dioxide Capture and Conversion Processes. *Ind. Eng. Chem. Res.* **55,** 3383–3419 (2016).

11. Miller, D. C., Litynski, J. T., Brickett, L. A. & Morreale, B. D. Toward Transformational Carbon Capture Systems. *AIChE J.* **62,** 1–10 (2016).

12. Songolzadeh, M., Soleimani, M., Takht Ravanchi, M. & Songolzadeh, R. Carbon dioxide separation from flue gases: a technological review emphasizing reduction in greenhouse gas emissions. *ScientificWorldJournal.* **2014,** 1–34 (2014).

13. Abotalib, M., Zhao, F. & Clarens, A. Deployment of a Geographical Information System Life Cycle Assessment Integrated Framework for Exploring the Opportunities and Challenges of Enhanced Oil Recovery Using Industrial CO_2 Supply in the United States. *ACS Sustain. Chem. Eng.* **4,** 4743–4751 (2016).

14. Agency, I. E. World Outlook Energy. *World Energy Outlook* 1–12 (2015). doi:10.1787/weo-2014-en

15. SaskPower.com. *Boundary Dam Integrated Carbon Capture and Storage Demonstration Project*. (2015).

16. Kong, Y., Shen, X., Fan, M., Yang, M. & Cui, S. Dynamic capture of low-concentration CO_2 on amine hybrid silsesquioxane aerogel. *Chem. Eng. J.* **283,** 1059–1068 (2016).

17. Arstad, B., Fjellvåg, H., Kongshaug, K. O., Swang, O. & Blom, R. Amine functionalised metal organic frameworks (MOFs) as adsorbents for carbon dioxide. *Adsorption* **14,** 755–762 (2008).

18. Builes, S., López-Aranguren, P., Fraile, J., Vega, L. F. & Domingo, C. Analysis of CO_2 Adsorption in Amine-Functionalized Porous Silicas by Molecular Simulations. *Energy & Fuels* **29,** 3855–3862 (2015).

19. Goeppert, A. *et al.* Carbon Dioxide Capture from the Air Using a Polyamine Based. *J. Am. Chem. Soc.* **133,** 20164–20167 (2011).

20. Corvo, M. C. *et al.* A Rational Approach to CO_2 Capture by Imidazolium Ionic Liquids: Tuning CO_2 Solubility by Cation Alkyl Branching. *ChemSusChem* **8,** 1935–1946 (2015).

21. Cadena, C. *et al.* Why is CO_2 so Soluble in Imidazolium-Based Ionic Liquids? *J. Am. Chem. Soc.* **126,** 5300–5308 (2004).

22. Bates, E. D., Mayton, R. D., Ntai, I. & Davis, J. H. CO_2 capture by a task-specific ionic liquid. *J. Am. Chem. Soc.* **124,** 926–7 (2002).

23. Rochelle, G. T. Amine scrubbing for CO2 capture. *Science* **325,** 1652–1654 (2009).

24. Markewitz, P. *et al.* Worldwide innovations in the development of carbon capture technologies and the utilization of CO_2. *Energy Environ. Sci.* **5,** 7281 (2012).

25. Merkel, T. C., Lin, H., Wei, X. & Baker, R. Power plant post-combustion carbon dioxide capture: An opportunity for membranes. *J. Memb. Sci.* **359,** 126–139 (2010).

26. Japip, S. *et al.* Highly permeable zeolitic imidazolate framework (ZIF)-71 nano-particles enhanced polyimide membranes for gas separation. *J. Memb. Sci.* **107,** 34–44 (2014).

27. Huang, Q. & Eić, M. Commercial adsorbents as benchmark materials for separation of carbon dioxide and nitrogen by vacuum swing adsorption process. *Sep. Purif. Technol.* **103,** 203–215 (2013).

28. Han, S. *et al.* High-throughput screening of metal-organic frameworks for CO2 separation. *ACS Comb. Sci.* **14,** 263–267 (2012).

29. Lively, R. P., Leta, D. P., DeRites, B. A., Chance, R. R. & Koros, W. J. Hollow fiber adsorbents for CO_2 capture: Kinetic sorption performance. *Chem. Eng. J.* **171,** 801–810 (2011).

30. Rownaghi, A. A. *et al.* Aminosilane-Grafted Zirconia–Titiania–Silica Nanoparticles/Torlon Hollow Fiber Composites for CO_2 Capture. *ChemSusChem* **9,** 1166–1177 (2016).

31. Koros, W. J. & Fleming, G. K. Membrane-based gas separation. *J. Memb. Sci.* **83,** 1–80 (1993).

32. Kosuri, M. R. & Koros, W. J. Asymmetric Hollow Fiber Membranes for Separation of CO_2 from Hydrocarbons and Fluorocarbons at High-Pressure Conditions Relevant to C_2F_4 Polymerization. *Ind. Eng. Chem. Res.* **48,** 10577–10583 (2009).

33. Favre, E. Carbon dioxide recovery from post-combustion processes: Can gas permeation membranes compete with absorption? *J. Memb. Sci.* **294,** 50–59 (2007).

34. Membrane Technology Research, *Membrane Process to Capture CO_2 from Coal-Fired Power Plant Flue Gas*. (2012).

35. Koros, W. J. Evolving beyond the thermal age of separation processes: Membranes can lead the way. *AIChE J.* **50,** 2326–2334 (2004).

36. Kim, T. J., Vrålstad, H., Sandru, M. & Hägg, M. B. Separation performance of PVAm composite membrane for CO_2 capture at various pH levels. *J. Memb. Sci.* **428,** 218–224 (2013).

37. Li, S. *et al.* Effects of Minor SO_2 on the Transport Properties of Fixed Carrier Membranes for CO_2 Capture. *Ind. Eng. Chem. Res.* **53,** 7758–7767 (2014).

38. Chen, H. Z., Thong, Z., Li, P. & Chung, T.-S. High performance composite hollow fiber membranes for CO_2/H_2 and CO_2/N_2 separation. *Int. J. Hydrogen Energy* **39,** 5043–5053 (2014).

39. Bae, T.-H. & Long, J. R. CO_2/N_2 separations with mixed-matrix membranes containing Mg_2(dobdc) nanocrystals. *Energy Environ. Sci.* **6,** 3565 (2013).

40. Zhao, Y. & Ho, W. S. W. CO_2 - Selective Membranes Containing Sterically Hindered Amines for CO_2/H_2 Separation. **3,** (2012).

41. Ramasubramanian, K., Verweij, H. & Winston Ho, W. S. Membrane processes for carbon capture from coal-fired power plant flue gas: A modeling and cost study. *J. Memb. Sci.* **421–422,** 299–310 (2012).

42. Tanh Jeazet, H. B., Staudt, C. & Janiak, C. Metal-organic frameworks in mixed-matrix membranes for gas separation. *Dalton Trans.* **41,** 14003–27 (2012).

43. Lively, R. P. *et al.* Hollow Fiber Adsorbents for CO_2 Removal from Flue Gas. *Ind. Eng. Chem. Res.* **48,** 7314–7324 (2009).

44. Labreche, Y. *et al.* Post-Spinning Infusion of Poly(ethyleneimine) into Polymer/Silica Hollow Fiber Sorbents for Carbon Dioxide Capture. *Chem. Eng. J.* **221,** 166–175 (2013).

45. Fan, Y. *et al.* Evaluation of CO_2 adsorption dynamics of polymer/silica supported poly (ethylenimine) hollow fiber sorbents in rapid temperature swing adsorption. *Int. J. Greenh. Gas Control* **21,** 61–71 (2014).

46. Phan, A. *et al.* Synthesis, structure, and carbon dioxide capture properties of zeolitic imidazolate frameworks. *Acc Chem Res* **43,** 58–67 (2010).

47. Liu, H. *et al.* Irreversible Change of the Pore Structure of ZIF-8 in Carbon Dioxide Capture with Water Coexistence. *J. Phys. Chem. C* **120,** 13287–13294 (2016).

48. Ma, X. *et al.* Ammonia-treated porous carbon derived from ZIF-8 for enhanced CO_2 adsorption. *Appl. Surf. Sci.* **369,** 390–397 (2016).

49. Chue, K.T., Kim, J.N., Yoo, Y.J., Cho, S.H., Yang, R. T. Comparison of activated carbon and zeolite 13X for CO_2 recovery from flue gas by pressure swing adsorption. *Ind. Eng. Chem. Res.* **34,** 591–598 (1995).

50. Patel, H. a. *et al.* High capacity carbon dioxide adsorption by inexpensive covalent organic polymers. *J. Mater. Chem.* **22,** 8431–8437 (2012).

51. Reich, T. E., Behera, S., Jackson, K. T., Jena, P. & El-Kaderi, H. M. Highly selective CO2/CH4 gas uptake by a halogen-decorated borazine-linked polymer. *J. Mater. Chem.* **22,** 13524–13528 (2012).

52. Choi, S., Drese, J. H. & Jones, C. W. Adsorbent materials for carbon dioxide capture from large anthropogenic point sources. *ChemSusChem* **2,** 796–854 (2009).

53. D.Ruthven. *Principles of adsorption processes*. *John Wiley &Sons,Inc.* (1984).

54. Hauchhum, L. & Mahanta, P. Carbon dioxide adsorption on zeolites and activated carbon by pressure swing adsorption in a fixed bed. *Int. J. Energy Environ. Eng.* **5,** 349–356 (2014).

55. Agarwal, A., Biegler, L.T., Zitney, S. E. A super structure-based optimal synthesis of PSA cycles for post-combustion CO_2 capture. *AIChE J* **56,** 1813–1828 (2010).

56. Merel, J., Clausse, M. & Meunier, F. Experimental Investigation on CO_2 Post-Combustion Capture by Indirect Thermal Swing Adsorption Using 13X and 5A Zeolites. *Ind. Eng. Chem. Res.* **47,** 209–215 (2008).

57. Chaffee AL, Knowles GP, Liang Z, Zhang J, Xiao P, W. P. CO_2 capture by adsorption materials and process development. *Int J Greenh Gas Control* **1,** 11–8 (2007).

58. Marx, D., Joss, L., Hefti, M. & Mazzotti, M. Temperature Swing Adsorption for Postcombustion CO_2 Capture: Single- and Multicolumn Experiments and Simulations. *Ind. Eng. Chem. Res.* **55,** 1401–1412 (2016).

59. T. Takeguchi, W. Tanakulrungsank, T. I. Separation and/or concentration of CO_2 from CO_2/N_2 gaseous mixture by pressure swing adsorption using metalincorporated microporous crystals with high surface area. *Gas Sep. Purif.* **7,** 3–9 (1993).

60. Leperi, K. T., Snurr, R. Q. & You, F. Optimization of Two-Stage Pressure/Vacuum Swing Adsorption with Variable Dehydration Level for Postcombustion Carbon Capture. *Ind. Eng. Chem. Res.* **55,** 3338–3350 (2016).

61. Rezaei, F. *et al.* MOF-74 and UTSA-16 film growth on monolithic structures and their CO_2 adsorption performance. *Chem. Eng. J.* **3,** http://dx.doi.org/10.1016/j.cej.2016.11.058 (2016).

62. Rezaei, F. & Webley, P. Structured adsorbents in gas separation processes. *Sep. Purif. Technol.* **70,** 243–256 (2010).

63. Rezaei, F. *et al.* Aminosilane-Grafted Polymer/Silica Hollow Fiber Adsorbents for CO_2 Capture from Flue Gas. *ACS Appl. Mater. Interfaces* **5,** 3921–3931 (2013).

64. Lively, R. P., Chance, R. R. & Koros, W. J. Enabling Low-Cost CO_2 Capture via Heat Integration. *Ind. Eng. Chem. Res.* **49,** 7550–7562 (2010).

65. Merel, J., Clausse, M. & Meunier, F. Carbon dioxide capture by indirect thermal swing adsorption using 13X zeolite. *Environ. Prog.* **25,** 327–333 (2006).

66. Ntiamoah, A., Ling, J., Xiao, P., Webley, P. A. & Zhai, Y. CO_2 Capture by Temperature Swing Adsorption: Use of Hot CO_2-Rich Gas for Regeneration. *Ind. Eng. Chem. Res.* **55,** 703–713 (2015).

67. Tlili, N., Grévillot, G. & Vallières, C. Carbon dioxide capture and recovery by means of TSA and/or VSA. *Int. J. Greenh. Gas Control* **3,** 519–527 (2009).

68. Plaza, M. G., García, S., Rubiera, F., Pis, J. J. & Pevida, C. Post-combustion CO_2 capture with a commercial activated carbon: Comparison of different regeneration strategies. *Chem. Eng. J.* **163,** 41–47 (2010).

69. J.Kärger, D. M. R. Diffusion in Zeolites and Other Microporous Solids. *John Wiley, New York* 1–605 (1992). doi:10.1524/zpch.1994.186.Part_2.269

70. Li, G., Xiao, P., Webley, P. a., Zhang, J. & Singh, R. Competition of CO_2/H_2O in adsorption based CO_2 capture. *Energy Procedia* **1,** 1123–1130 (2009).

71. D. Ruthven, S. Farooq, K. K. *Pressure Swing Adsorption*. (VCH Publishers,Inc., 1994).

72. Hossain, M. M., Lasa, H. I. De & de Lasa, H. I. Chemical-looping combustion (CLC) for inherent separations—a review. *Chem. Eng. Sci.* **63,** 4433–4451 (2008).

73. Romeo, L. M., Usón, S., Valero, A. & Escosa, J. M. Exergy analysis as a tool for the integration of very complex energy systems: The case of carbonation/calcination CO2 systems in existing coal power plants. *Int. J. Greenh. Gas Control* **4,** 647–654 (2010).

74. Martínez, I., Murillo, R., Grasa, G. & Abanades, J. C. Integration of a Ca-looping system for CO2 capture in an existing power plant. *Energy Procedia* **4,** 1699–1706 (2011).

75. Martínez, A., Lara, Y., Lisbona, P. & Romeo, L. M. Energy penalty reduction in the calcium looping cycle. *Int. J. Greenh. Gas Control* **7,** 74–81 (2012).

76. Ozcan, D. C. *et al.* Ca-Cu looping process for CO_2 capture from a power plant and its comparison with Ca-looping, oxy-combustion and amine-based CO_2 capture processes. *Int. J. Greenh. Gas Control* **43,** 198–212 (2015).

77. Symonds, R. T., Lu, D. Y., Manovic, V. & Anthony, E. J. Pilot-scale study of CO_2 capture by CaO-based sorbents in the presence of steam and SO_2. *Ind. Eng. Chem. Res.* **51,** 7177–7184 (2012).

78. N. Rodrı´guez, M. Alonso, and J. C. A. Experimental Investigation of a Circulating Fluidized-Bed Reactor to Capture CO_2 with CaO. *AIChE J.* **57,** 1356–1366 (2011).

79. Charitos, A. *et al.* Parametric investigation of the calcium looping process for CO2 capture in a 10 kWth dual fluidized bed. *Int. J. Greenh. Gas Control* **4,** 776–784 (2010).

80. Agency, I. E. Technology roadmap - Carbon capture and Storage. *IEA Rep.* 1–59 (2013). doi:10.1007/SpringerReference_7300

81. Lackner, K. S. Capture of carbon dioxide from ambient air. *Eur. Phys. J. Spec. Top.* **176,** 93–106 (2009).

82. Lackner, K., Grimes, P. & Ziock, H. Capturing carbon dioxide from air. *Carbon Sequestration* (2001). http://www.netl.doe.gov/publications/proceedings/01/carbon_seq/7b1.pdf

83. Lackner, K. S. *et al.* The urgency of the development of CO_2 capture from ambient air. *Proc. Natl. Acad. Sci. U. S. A.* **109,** 13156–13162 (2012).

84. Jones, C. W. CO_2 capture from dilute gases as a component of modern global carbon management. *Annu. Rev. Chem. Biomol. Eng.* **2,** 31–52 (2011).

85. Sanz-Pérez, E. S., Murdock, C. R., Didas, S. A. & Jones, C. W. Direct Capture of CO_2 from Ambient Air. *Chem. Rev.* **116,** 11840−11876 (2016).

86. Lively, R. P. & Realff, M. J. On Thermodynamic Separation Efficiency: Adsorption Processes. *AIChE J.* **62,** 3699–3705 (2016).

87. Esteves, I. A. A. C., Mota, J. P. B., Quimica, D., Q, C. De & Ck, F. De. Simulation of a New Hybrid Membrane/Pressure Adsorption Process for Gas Separation. *Desalination* **148,** 275–280 (2002).

88. Belaissaoui, B., Le Moullec, Y., Willson, D. & Favre, E. Hybrid membrane cryogenic process for post-combustion CO_2 capture. *J. Memb. Sci.* **415–416,** 424–434 (2012).

89. Scholes, C. A., Ho, M. T., Wiley, D. E., Stevens, G. W. & Kentish, S. E. Cost competitive membrane-cryogenic post-combustion carbon capture. *Int. J. Greenh. Gas Control* **17,** 341–348 (2013).

90. Zhao, L., Primabudi, E. & Stolten, D. Investigation of a Hybrid System for Post-Combustion Capture. *Energy Procedia* **63,** 1756–1772 (2014).

91. Scholz, M., Frank, B., Stockmeier, F., Falß, S. & Wessling, M. Techno-economic analysis of hybrid processes for biogas upgrading. *Ind. Eng. Chem. Res.* **52,** 16929–16938 (2013).

92. Hasse, D. *et al.* CO_2 capture by cold membrane operation. *Energy Procedia* **63,** 186–193 (2014).

93. Song, C., Kansha, Y., Fu, Q., Ishizuka, M. & Tsutsumi, A. Reducing energy consumption of advanced PTSA CO_2 capture process—Experimental and numerical study. *J. Taiwan Inst. Chem. Eng.* **64,** 69–78 (2016).

94. Wurzbacher, J. A., Gebald, C. & Steinfeld, A. Separation of CO_2 from air by temperature-vacuum swing adsorption using diamine-functionalized silica gel. *Energy Environ. Sci.* **4,** 3584 (2011).

95. Wurzbacher, J. A., Gebald, C., Brunner, S. & Steinfeld, A. Heat and mass transfer of temperature-vacuum swing desorption for CO_2 capture from air. *Chem. Eng. J.* **283,** 1329–1338 (2016).

96. Aresta, M. *Carbon Dioxide as Chemical Feedstock*. *Carbon Dioxide as Chemical Feedstock* (2010). doi:10.1002/9783527629916

97. Aresta, M., E. carbon dioxide recovery and utilisation. *Kluwer Acad. Publ.* (2003).

98. Hu, B., Guild, C. & Suib, S. L. Thermal, electrochemical, and photochemical conversion of CO2 to fuels and value-added products. *J. CO2 Util.* **1,** 18–27 (2013).

99. Aresta, M., Dibenedetto, A. & Angelini, A. Catalysis for the valorization of exhaust carbon: From CO_2 to chemicals, materials, and fuels. technological use of CO_2. *Chem. Rev.* **114,** 1709–1742 (2014).

100. Melzer, L. Stephen, C. C. and A. C. F. C. D. Carbon Dioxide Enhanced Oil Recovery. 18 (2012).

101. Lake, L., Johns, R., Rossen, W. & Pope, G. *Fundamentals of enhanced oil recovery*. (2014).

102. Tunio, S. Q., Mehran, A. H. T., Ghirano, N. A. & Adawy, Z. M. El. Comparison of Different Enhanced Oil Recovery Techniques for Better Oil Productivity. *Int. J. Appl. Sci. Technol.* **1,** 143–153 (2011).

103. Perera, M. *et al.* A Review of CO_2-Enhanced Oil Recovery with a Simulated Sensitivity Analysis. *Energies* **9,** 481 (2016).

104. Gozalpour, F., Ren, S. R. & Tohidi, B. CO_2 EOR and storage in oil reservoirs. *Oil Gas Sci. Technol.* **60,** 537–546 (2005).

105. Cho, J., Kim, T. H. & Lee, K. S. Modeling of CO_2 EOR Process Combined with Intermediate Hydrocarbon. (2016).

106. Klins, M. A. *Carbon dioxide flooding: Basic mechanisms and project design*. (1984).

107. Panda, M., Nottingham, D. & Lenig, D. Systematic Surveillance Techniques for a Large Miscible WAG Flood. *SPE Reserv. Eval. Eng.* **14,** 27–30 (2011).

108. Hajeri, S. Al, Negahban, S., Al-yafei, G. & Basry, A. Al. Design and Implementation of the first CO_2-EOR Pilot in Abu Dhabi , UAE. *Spe* (2010).

109. Pizarro, J. O. D. S. A. & Branco, C. C. M. Challenges in implementing an EOR project in the Pre-Salt province in deep offshore Brasil. *Soc. Pet. Eng. - SPE EOR Conf. Oil Gas West Asia 2012, OGWA - EOR Build. Towar. Sustain. Growth* **2,** 954–966 (2012).

110. Ampomah, W., Balch, R. S., Grigg, R. B., Recovery, P. & Will, R. Farnsworth Field CO 2 -EOR Project : Performance Case History. (2016).

111. A.Goeppert,M.Czaun,G.K.Surya Prakash, G. A. O. No Title. *Energy Environ. Sci.* **5,** 7833 (2012).

112. No Title. *https://www3.epa.gov/climatechange/ghgemissions/gases.html*

113. M.S.Fan, A. Z. A. and S. B. No Title. *ChemCatChem* **1,** 192–208 (2009).

114. Aresta, M. & Dibenedetto, A. Utilisation of CO_2 as a chemical feedstock: opportunities and challenges. *Dalton Trans.* 2975–2992 (2007). doi:10.1039/b700658f

115. Song, C. Global Challenges and Strategies for Control, Conversion and Utilization of CO_2 for Sustainable Development Involving Energy, Catalysis, Adsorption and Chemical Processing. *Catal. Today* **115,** 2–32 (2006).

116. Matsubu, J. C., Yang, V. N. & Christopher, P. Isolated metal active site concentration and stability control catalytic CO_2 reduction selectivity. *J. Am. Chem. Soc.* **137,** 3076–3084 (2015).

117. J. Graciani, K. Mudiyanselage, F., Xu, A. E. Baber, J. Evans, S. D. Senanayake, D. J. Stacchiola, P. & Liu, J. Hrbek, J. F. Sanz, J. A. R. No Title. *Science (80-.).* **345,** 546–550 (2014).

118. G.laurenczy. Hydrogen Storage and Delivery: The Carbon Dioxide – Formic Acid Couple. *Chimia (Aarau).* **65,** 663–666 (2011).

119. P.F.Tropschuh, E. P. Sustainable automotive technologies, in: Proceedings of the 5th International Conference ICSAT 2013. *Springer Int. Publ.* 185–190 (2013).

120. S. Kuld, C. Conradsen, P. G. Moses, I. C. and & J. Sehested, A. No Title. *Chem.,Int.* **53,** 5941–5945 (2014).

121. W. J. Cai, P. R. de la Piscina, J. T. and N. H. No Title. *Catal.Today* **242,** 193–199 (2015).

122. Urakawa, A. B. and A. No Title. *J.Catal.* **309,** 66–70 (2014).

123. Porosoff, M. D., Yan, B. & Chen, J. G. Catalytic reduction of CO_2 by H_2 for synthesis of CO, methanol and hydrocarbons: challenges and opportunities. *Energy Environ. Sci.* **2,** 303 (2015).

124. Kattel, S. *et al.* CO_2 Hydrogenation over Oxide-Supported PtCo Catalysts: The Role of the Oxide Support in Determining the Product Selectivity. *Angew. Chem. Int. Ed. Engl.* **55,** 1–7 (2016).

125. Markley, B. & Rodriguez-santiago, V. Utilization of Carbon Dioxide from Coal-Fired Power Plant for the Production of Value-Added Products. (2006).

126. Dayton, D. C.; Turk, B.; Gupta, R. Syngas Cleanup, Conditioning, and Utilization. *John Wiley Sons, Inc.* 78−123 (2011).

127. Gangadharan, P., et al. Evaluation of the economic and environmental impact of combining dry reforming with steam reforming of methane. *Chem. Eng. Res. Des.* 2012

128. Hartley, M., Tam, I. Non-Sequestration Utilization Options for Carbon Dioxide (CO_2). *Nexant´s ChemSystems* (2012).

129. Song, C., Gaffney, A. M., F. K. CO_2 Conversion and Utilization. *Am. Chem. Soc. Symp. Ser.* **809,** (2000).

130. Araújo, O. D. Q. F., Medeiros, J. L. De & Alves, R. M. B. CO 2 Utilization : A Process Systems Engineering Vision. *B. Chapter* (2014).

131. Jiang, Z.; Liao, X.; Zhao, Y. Comparative study of the dry reforming of methane on fluidized aerogel and xerogel Ni/Al2O3 catalysts. *Appl. Petrochemical Res.* 1–9 (2013).

132. Kahle, L. C. S., Roussière, T., Maier, L., Delgado, K.H., Wasserschaff, G., S. & S.A., Deutschmann, O. Methane Dry Reforming at High Temperature and Elevated Pressure: Impact of Gas-Phase Reactions. *ndustrial Eng. Chem. Res.* 34 (2013).

133. Kaiser, P., Unde, R.B., Kern, C., J. Production of Liquid Hydrocarbons with CO_2 as Carbon Source based on Reverse Water-Gas Shift and Fischer-Tropsch Synthesis. *Chemie Ing. Tech.* **85,** 489–499 (2013).

134. J.R.H.Ross. No Title. *Catal.Today* **100,** 151–158 (2005).

135. Urlan, F., Marcu, I.-C. & Sandulescu, I. Oxidative dehydrogenation of n-butane over titanium pyrophosphate catalysts in the presence of carbon dioxide. *Catal. Commun.* **9,** 2403–2406 (2008).

136. Liu, H., Zhang, Z., Li, H. & Huang, Q. Intrinsic kinetics of oxidative dehydrogenation of propane in the presence of CO_2 over Cr/MSU-1 catalyst. *J. Nat. Gas Chem.* **20,** 311–317 (2011).

137. Deven, P. E. & Copéret, C. The Role of Proton Transfer in Heterogeneous Transformations of Hydrocarbons. *Chimia (Aarau).* **69,** 321–326 (2015).

138. Cheng, Y. *et al.* Oxidative dehydrogenation of ethane with CO2 over Cr supported on submicron ZSM-5 zeolite. *Chinese J. Catal.* **36,** 1242–1248 (2015).

139. Koirala, R., Buechel, R., Krumeich, F., Pratsinis, S. E. & Baiker, A. Oxidative Dehydrogenation of Ethane with CO2 over Flame-Made Ga-Loaded TiO_2. *ACS Catal.* **5,** 690–702 (2015).

140. Muller, K., Baumgartner, A., Mokrushina, L. & Arlt, W. Increasing the Equilibrium Yield of Oxidative Dehydrogenation with CO_2 by Secondary Reactions. *Chem. Eng. Technol.* **37,** 1261–1264 (2014).

141. Wang, S. & Zhu, Z. H. Catalytic Conversion of Alkanes to Olefins by Carbon Dioxide Oxidative DehydrogenationsA Review. 1126–1139 (2004). doi:10.1021/ef0340716

142. Ansari, M. B. & Park, S.-E. Carbon dioxide utilization as a soft oxidant and promoter in catalysis. *Energy Environ. Sci.* **5,** 9419–9437 (2012).

143. N. MacDowell, N. Florin, A. Buchard, J. Hallett, A. G., G. Jackson, C. S. Adjiman, C. K. Williams, N. S. and & Fennell, P. Energy Environ. Sci., 2010, 3, 1645–1669. *Energy Environ. Sci.* **3,** 1645–1669 (2010).

144. Styring, Peter. de Coninck,Heleen .Reith, H. Carbon Capture and Utilisation in the green economy. *Cent. Low Carbon Futur.* (2011).

145. Bell, A. T. & Marks, T. J. *Carbon Management: Implications for R & D in the Chemical Sciences and Technology*. (2001).

146. After Major Downturn, Global Demand for Polycarbonate Growing Again, Says IHS Chemical Report; IHS. *http//press.ihs.com/pressrelease/ Commod. polycarbonate-growing-agai.* **13,** (2012).

147. Sen, C. Cong Sen Master of Science Thesis Stockholm 2012. (2012).

148. Intergovernmental Panel on Climate Change: Special Report on Carbon Dioxide Capture and Storage. *IPCC, Cambridge Univ. Press. Cambridge* (2005).

149. Cuellar-Franca, R. M. & Azapagic, A. Carbon capture, storage and utilisation technologies: A critical analysis and comparison of their life cycle environmental impacts. *J. CO2 Util.* **9,** 82–102 (2015).

150. Sanna, A., Uibu, M., Caramanna, G., Kuusik, R. & Maroto-Valer, M. M. A review of mineral carbonation technologies to sequester CO_2. *Chem. Soc. Rev.* **43,** 8049–8080 (2014).

151. Pan, Shu-Yuan; Chiang, Adrew; Chang, E-E; Lin, Yi-Pin; Kim, Hyunook; Chiang, P.-C. An Innovative Approach to Integrated Carbon Mineralization and Waste Utilization: A Review. *Aerosol Air Qual. Res.* **2015,** 1072–1091 (2015).

152. Metz, B. O. D. H. de C. M. L. L. L. M. *IPCC Special Report on Carbon Dioxide Capture and Storage*. *CAMBRIDGE UNIVERSITY PRESS* (2005). doi:10.1021/es200619j

153. Sanna, A., Hall, M. R. & Maroto-Valer, M. Post-processing pathways in carbon capture and storage by mineral carbonation (CCSM) towards the introduction of carbon neutral materials. *Energy Environ. Sci.* **5,** 7781 (2012).

154. Huijgen, W. J. J. Carbon dioxide sequestration by mineral carbonation. Feasibility of enhanced natural weathering as a CO_2 emission reduction technology. *Carbon Dioxide Sequestration by Mineral Carbonation Wouter J . J . Huijgen*. (2016).

155. Weijun Bao , Huiquan Li, and Y. Z. Experimental investigation of enhanced carbonation by solvent extraction for indirect CO_2 mineral sequestration. *Greenh. Gases Sci. Technol.* **4,** 785–799 (2014).

156. Matter, J.M., Stute, M., Snæbjörnsdottir, S.Ó., Oelkers, E.H., Gislason, S.R., Aradottir, E.S., Sigfusson, B., Gunnarsson, I., Sigurdardottir, H., Gunnlaugsson, E. and Axelsson, G. Rapid carbon mineralization for permanent disposal of anthropogenic carbon dioxide emissions. *Science (80-.).* **352,** 1312–1314 (2016).

157. Evangelos Georgakopoulos, Rafael M. Santos, YiWai Chiang, V. M. Influence of process parameters on carbonation rate and conversion of steelmaking slags – Introduction of the 'carbonation weathering rate'. *Greenh. Gases Sci. Technol.* **6,** 470–491 (2016).

158. Monkman, S. & Shao, Y. Assessing the Carbonation Behavior of Cementitious Materials. *J. Mater. Civ. Eng.* **18,** 768–776 (2006).

159. Reddy, K. J. *et al.* Simultaneous capture and mineralization of coal combustion flue gas carbon dioxide (CO_2). *Energy Procedia* **4,** 1574–1583 (2011).

160. Bijl, D. L., Bogaart, P. W., Kram, T., de Vries, B. J. M. & van Vuuren, D. P. Long-term water demand for electricity, industry and households. *Environ. Sci. Policy* **55,** 75–86 (2016).

161. Metz, B., Davidson, O., de Coninck, H., Loos, M. & Meyer, L. *Carbon dioxide capture and storage*. (2012).

162. McCutcheon, J. L. & McGinnis, R. L. The Ammonia-Carbon Dioxide Forward Osmosis Desalination Process. *Water Cond. Purif.* 1–4 (2006).

163. Rongved, P. I. Sea water desalination using CO_2 gas from combustion exhaust. **1,** 0–4 (2001).

164. Williams, V. C. Hydrate forming saline water conversion process. (1964).

165. Max, M. D. Desalination and Concomitant Carbon Dioxide Capture Yielding Liquid Carbon Dioxide. **1,** (2002).

166. Spencer, D. F. & North, W. J. Method for the production of carbon dioxide hydrates. 0–4 (1996).

167. Dawoud, M. a & Mulla, M. M. Al. Environmental Impacts of Seawater Desalination : Arabian Gulf Case Study. *Int. J. Environ. Sustain.* **1,** 22–37 (2012).

168. Latteman, S. *Development of an environmental impact assessment and decision support system for seawater desalination plants*. (2010).

169. Dindi, A., Quang, D. V. & Abu-Zahra, M. R. M. Simultaneous carbon dioxide capture and utilization using thermal desalination reject brine. *Appl. Energy* **154,** 298–308 (2015).

170. DOE/NETL-2012/1588. Novel CO2 Utilization Concepts: Working Paper. *US Dep. Energy, Off. Foss. Energy* 1–50 (2013). doi:10.1016/j.enconman.2007.12.029

171. Buonomenna, M. G. & Golemme, G. *Advanced Materials for Membrane Preparation*. (2012). at Bentham eBooks

172. Chen, H., Zhang, H. & Yan, Y. Catalytic combustion of volatile organic compounds over a structured zeolite membrane reactor. *Ind. Eng. Chem. Res.* **52,** 12819–12826 (2013).

173. Avila, A. M., Yu, Z., Fazli, S., Sawada, J. a. & Kuznicki, S. M. Hydrogen-selective natural mordenite in a membrane reactor for ethane dehydrogenation. *Microporous Mesoporous Mater.* **190,** 301–308 (2014).

174. Hufton, J. R., Mayorga, S. & Sircar, S. Sorption-enhanced reaction process for hydrogen production. *AIChE J.* **45,** 248–256 (1999).

175. Carvill, B. T., Hufton, J. R., Anand, M. & Sircar, S. Sorption-enhanced reaction process. *AIChE J.* **42,** 2765–2772 (1996).

176. Jang, H. M., Lee, K. B., Caram, H. S. & Sircar, S. High-purity hydrogen production through sorption enhanced water gas shift reaction using K_2CO_3-promoted hydrotalcite. *Chem. Eng. Sci.* **73,** 431–438 (2012).

177. Selow, E. R. Van, Cobden, P. D., Verbraeken, P. a, Hufton, J. R. & Brink, R. W. Van Den. Carbon Capture by Sorption-Enhanced Water - Gas Shift Reaction Process using Hydrotalcite-Based Material. *Ind. Eng. Chem. Res.* **48,** 4184–4193 (2009).

178. Stevens, R. W., Shamsi, A., Carpenter, S. & Siriwardane, R. Sorption-enhanced water gas shift reaction by sodium-promoted calcium oxides. *Fuel* **89,** 1280–1286 (2010).

179. Duyar, M. S., Farrauto, R. J., Castaldi, M. J. & Yegulalp, T. M. In Situ CO_2 Capture Using CaO/γ -Al_2O_3 Washcoated Monoliths for Sorption Enhanced Water Gas Shift Reaction. *Ind. Eng. Chem. Res.* **53,** 1064–1072 (2014).

180. Gruene, P., Belova, A. G., Yegulalp, T. M., Farrauto, R. J. & Castaldi, M. J. Dispersed Calcium Oxide as a Reversible and Efficient CO_2-Sorbent at Intermediate Temperatures. *Ind. Eng. Chem. Res.* **50,** 4042–4049 (2011).

181. Song, C. & Pan, W. Tri-reforming of methane: A novel concept for catalytic production of industrially useful synthesis gas with desired H_2/CO ratios. *Catal. Today* **98,** 463–484 (2004).

182. Song, C. Global challenges and strategies for control, conversion and utilization of CO_2 for sustainable development involving energy, catalysis, adsorption and chemical processing. *Catal. Today* **115,** 2–32 (2006).

183. Minutillo, M. & Perna, a. A novel approach for treatment of CO_2 from fossil fired power plants, Part A: The integrated systems ITRPP. *Int. J. Hydrogen Energy* **34,** 4014–4020 (2009).

184. Farrauto, R. J., Duyar, M. S. & Arellano, M. a. Dual function materials for CO_2 capture and conversion using renewable H2. *Appl. Catal. B Environ.* **168,** 370–376 (2015).

185. Duyar, M. S., Wang, S., Arellano-Treviño, M. A. & Farrauto, R. J. CO_2 utilization with a novel dual function material (DFM) for capture and catalytic conversion to synthetic natural gas: An update. *J. CO_2 Util.* **15,** 65–71 (2016).

186. Zheng, Q., Farrauto, R. & Chau Nguyen, A. Adsorption and Methanation of Flue Gas CO_2 with Dual Functional Catalytic Materials: A Parametric Study. *Ind. Eng. Chem. Res.* **55,** 6768–6776 (2016).

187. Im, S. I. & Lee, K. B. Novel Sorption-Enhanced Methanation with Simultaneous CO_2 Removal for the Production of Synthetic Natural Gas. *Ind. Eng. Chem. Res.* **55,** 9244–9255 (2016).

188. Lao, D. B., Galan, B. R., Linehan, J. C. & Heldebrant, D. J. The steps of activating a prospective CO2 hydrogenation catalyst with combined CO_2 capture and reduction. *Green Chem.* **18,** 4871–4874 (2016).

II. DEVELOPMENT OF POTASSIUM- AND SODIUM-PROMOTED CAO ADSORBENTS FOR CO_2 CAPTURE AT HIGH TEMPERATURES

Ahmed Al-Mamoori, Harshul Thakkar, Xin Li, Ali A. Rownaghi, Fateme Rezaei*

Department of Chemical & Biochemical Engineering, Missouri University of Science and Technology, 1101 N State Street, Rolla, MO, 65409, United States

ABSTRACT

Development of highly efficient adsorbents for high temperature CO_2 capture process is crucial for large scale implementation of this technology. In this work, development of novel potassium- and sodium-promoted CaO adsorbents (K-Ca and Na-Ca) is discussed and their CO_2 capture performance at high temperatures is presented. A series of K-Ca and Na-Ca adsorbents with various K/Ca or Na/Ca molar ratios were developed and tested for CO_2 capture at high temperatures ranging from 300 to 400 °C. The structural, chemical, and morphological characteristics of the double salts were systematically evaluated before and after exposure to CO_2. Our results indicated that CO_2 capacity is largely influenced by both K or Na concentration and adsorption temperature. A maximum capacity of 3.8 and 3.2 mmol/g were obtained for K-Ca and Na-Ca double salts, respectively, at 375 °C and 1 bar. Further investigation of the effect of temperature revealed that the window temperature for operation ranges from 300 to 650 °C while beyond 650 °C, the double salts start to decompose and lose capacity. Moreover, it was found that both adsorption kinetics and capacity improve with temperature, with CO_2 uptake reaching a maximum 10.7 mmol/g at 650 °C over K-Ca double salt. This study

represents alkali metal-promoted CaO adsorbents as potential high-temperature adsorbents with similar performance to their MgO-based analogues.

1. INTRODUCTION

CO_2 emissions are continuously increasing due to ever increasing energy demand and population growth. Climate change that has recently affected various places around the world is a result of such excessive emissions which necessitates extensive effort to alleviate the greenhouse gas emissions. One of the most promising technologies to mitigate CO_2 emissions is adsorption due to its easy installation, relatively low cost, and low required energy, in comparison to the benchmark amine scrubbing process.[1–3] Recently, CO_2 adsorption at high temperature has attracted a great deal of attention since it offers various opportunities in processes such as sorption enhanced reaction (SER) and integrated gasification combined cycle (IGCC).[4,5] Additionally, there is no need to cool down flue gas to the ambient temperature and thus lose a lot of energy.[6] Furthermore, development of high temperature adsorbents for simultaneous CO_2 capture and conversion process in which CO_2 is first separated from flue gas and then is converted to commodity chemicals or fuels has recently gained interest among researchers worldwide.[1,7] However, selecting a suitable adsorbent is still challenging due to the high capacity, stability, selectivity, and fast adsorption/desorption kinetics requirements.[8] In addition to these criteria, the adsorbents are required to be practical, inexpensive, and regenerable.

To this end, there has been a wide variety of porous materials developed for CO_2 capture at both low and high temperatures.[9–14] Among solid adsorbents investigated so far,

only a few materials such as calcium oxide (CaO), hydrotalcite (HT), calcium chabazite (CHA), alumina, and a few mixed-metal oxides have demonstrated favorable characteristics at elevated temperatures.[8,15–18] In large-scale CO_2 capture applications, CaO is advantageous compared to other adsorbents on account of higher capture capacity (~17.9 mmol/g at above 600 °C), low cost, and wide availability of precursors such as limestones or dolomites,[15,19–21] however, high temperature regeneration (i.e., above 800 °C) and low stability due to sintering could outweigh these benefits. Additionally, slow sorption kinetics due to the formation of $CaCO_3$ which results in limited CO_2 diffusion is another challenge associated with the practical use of CaO-based adsorbents.[17] The HTs, also known as layered double hydroxides (LDH), are composed of positively charged brucite-like layers with trivalent cations partially substituting divalent cations. This class of adsorbents shows good stability in the presence of water vapor and enhanced capacity when impregnated with alkali metals.[19,22–25] Despite these noticeable advantages, their relatively low capacity is still challenging for industrial applications.[22] Recently, Kim et al.[26] reported a high CO_2 uptake (ca. 9.27 mmol/g) over HT at 240 °C and 1 bar, but the capacity dropped dramatically to below 3.0 mmol/g after 16 cycles. CHA consists of double-six ring (D6R) units arranged in layers that are linked together by tilted 4-membered rings and is capable of yielding high CO_2 selectivity due to the molecular sieving effect.[8,27,28] To enhance CO_2 capacity of CHA, ion exchange can be done with Na, Ca, K, Mg, Li, and Ba ions.[28,29]

Development of more efficient adsorbents is needed for CO_2 capture at high temperatures (i.e., 300-400 °C). Recent works have demonstrated the potential of double salts for effectively capturing CO_2 with reasonable stability.[18,26,30–33] Harada and Hatton[30] prepared colloidal nanoclusters of MgO coated with Li, Na, and K nitrates/nitrites with

various salts loadings and showed that both CO_2 uptake and adsorbent regenerability can be enhanced by introduction of nitrite salts to the coating layer of MgO particles through the formation of magnesium nitro or nitrate species. In another investigation, Lee et al.[18] studied the effect of pH on double salt potassium based magnesium K-Mg by using different precursors for potassium (KOH/K_2CO_3). The authors showed that CO_2 capacity improves upon increasing pH of the potassium precursor. They also reported that K-Mg double salt has a rapid adsorption/desorption kinetics. Lee et al.[33] prepared a Na-Mg double salt by precipitation method and investigated for CO_2 capture. The authors reported a relatively high CO_2 uptake (3.48 mmol/g), good stability, and quick sorption kinetics at 375 °C and 1 bar.

Most of double salts adsorbents investigated so far are based on MgO coated or doped with molten salts of alkali earth metals such as lithium, sodium or potassium. Most recently, Huang et al.[35] reported development and evaluation of sorption performance of a series of alkali carbonate molten salt-coated CaO adsorbents. On the basis of their experimental results, the authors concluded that $(Li\text{-}K)_2CO_3$ molten salt coating not only enhances CO_2 uptake, but also facilitates the CO_2 desorption from CaO. They correlated this uptake enhancement to the role of coated molten salts in preventing the formation of a rigid $CaCO_3$ layer on the surface of CaO particles and providing a continuous delivery of CO_3^{2-} to promote CO_2 capture. Generally, MgO-based adsorbents exhibit much lower capacity at higher temperatures (> 400 °C) than CaO-based double salts, thus they are suitable for use at milder temperatures. On the other hand, although CaO-based adsorbents exhibit improved uptake with increasing temperature, they suffer from sintering during regeneration, as stated above, displaying reduction in their cyclic capacity. Significant

efforts have been put forth to overcome this issue including the use of a porous support for CaO particles, the use of other naturally occurring precursors instead of limestone, or obtaining CaO from sintering-resistant precursors, among others.[36,37]

Motivated by the search for a better high-temperature CO_2 adsorbent and the need for an active adsorbent as a catalyst support that could be used in simultaneous CO_2 capture and conversion process, the objective of this study was to develop practical adsorbents that could be used in hybrid CO_2 capture (from flue gas) and conversion process at high temperatures (i.e., 300-400 °C). More specifically, this work focused on development of a series of double salts such as potassium-promoted calcium (K-Ca) and sodium-promoted calcium (Na-Ca) adsorbents for CO_2 capture that could later be used for development of hybrid adsorbent-catalyst materials.

2. EXPERIMENTAL SECTION

2.1. PREPARATION OF DOUBLE SALTS

2.1.1. Double Salts K-Ca. Potassium-promoted calcium oxide adsorbents were prepared according to the procedure described in the literature.[18] Briefly, a desired amount of potassium carbonate (K_2CO_3) was added to appropriate volume of distilled water. Potassium hydroxide (KOH) dissolved in distilled water was then added to the K_2CO_3 solution. In the next step, the new solution was added drop-wise to the calcium nitrate tetrahydrate ($Ca(NO_3)_2.4H_2O$) dissolved in distilled water. The final solution was stirred for 1 h at 700 rpm and allowed to settle down. After that, the precipitated particles were filtered using vacuum filtration, then dried in the oven over night at 120 °C, and finally

calcined at 700 °C for 5 h with ramping step of 10 °C/min. The molar ratios of the precursors are presented in Table 1. The samples were labeled as K-Ca-1, K-Ca-2, and K-Ca-3.

Table 1. K-Ca double salts composition.

Name	K/Ca mol ratio	K_2CO_3 weight (g)	KOH weight (g)	$Ca(NO_3)_2.4H_2O$ weight (g)
K-Ca-1	3.3	12.09	0.79	41.33
K-Ca-2	6.7	24.19	1.57	41.33
K-Ca-3	10	36.28	2.36	41.33

2.1.2. Double Salts Na-Ca. Sodium-promoted calcium oxide adsorbents were synthesized according to a previously reported procedure.[33] Briefly, 8.1 g of $Ca(NO_3)_2.4H_2O$ was dissolved in 100 mL distilled water and then desired amounts of sodium carbonate (Na_2CO_3) were added gradually to the solution and stirred for 1 h at 500 rpm. In the next step, the solution was allowed to precipitate and then dried at 110 °C overnight before calcination at 700 °C for 3 h with ramping step of 10 °C/min. The samples were labeled as Na-Ca-1, Na-Ca-2, and Na-Ca-3 with the compositions shown in Table 2.

2.2. CHARACTERIZATION OF DOUBLE SALTS

Phase analysis of adsorbents before and after CO_2 exposure was performed by XRD experiments using PANalytical X'Pert Multipurpose X-ray Diffractometer with scan step size of 0.02 °/step at the rate of 147.4 s/step. Surface area and total pore volume of the adsorbents were estimated from N_2 physisorption data obtained by measurements

performed on a Micromeritics 3Flex gas analyzer at 77 K. FT-IR experiments were carried out on a Nicolet Nexus 470 optical bench.

Table 2. Na-Ca double salts composition.

Name	Na/Ca mol ratio (%)	Na_2CO_3 weight (g)	$Ca(NO_3)_2.4H_2O$ weight (g)
Na-Ca-1	2.8	10	8.1
Na-Ca-2	4.2	15	8.1
Na-Ca-3	5.6	20	8.1

For FT-IR measurements, around 1 mg of sample was mixed with 100 mg of KBr and pressed to pellets for analysis. Hitachi S4700 Field Emission Scanning Electron Microscopy (SEM) was used to evaluate the structural morphology of double salt adsorbents before and after CO_2 adsorption.

2.3. CO_2 ADSORPTION ISOTHERM MEASUREMENTS

CO_2 adsorption isotherms were collected on the 3Flex at different temperatures. For the isotherm measurements, the samples were first degassed at 450 °C for 2 h under vacuum. The isotherms were collected at 300, 350, and 375 °C. In addition, TGA (Q500, TA Instruments) was utilized to analyze CO_2 adsorption over time and to perform cyclic measurements. For the TGA measurements, the temperature was first ramped from ambient temperature to 450 °C at the rate of 10 °C/min under N_2 flow to degas the samples before exposure to a gas mixture containing 10% CO_2 in N_2 at a desired adsorption temperature.

3. RESULTS AND DISCUSSION

3.1. CHARACTERIZATION AND ADSORPTION PERFORMANCE OF DOUBLE SALTS

Figure 1a-b shows the comparison of XRD spectra for three K-Ca and three Na-Ca double salts. It is clear from Figure 1a that the main components of K-Ca adsorbents are CaO, K_2CO_3, $CaCO_3$, and $Ca(OH)_2$ whereas the XRD spectra in Figure 1b indicate that the main components of Na-Ca adsorbents are CaO, Na_2CO_3, $NaNO_3$, and $Ca(OH)_2$. It should also be noted that by increasing the K/Ca molar ratio, the intensity of K_2CO_3 peaks increased while similarly, higher Na/Ca molar ratio resulted in higher intensity of $NaNO_3$ and Na_2CO_3 characteristic peaks. The components $CaCO_3$ and $NaNO_3$ were formed after the thermal treatment (calcination) of the samples at 700 °C. Also for both cases, small amount of $Ca(OH_3)_2$ was formed at higher K/Ca or Na/Ca molar ratio. These XRD results confirm the successful formation of K-Ca and Na-Ca double salts. The characteristic peaks of bare (unpromoted) CaO can also be observed in Figure S1 (Supporting Information).

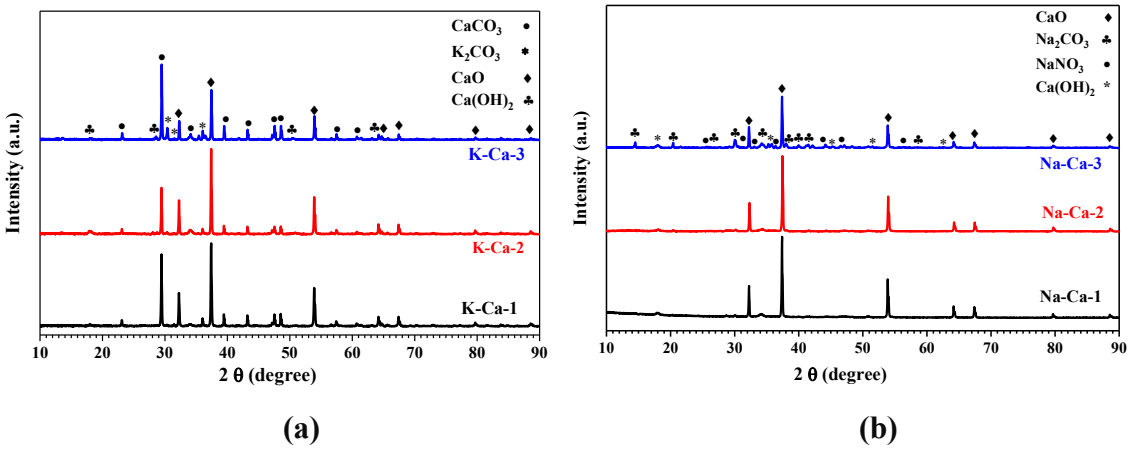

Figure 1. XRD patterns of (a) K-Ca double salts and (b) Na-Ca double salts.

Figure 2a-b shows N_2 physisorption profiles of the K-Ca and Na-Ca double salts. These physisorption profiles show noticeable N_2 uptake at partial pressures greater than 0.6 ($P/P_0 > 0.6$), which indicates the presence of mesopores in the structure of the samples. Furthermore, the hysteresis loop confirms the presence of large void spaces between the crystals in double salts. For K-Ca materials, increasing the K concentration resulted in a decrease in N_2 uptake, whereas for Na-Ca adsorbents, the N_2 uptake first exhibited a sharp increase followed by a drop upon increasing the concentration of Na. These N_2 physisorption isotherms obtained for K-Ca double salts are similar to the previously reported results for K-Mg materials which exhibited the decrease in porosity with increasing the K/Mg concentration ratio.[38,39]

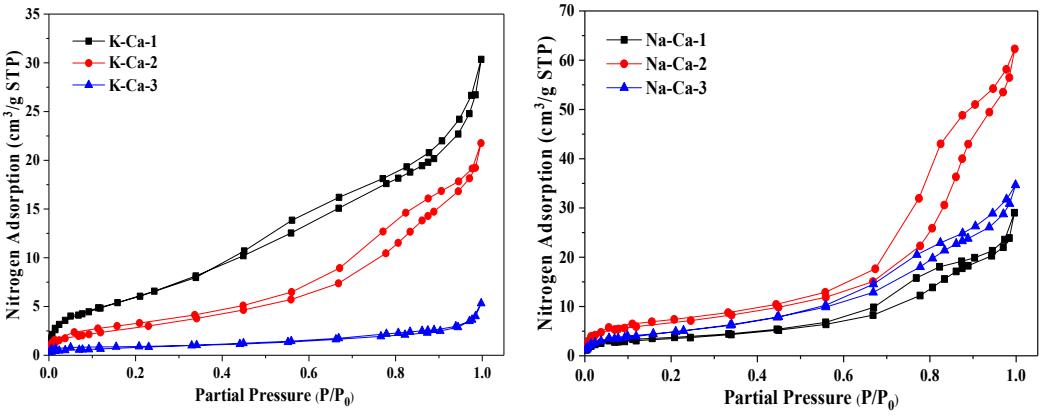

Figure 2. N_2 physisorption isotherms for (a) K-Ca and (b) Na-Ca double salts.

Table 3 shows the BET surface area (m^2/g), total pore volume (cm^3/g) of the materials estimated at a partial pressure of 0.99, and pore size values obtained from N_2 physisorption isotherms. It can be noted that upon increasing the amount of K, the surface area and pore volume decreased from respectively, 24 m^2/g and 0.04 cm^3/g for K-Ca-1 to

3 m^2/g and 0.01 cm^3/g for K-Ca-3. On the contrary, upon increasing Na content, both surface area and pore volume increased respectively, from 12 m^2/g and 0.04 cm^3/g for Na-Ca-1 to 18 m^2/g and 0.05 cm^3/g for Na-Ca-3. K-Ca-2 and Na-Ca-2 exhibited respectively, a surface area of 11 and 24 m^2/g, a pore volume of 0.03 and 0.09 cm^3/g, and an average pore size of 7 and 9 nm. Moreover, for bare CaO, a BET surface area of 312 m^2/g and a pore volume of 0.32 cm^3/g were obtained and as it is clear from the data in Table 3, upon CaO promotion with K and Na, both surface area and pore volume decreased drastically compared to unpromoted CaO. Similar behavior was reported for MgO-based double salts.[38]

Table 3. N_2 physisorption data for K-Ca-2 and Na-Ca-2 adsorbents.

Adsorbent	**S_{BET}** (m^2/g)	**Pore volume** (cm^3/g)	**Pore size** (nm)
K-Ca-1	24	0.04	5
K-Ca-2	11	0.03	7
K-Ca-3	3	0.01	10
Na-Ca-1	12	0.04	8
Na-Ca-2	24	0.09	9
Na-Ca-3	18	0.05	7

The CO_2 adsorption isotherms obtained at 375 °C for three K-Ca and three Na-Ca double salts are presented in Figure 3a-b. In both cases, the double salt with the lowest amount of K or Na (K-Ca-1 and Na-CA-1) exhibited the lowest CO_2 uptake. Also, it can

be observed that by increasing the K and Na composition, the CO_2 adsorption increased first (for K-Ca-2 and Na-Ca-2) and then experienced a decreasing trend upon further increase of the K and Na contents (for K-Ca-3 and Na-Ca-3). These results are in agreement with Zhang et al.[32] Moreover, Huang et al.[35] observed the same behavior and correlated the strong dependence of CO_2 uptake on the molar ratio of the $(Li\text{-}K)_2CO_3$/CaO salts to the dependency of melting points of $(Li\text{-}K)_2CO_3$ on different Li/K ratios. Similarly, we can argue here that for intermediate molar ratios (i.e., K-Ca-2 and Na-Ca-2), the melting point of K_2CO_3 or Na_2CO_3 was likely lower than that of samples with other molar ratios. According to Harada et al.,[40] for double salt adsorbents, CO_2 uptake can only be promoted at adsorption temperatures above the melting points of the molten salts coating the particles. This suggests that low and high K/Na content samples for each class (1 and 3) have melting points above 375 °C. It should also be mentioned here that It should be mentioned here that as a control experiment, we measured the CO_2 uptake over bare (unpromoted) CaO and as Figure S2 (Supporting Information) shows, the adsorption capacity was very low compared with the K- and Na-promoted CaO, reaching 0.4 mmol/g, as also shown by other researchers.[35]

Moreover, in both cases a general trend could be observed where the uptake increases sharply at lower pressures up to 0.02 bar followed by a gradual increase over higher pressures until 1 bar. For K-Ca-2, the CO_2 capacity reached 3.8 mmol/g and for Na-Ca-2, the capacity was found to be 3.2 mmol/g at 1 bar. Lee et al.[33] reported a CO_2 uptake of 3.48 mmol/g over Na-Mg double salt at the same temperature and pressure. For the rest of analysis, we picked K-Ca-2 and Na-Ca-2 double salts that exhibited the highest adsorption uptake among their adsorbent counterparts.

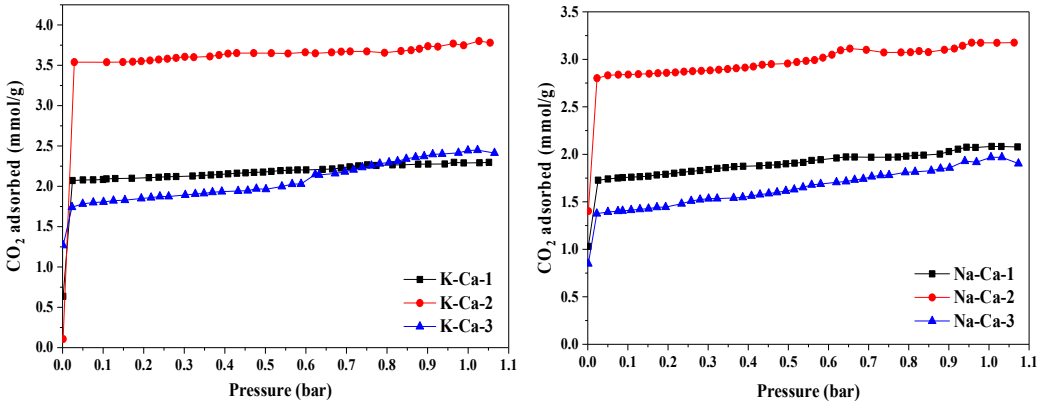

(a) **(b)**

Figure 3. CO_2 adsorption isotherms for (a) K-Ca double salts and (b) Na-Ca double salts obtained at 375 °C.

3.2. ADSORPTION PERFORMANCE OF K-CA-2 AND NA-CA-2

The effect of adsorption temperature on CO_2 uptake over K-Ca-2 and Na-Ca-2 double salts is demonstrated in Figure 4a-b. It can be seen that as the temperature increased from 300 to 375 °C, the uptake increased dramatically from 0.6 to 3.8 mmol/g for K-Ca-2 and from 1.1 to 3.2 mmol/g for Na-Ca-2 at 1 bar. The higher uptake at higher temperatures could be attributed to the formation of more carbonates that contribute more toward the adsorption of CO_2 molecules. Huang et al.[35] reported the same behavior for Li-K-promoted CaO, for which the capacity increased from 4.9 to 10.6 mmol/g upon temperature rise from 400 to 700 °C. For Mg-based materials, although similar increasing trend has been reported,[18] the operating window is narrower and the uptake starts to decrease at temperatures above 400 °C.

Comparing the XRD patterns of the K-Ca-2 adsorbent before and after CO_2 adsorption at 375 °C in Figure 5a, it is apparent that no additional peaks were appeared after CO_2 capture, however, as can be clearly noted, the intensity of the calcium oxide

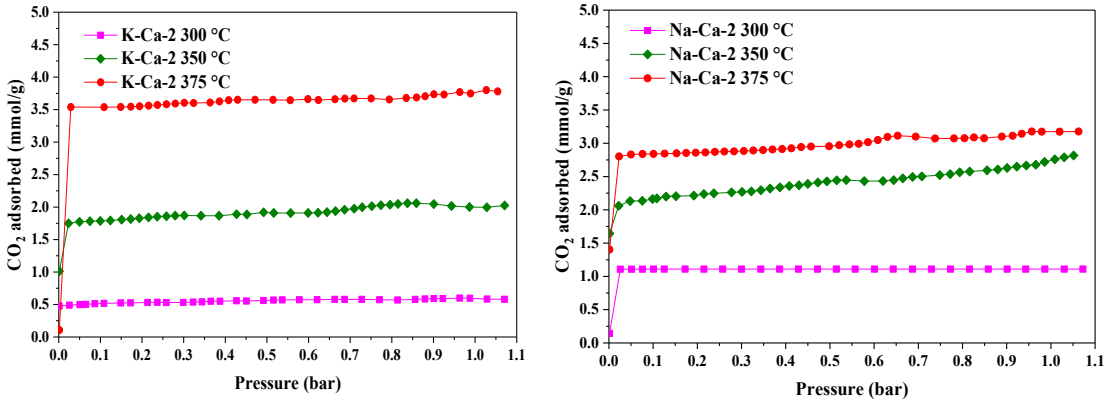

(a) **(b)**

Figure 4. CO_2 adsorption isotherms for (a) K-Ca double salts and (b) Na-Ca double salts obtained at 375 °C.

(CaO) peaks decreased because of the reaction of calcium oxide with CO_2 while the intensity of the peaks corresponding to calcium hydroxide ($Ca(OH)_2$) decreased. Further, potassium calcium carbonate ($K_2Ca(CO_3)_2$) phase formed after CO_2 exposure. For Na-Ca-2, investigating the XRD spectra presented in Figure 5b, it was found that sodium calcium carbonate ($Na_2Ca(CO_3)_2$) phase formed upon CO_2 adsorption while like K-Ca-2, the remaining CaO peaks were weak. In addition, new peaks associated with $CaCO_3$ were appeared confirming that the molten salts facilitate the formation of $CaCO_3$ during CO_2 adsorption. This however was not the case for K-Ca-2 mainly because the $CaCO_3$ phase was present in the fresh material. The formation of $K_2Ca(CO_3)_2$ and $Na_2Ca(CO_3)_2$ is according to the following reactions on the K-Ca-2 and Na-Ca-2 double salts, respectively, as suggested by Lee et al.[33] for MgO- based materials:

$$K_2CO_3 + CaO + CO_2 \leftrightarrow K_2Ca(CO_3)_2$$

$$Na_2CO_3 + CaO + CO_2 \leftrightarrow Na_2Ca(CO_3)_2$$

The XRD spectra of unpromoted CaO before and after CO_2 adsorption are also presented in Figure S1 (Supporting Information). The appearance of several peaks related to $CaCO_3$ and $Ca(OH)_2$ was noticeable after CO_2 adsorption while the intensity of CaO characteristic peaks decreased in a similar fashion to the promoted samples.

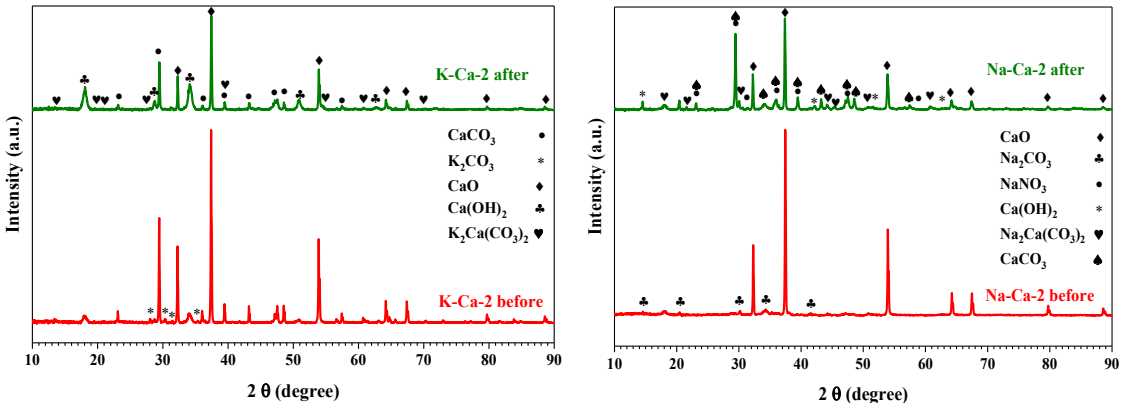

Figure 5. XRD patterns of (a) K-Ca-2 and (b) Na-Ca-2 before and after CO_2 exposure at 375 °C.

To probe changes to the chemical properties of the double salts, the FT-IR spectra of the candidate double salts before and after CO_2 adsorption were compared. As Figure 6a-b demonstrates, both materials retained their chemical structure and displayed similar characteristic peaks before and after exposure to CO_2. The only noticeable change is the intensity of the characteristic peaks which was much stronger after CO_2 adsorption confirming the formation of more $CaCO_3$ on K- and Na-promoted double salts. Comparing the peak intensities of the K-Ca and Na-Ca after CO_2 adsorption, it follows that the increase was more pronounced for Na-Ca-2 than for K-Ca-2, despite its lower uptake capacity. This could be explained by the fact the fresh K-Ca-2 contains $CaCO_3$ in its structure, as opposed

to Na-Ca-2 (as confirmed by XRD results), hence after CO_2 adsorption, the intensity of the bands corresponding to the formation of carbonate is higher for Na-Ca-2.

The FT-IR spectra of K-Ca-2 and Na-Ca-2 after CO_2 capture show clear peaks related to $CaCO_3$ at 713, 874, 1484, 1797, and 2518 cm^{-1}. The presence of these $CaCO_3$ characteristic peaks are also noticeable in the spectrum of bare CaO after CO_2 adsorption (Figure S3, Supporting Information). The bands at 1072 and 858 cm^{-1} represent symmetric stretching and out-of-plane bending modes of the carbonate ion, respectively,[41] whereas the peak at 713 cm^{-1} represents in-plane bending mode of the carbonate ion.[42] Moreover, the broad peak at 1484 cm^{-1} corresponds to stretching vibrations of C-O bonds, whereas the peaks at 1798 and 3641 cm^{-1} are assigned to C=O and O-H bonds, respectively.[42]

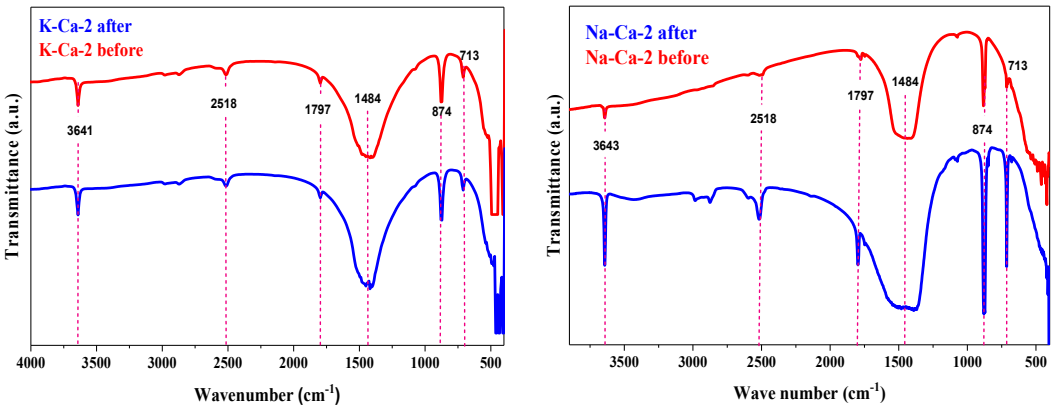

(a) **(b)**

Figure 6. FT-IR spectra of (a) K-Ca-2 and (b) Na-Ca-2 before and after CO_2 exposure at 375 °C.

The SEM images shown in Figure 7a-d reveal the morphology of the adsorbents before and after CO_2 exposure to CO_2 at 375 °C. For fresh materials, a relatively dense structure with less degree of agglomeration was found for both materials. Also, the particle

size appeared to be uniform in both cases ranging from 100 to 200 nm. After CO_2 exposure, the materials retained their porous structure and the particles were still well dispersed, although relatively large aggregates formed in the form of agglomerated clusters with small cracks on their external surface, as can be seen from Figures 7b and 7d.

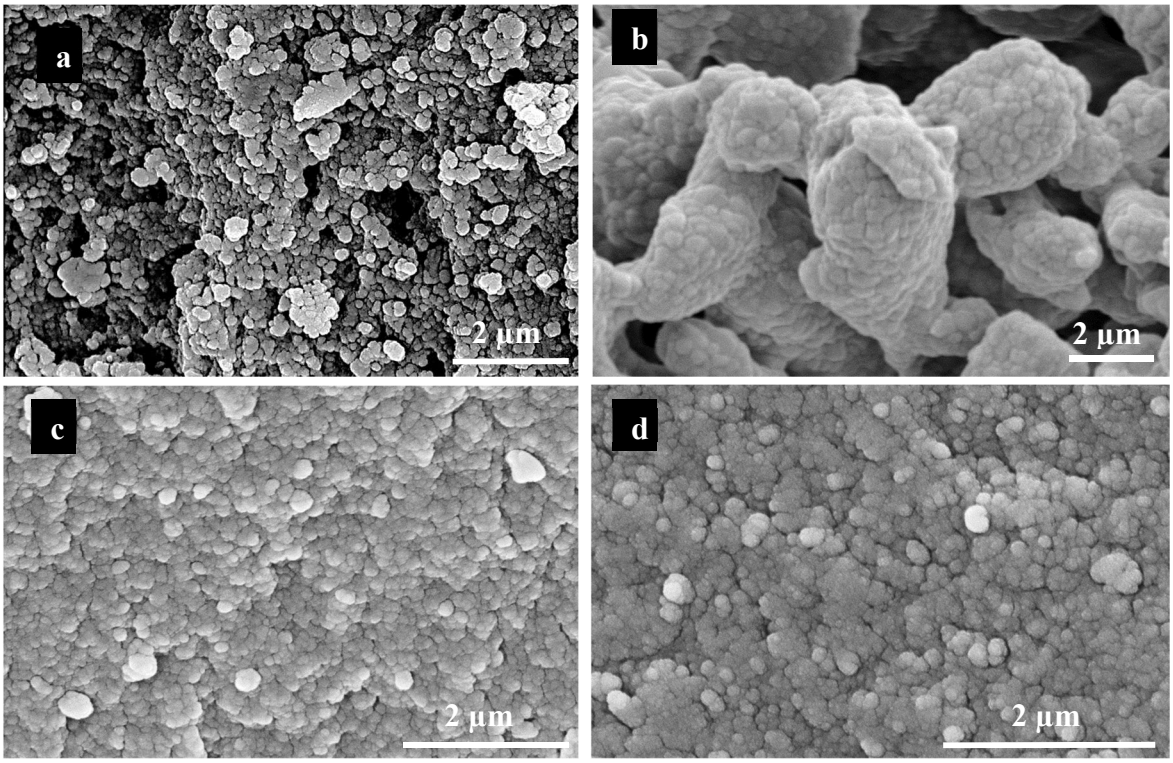

Figure 7. SEM images of (a-b) K-Ca-2 and (c-d) Na-Ca-2 before and after CO_2 adsorption at 375 °C.

To identify the operating window for adsorption of CO_2 over K-Ca and Na-Ca double salts, the mass degradation experiments were performed under the flow of N_2 and 10% CO_2/N_2 (as simulated flue gas) using TGA. Figure 8a-b shows the weight change of K-Ca-2 and Na-Ca-2 over the temperature range of 100 to 800 °C. Under N_2 flow, a significant weight loss (~22.5% for K-Ca and 32% for Na-Ca) was observed at

temperatures above 600 °C, whereas under 10% CO_2/N_2 gas flow, a CO_2 adsorption region between 300-700 °C was observed, as characterized by the increase in the weight (~12 wt% for K-Ca and 20 wt% for Na-Ca), suggesting the window operation for CO_2 capture. Above 700 °C, both K-Ca and Na-Ca adsorbents started to lose their capacity as a result of both CO_2 desorption and materials degradation. Interestingly, Na-Ca-2 retained 82% of its original weight above 700 °C while K-Ca-2 showed 22.5% weight loss under 10% CO_2/N_2 flow, similar to its weight loss under pure N_2.

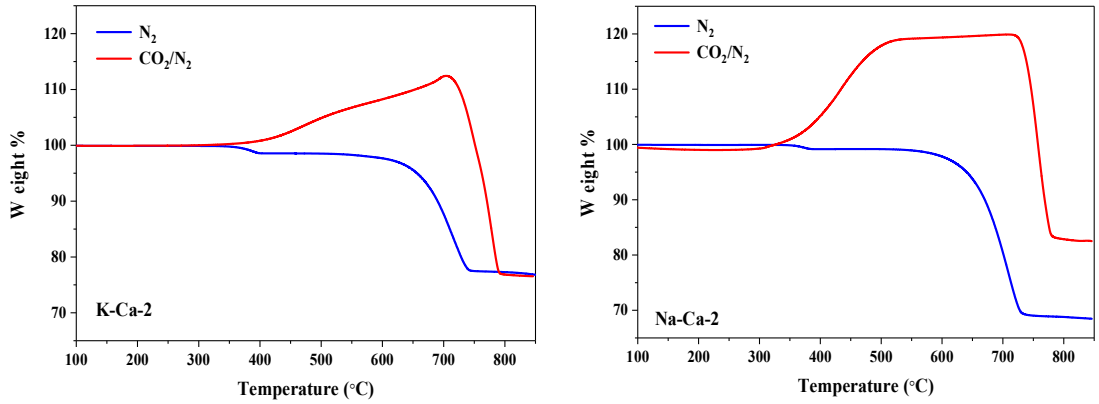

Figure 8. K-Ca-2 weight change of (a) K-Ca-2 and (b) Na-Ca-2 with increasing temperature under N_2 and CO_2/N_2 gas flow.

The effect of adsorption temperature on adsorption kinetics and CO_2 capacity of K-Ca-2 and Na-Ca-2 adsorbents is illustrated in Figure 9a-b. It can be noticed that the capacity increased as the temperature was raised from 300 to 650 °C. However, further increase to 700 °C resulted in dramatic capacity loss in both cases, mainly due to the decomposition of the materials, as discussed earlier. The maximum obtained CO_2 uptakes were found to be 10.7 and 9.5 mmol/g for K-Ca-2 and Na-Ca-2 respectively, which were obtained at 650

°C after 300 min adsorption time. Notably, at higher temperatures, materials exhibited faster sorption kinetics by displaying a sharp increase in CO_2 uptake at the beginning of the adsorption. For instance, at 650 °C, K-Ca-2 and Na-Ca-2 achieved ~43% of their equilibrium capacities in the first 10 min of adsorption. A rapid initial uptake followed by slow adsorption over a longer timescale was also reported previously for K-Mg double salts.[18]

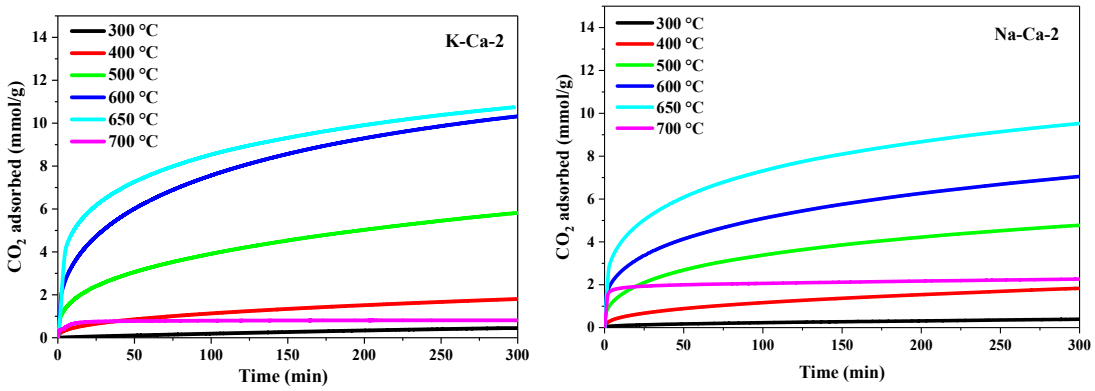

(a) **(b)**

Figure 9. CO_2 uptake over (a) K-Ca-2 and (b) Na-Ca-2 double salts as a function of temperature.

To further assess the stability of the K-Ca and Na-Ca double sites, cyclic adsorption measurements were performed using 10% CO_2/N_2 at 375 °C. Figure 10a-b shows the CO_2 capacities over 10 cycles for K-Ca-2 and Na-Ca-2 adsorbents. It is clear from these profiles that both adsorbents experienced a capacity loss over consecutive cycles, however, the loss was more pronounced for Na-Ca double salt. The K-Ca-2 double salt retained 85% of its initial capacity whereas, Na-Ca-2 experienced 37% capacity loss after the 10^{th} cycle. The loss in CO_2 capture capacity and rapid deactivation of CaO sorbents over multiple cycles

is well-known and has been correlated to the sintering of CaO particles under high regeneration temperature.[43,44] For instance, Dean et al.[43] reported a ~ 40% capacity loss after 50 CO_2 capture-release cycles over Cao adsorbent.[43] Our results indicated that CaO promotion with K and Na positively affects the stability of CaO sorbents, especially in the case of K-Ca. Nonetheless, a much lower drop in capacity was reported for Na-Mg by Lee et al.[33] (only ~ 1% after 7th cycle) in comparison to Na-Ca (Figure 10b). Such higher capacity loss may be due to the sintering of CaO particles. Another reason could be due to rearrangement of the molten phase of Na_2CO_3 in the adsorbent structure during the first cycle. This however requires more investigation to fully understand the cause for deteriorated cyclic capacity of Na-promoted CaO adsorbents.

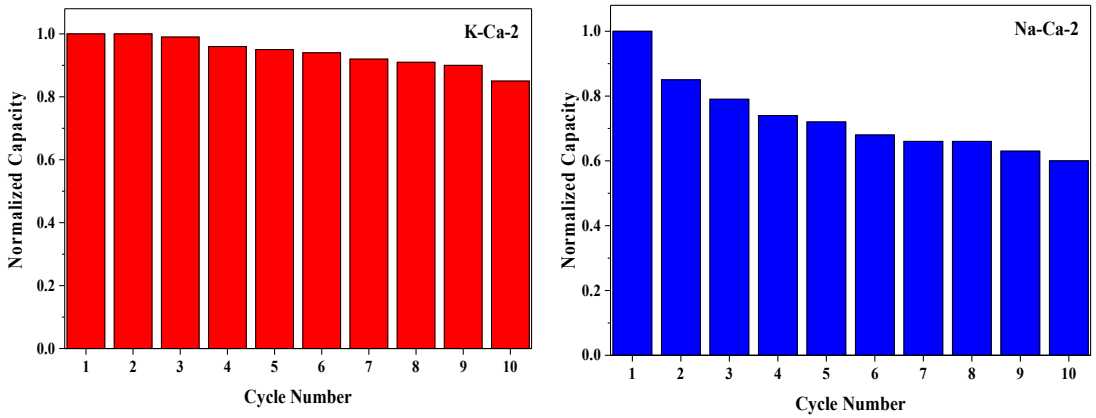

Figure 10. Normalized capacity of (a) K-Ca-2 and (b) Na-Ca-2 over 10 cycles of adsorption and desorption at 375 °C using 10% CO_2/N_2.

Moreover, unlike K-Ca, a dramatic CO_2 uptake reduction (~ 40%) was reported for K-Mg after 10 adsorption/desorption cycles and the authors attributed this drop to the rearrangement of the molten phase of KNO_3 during the first cycle.[18]

4. CONCLUSIONS

This work illustrates development and evaluation of a series of inexpensive CaO-based adsorbents promoted by potassium and sodium carbonate salts for use in high temperature CO_2 capture process. The physical, chemical, and morphological properties of the adsorbents were assessed systematically and their CO_2 capture performance was evaluated taking into account the effects of K or Na concentration and adsorption temperature. It was shown that the K- and Na-prompted CaO adsorbents with optimum K/Ca and Na/Ca molar ratios exhibit relatively high capacity, fast kinetics, and good stability (in the case of K-Ca) at high temperatures. Our results highlighted the effectiveness of K-Ca and Na-Ca double salts in adsorption of CO_2 at temperatures above 300 °C. These materials could be used as suitable catalyst supports in development of hybrid adsorbent-catalyst materials for use in simultaneous capture-conversion process. In that regard, the future task should focus on improving their relatively low surface area, which could be achieved by supporting them on a high surface area support such as alumina or silica.

ACKNOWLEDGEMENT

This work was supported by the University of Missouri Research board (UMRB). The authors acknowledge the Material Research Center (MRC) at Missouri University of Science & Technology for SEM and XRD.

REFERENCES

(1) Al-Mamoori, A.; Krishnamurthy, A.; Rownaghi, A. A.; Rezaei, F. Carbon Capture and Utilization Update. *Energy Technol.* **2017**, *5* (6), 834–849..

(2) Chaffee, A. L.; Knowles, G. P.; Liang, Z.; Zhang, J.; Xiao, P.; Webley, P. A. CO_2 Capture by Adsorption: Materials and Process Development. *Int. J. Greenh. Gas Control* **2007**, *1* (1), 11–18.

(3) Rezaei, F.; Webley, P. Structured Adsorbents in Gas Separation Processes. *Sep. Purif. Technol.* **2010**, *70* (3), 243–256.

(4) Hufton, J. R.; Mayorga, S.; Sircar, S. Sorption-Enhanced Reaction Process for Hydrogen Production. *AIChE J.* **1999**, *45* (2), 248–256.

(5) Duyar, M. S.; Farrauto, R. J.; Castaldi, M. J.; Yegulalp, T. M. In Situ CO_2 Capture Using CaO/γ -Al_2O_3 Washcoated Monoliths for Sorption Enhanced Water Gas Shift Reaction. *Ind. Eng. Chem. Res.* **2014**, *53*, 1064–1072.

(6) Chang, Y.; Chen, Y.; Chang, P.; Chen, S. Synthesis, Characterization , and CO_2 Adsorptive Behavior of Mesoporous AlOOH-Supported Layered Hydroxides. *ChemSusChem* **2012**, *5*, 1249–1257.

(7) Duyar, M. S.; Wang, S.; Arellano-Treviño, M. A.; Farrauto, R. J. CO_2 Utilization with a Novel Dual Function Material (DFM) for Capture and Catalytic Conversion to Synthetic Natural Gas: An Update. *J. CO_2 Util.* **2016**, *15*, 65–71.

(8) Lee, A.; Xiao, G.; Xiao, P.; Joshi, K.; Singh, R.; Webley, P. A. High Temperature Adsorption Materials and Their Performance for Pre-Combustion Capture of Carbon Dioxide. *Energy Procedia* **2011**, *4*, 1199–1206.

(9) Choi, S.; Drese, J. H.; Jones, C. W. Adsorbent Materials for Carbon Dioxide Capture from Large Anthropogenic Point Sources. *ChemSusChem* **2009**, *2* (9), 796–854.

(10) Rownaghi, A. A.; Rezaei, F.; Labreche, Y.; Brennan, P. J.; Johnson, J. R.; Li, S.; Koros, W. J. In Situ Formation of a Monodispersed Spherical Mesoporous Nanosilica –Torlon Hollow-Fiber Composite for Carbon Dioxide Capture. *ChemSusChem* **2015**, *8*, 3439–3450.

(11) Rownaghi, A. A.; Kant, A.; Li, X.; Thakkar, H.; Hajari, A.; He, Y.; Brennan, P. J.; Hosseini, H.; Koros, W. J.; Rezaei, F. Aminosilane-Grafted Zirconia–Titiania–Silica Nanoparticles/Torlon Hollow Fiber Composites for CO_2 Capture. *ChemSusChem* **2016**, *9*, 1166–1177.

(12) Thakkar, H. V.; Eastman, S.; Hajari, A.; Rownaghi, A. A.; Knox, J. C.; Rezaei, F. 3D-Printed Zeolite Monoliths for CO_2 Removal from Enclosed Environments. *ACS Appl. Mater. Interfaces* **2016**, *8*, 27753−27761.

(13) Thakkar, H.; Eastman, S.; Al-Mamoori, A.; Hajari, A.; Rownaghi, A. A.; Rezaei, F. Formulation of Aminosilica Adsorbents into 3D-Printed Monoliths and Evaluation of Their CO_2 Capture Performance. *ACS Appl. Mater. Interfaces* **2017**, *9*, 7489–7498.

(14) Rezaei, F.; Mosca, A.; Webley, P.; Hedlund, J.; Xiao, P. Comparison of Traditional and Structured Adsorbents for CO_2 Separation by Vacuum-Swing Adsorption. *Ind. Eng. Chem. Res.* **2010**, No. 49, 4832–4841.

(15) Manovic, V.; Anthony, E. J. Lime-Based Sorbents for High-Temperature CO_2 Capture-a Review of Sorbent Modification Methods. *Int. J. Environ. Res. Public Health* **2010**, *7* (8), 3129–3140.

(16) Yong, Z.; Mata, V.; Rodrigues, A. E. Adsorption of Carbon Dioxide at High Temperature-a Review. *Sep. Purif. Technol.* **2002**, *26* (2), 195–205.

(17) Gruene, P.; Belova, A. G.; Yegulalp, T. M.; Farrauto, R. J.; Castaldi, M. J. Dispersed Calcium Oxide as a Reversible and Efficient CO_2-Sorbent at Intermediate Temperatures. *Ind. Eng. Chem. Res.* **2011**, *50*, 4042–4049.

(18) Lee, H. C.; Kwon, S.; Jeon, S. G.; Lee, K. B.; Hyun, C.; Jae, H.; Chul, H.; Kwon, S.; Goo, S.; Bong, K. Effect of pH-Controlled Synthesis on the Physical Properties and Intermediate-Temperature CO_2 Sorption Behaviors of K–Mg Double Salt-Based Sorbents. *Chem. Eng. J.* **2016**, *294*, 439–446.

(19) Oliveira, E. L. G.; Grande, C. a.; Rodrigues, A. E. $CO2$ Sorption on Hydrotalcite and Alkali-Modified (K and Cs) Hydrotalcites at High Temperatures. *Sep. Purif. Technol.* **2008**, *62* (1), 137–147.

(20) Broda, M.; Kierzkowska, A. M.; Müller, C. R. Influence of the Calcination and Carbonation Conditions on the CO_2 Uptake of Synthetic Ca-Based CO_2 Sorbents. *Environ. Sci. Technol.* **2012**, *46* (19), 10849–10856.

(21) Yu, C.; Kuo, H.; Chen, Y. Carbon Dioxide Removal Using Calcium Aluminate Carbonates on Titanic Oxide under Warm-Gas Conditions. *Appl. Energy* **2016**, *162*, 1122–1130.

(22) Wang, Q.; Tay, H. H.; Guo, Z.; Chen, L.; Liu, Y.; Chang, J.; Zhong, Z.; Luo, J.; Borgna, A. Morphology and Composition Controllable Synthesis of Mg-Al-CO_3 Hydrotalcites by Tuning the Synthesis pH and the CO2 Capture Capacity. *Appl. Clay Sci.* **2012**, *55*, 18–26.

(23) Wang, Q.; Luo, J.; Zhong, Z.; Borgna, A. CO2 Capture by Solid Adsorbents and Their Applications: Current Status and New Trends. *Energy Environ. Sci.* **2011**, *4* (1), 42–55.

(24) Wang, Q.; Wu, Z.; Tay, H. H.; Chen, L.; Liu, Y.; Chang, J.; Zhong, Z.; Luo, J.; Borgna, A. High Temperature Adsorption of CO_2 on Mg-Al Hydrotalcite: Effect of the Charge Compensating Anions and the Synthesis pH. *Catal. Today* **2011**, *164* (1), 198–203.

(25) Palomares, A.; López-Nieto, J. Reactivity in the Removal of SO_2 and NO_x on Co/Mg/Al Mixed Oxides Derived from Hydrotalcites. *Appl. Catal. B …* **1999**, *20*, 257–266.

(26) Kim, S.; Jeon, S. G.; Lee, K. B. High-Temperature CO_2 Sorption on Hydrotalcite Having a High Mg/Al Molar Ratio. *ACS Appl. Mater. Interfaces* **2016**, *8* (9), 5763–5767.

(27) Fang, H.; Kulkarni, A.; Kamakoti, P.; Awati, R.; Ravikovitch, P. I.; Sholl, D. S. Identification of High-CO_2 -Capacity Cationic Zeolites by Accurate Computational Screening. *Chem. Mater.* **2016**, *26*, 3887–3896.

(28) Hong, S.-H.; Jang, M.-S.; Cho, S. J.; Ahn, W.-S. Chabazite and Zeolite 13X for CO_2 Capture under High Pressure and Moderate Temperature Conditions. *Chem. Commun. (Camb).* **2014**, *50* (38), 4927–4930.

(29) Zhang, J.; Singh, R.; Webley, P. A. Alkali and Alkaline-Earth Cation Exchanged Chabazite Zeolites for Adsorption Based CO_2 Capture. **2008**, *111*, 478–487.

(30) Harada, T.; Hatton, T. A. Colloidal Nanoclusters of MgO Coated with Alkali Metal Nitrates/Nitrites for Rapid, High Capacity CO_2 Capture at Moderate Temperature. *Chem. Mater.* **2015**, *27* (23), 8153–8161.

(31) Ding, Y.-D.; Song, G.; Liao, Q.; Zhu, X.; Chen, R. Bench Scale Study of CO_2 Adsorption Performance of MgO in the Presence of Water Vapor. *Energy* **2016**, *112*, 101–110.

(32) Zhang, K.; Li, X. S.; Chen, H.; Singh, P.; King, D. L. Molten Salt Promoting Effect in Double Salt CO_2 Absorbents. *J. Phys. Chem. C* **2016**, *120* (2), 1089–1096.

(33) Lee, C. H.; Mun, S.; Lee, K. B. Characteristics of Na-Mg Double Salt for High-Temperature CO_2 Sorption. *Chem. Eng. J.* **2014**, *258*, 367–373.

(34) Hyun, C.; Jae, H.; Chul, H.; Kwon, S.; Goo, S.; Bong, K. Effect of pH-Controlled Synthesis on the Physical Properties and Intermediate-Temperature CO_2 Sorption Behaviors of K – Mg Double Salt-Based Sorbents. *Chem. Eng. J.* **2016**, *294*, 439–446.

(35) Huang, L.;Y.; Gao, W.; Harada, T.; Qin, Q.; Zheng, Q.; Hatton, A.; Wang, Q. Alkali Carbonate Molten Salt-Coated CaO with Highly Improved CO_2 Capture Capacity. *Energy Technol.* **2017**, 5, 1-11.

(36) Valverde, J. M.; Perejon, A.; Perez-Maqueda, L. A. Enhancement of Fast CO2 Capture by a Nano-SiO_2/CaO Composite at Ca-Looping Conditions. *Environ. Sci. Technol.* **2012**, *46* (11), 6401–6408.

(37) Hu, Y.; Liu, W.; Chen, H.; Zhou, Z.; Wang, W.; Sun, J.; Yang, X.; Li, X.; Xu, M. Screening of Inert Solid Supports for CaO-Based Sorbents for High Temperature CO_2 Capture. *Fuel* **2016**, *181*, 199–206.

(38) Vu, A. T.; Ho, K.; Jin, S.; Lee, C. H. Double Sodium Salt-Promoted Mesoporous MgO Sorbent with High CO_2 Sorption Capacity at Intermediate Temperatures under Dry and Wet Conditions. *Chem. Eng. J.* **2016**, *291*, 161–173.

(39) Xiao, G.; Singh, R.; Chaffee, A.; Webley, P. Advanced Adsorbents Based on MgO and K_2CO_3 for Capture of CO_2 at Elevated Temperatures. *Int. J. Greenh. Gas Control* **2011**, *5* (4), 634–639.

(40) Harada, T.; Simeon, F.; Hamad, E. Z.; Hatton, T. A. Alkali Metal Nitrate-Promoted High-Capacity MgO Adsorbents for Regenerable CO_2 Capture at Moderate Temperatures. *Chem. Mater.* **2015**, *27* (6), 1943–1949.

(41) Sagar, T. V.; Surendar, M.; Padmakar, D.; Parameswaram, G.; Lingaiah, N.; Rao, K. S. R.; Reddy, I. A. K.; Sumana, C.; Prasad, P. S. S. Selectivity Reversal in Oxidative Dehydrogenation of Ethane with CO_2 on CaO–NiO/Al_2O_3 Catalysts. *Catal. Letters* **2017**, *147*, 82–89.

(42) Galván-Ruiz, M.; Hernández, J.; Baños, L.; Noriega-Montes, J.; Rodríguez-García, M. E. Characterization of Calcium Carbonate, Calcium Oxide, and Calcium Hydroxide as Starting Point to the Improvement of Lime for Their Use in Construction. *J. Mater. Civ. Eng.* **2009**, *21* (11), 694–698.

(43) Dean, C. C.; Blamey, J.; Florin, N. H.; Al-Jeboori, M. J.; Fennell, P. S. The Calcium Looping Cycle for CO_2 Capture from Power Generation, Cement Manufacture and Hydrogen Production. *Chem. Eng. Res. Des.* **2011**, *89* (6), 836–855.

(44) Hu, Y.; Liu, W.; Sun, J.; Yang, X.; Zhou, Z.; Zhang, Y.; Xu, M. High Temperature CO_2 Capture on Novel Yb_2O_3-Supported CaO-Based Sorbents. *Energy and Fuels* **2016**, *30* (8), 6606–6613.

III. COMBINED CAPTURE AND UTILIZATION OF CO_2 FOR SYNGAS PRODUCTION OVER DUAL-FUNCTION MATERIALS

Ahmed Al-Mamoori, Ali A. Rownaghi, Fateme Rezaei*

Department of Chemical & Biochemical Engineering, Missouri University of Science and Technology, 1101 N State Street, Rolla, MO, 65409, United States

ABSTRACT

The integration of CO_2 capture and conversion has been recently demonstrated as a promising approach to address CO_2 emissions while producing value-added chemicals and fuels. Herein, we report *in-situ* capture and utilization of CO_2 in syngas production from dry reforming of ethane (DRE) over dual-function materials (DFMs) consisting of Ni-impregnated CaO and MgO-based double salts supported on γ-Al_2O_3. The N_2 physisorption, XRD, CO_2-TPD, NH_3-TPD, H_2-TPR, and XPS analyses were performed to characterize the obtained DFMs. The CO_2 adsorption-desorption performance of γ-Al_2O_3-supported adsorbent-catalyst materials at 650 °C indicated that 100% of the adsorbed CO_2 was desorbed from the DFMs surface for subsequent reaction with C_2H_6. At reaction temperature of 650 °C and WHSV of 2250 mL/g.h, the Ni_{20}@$(K\text{-}Ca)_{50}$/$(\gamma\text{-}Al_2O_3)_{50}$ and Ni_{20}@$(Na\text{-}Ca)_{50}$/$(\gamma\text{-}Al_2O_3)_{50}$ showed the best activity with 100% C_2H_6 conversion and 65 and 75% CO_2 conversion, respectively. Analysis of the spent DFMs revealed low degree of coke formation (~9 wt%) which reduced the stability of DFMs by only 5%. The results reported in this investigation highlight the importance of combined capture-reaction system

as a cost-effective technology for utilizing the emitted CO_2 as a feedstock to make valuable chemicals, materials and fuels.

Keywords: CO_2 capture, adsorbent-catalyst, CO_2 utilization, syngas, dry ethane reforming.

1. INTRODUCTION

The U.S. energy-related CO_2 emissions are expected to increase by 3% from 2013 to 2040 while the U.S. energy consumption grows 0.3%/year from 2013 through 2040, thus finding cost-effective approaches to capture and utilize the emitted CO_2 will open avenues to sustainable creation of energy with less environmental impacts.[1–4] The hybrid capture-utilization system that simultaneously captures and utilizes CO_2 in production of fuels or chemicals directly from industrial flue gas offers a unique solution to emissions control and energy supply challenges. This integrated process that is operated in a single-unit system under isothermal condition can eliminate the need for adsorbent regeneration and also the infrastructure required for transportation and storage of captured CO_2 that are typical energy-intensive steps in carbon capture and storage technology.

The combined capture-utilization system is based on dual-function materials (DFMs) that can efficiently concentrate dilute waste gases on their surface before subsequent utilization in chemical reaction. This approach has been recently reported by several research groups for direct methanation of CO_2 from flue gas in a sorptive reactor that is operated at 300–350 °C and low pressure (< 2.5 bar) using H_2.[5–9] Farrauto and co-workers[5–8] used a series of DFMs consisting of Ru and CaO, as adsorbent and catalyst components, respectively, supported on γ-Al_2O_3 for coupling CO_2 capture and CO_2

hydrogenation reaction. The authors demonstrated that the CO_2 capture by CaO and spillover to Ru catalyst sites increases methane turnover and methanation capacity. In another investigation, Bobadilla et al.[10] reported the use of FeCrCu/K-MgO-Al_2O_3 as a DFM for capturing and converting CO_2 to syngas in a two-reactor unit at 450 °C. Their CO_2 capture-conversion process involving capture of CO_2, release of CO_2, direct catalytic reduction of stored CO_2 by hydrogen, and catalyst regeneration was operated alternately and isothermally. Most recently, Miguel at al.[9] proposed an adsorption-reaction process using a sorptive reactor with different layers of adsorbent (K-HTC) and catalyst (Ni) for production of synthetic methane from reaction of adsorbed CO_2 with H_2. The authors reported complete conversion of the captured CO_2 (0.3 mol/kg) into CH_4 with a methane productivity of 2.36 mol/kg/h at 350 °C.

One of the drawbacks of the current proposed DFMs investigated for *in-situ* capture-utilization processes is low CO_2 uptake capacity at high temperatures which compromises their overall performance to effectively capture CO_2 before subsequent conversion. To have an efficient and cost-effective integrated process, the DFMs are required to not only exhibit high catalytic activity and stability but also high adsorption capacity. In our previous investigation,[11] we developed a series of high temperature CO_2 adsorbents based on potassium- and sodium-promoted CaO (K-Ca and Na-Ca) and reported high CO_2 uptake (c.a. 10.7 and 9.5 mmol/g for K-Ca and Na-Ca, respectively) at 650 °C and 100% CO_2. On the basis of the obtained results, the double slat adsorbents appeared to be good candidates for high temperature CO_2 adsorption.

Synthesis gas (syngas) is an industrially important feedstock for production of methanol through Fisher-Tropsch process. It is produced commercially by steam methane

reforming (SMR) process.[12] Another alternative route to produce syngas is dry methane reforming (DMR) by which two greenhouse gases, CH_4 and CO_2, are reacted.[13] However, DMR is highly endothermic and requires high temperature (800-900 °C) to obtain equilibrium conversion. Moreover, the highly endothermic nature of this reaction leads to severe catalyst coking and fast deactivation.[14] To address this issue, dry ethane reforming (DER) which is performed at lower temperature (*i.e.,* 100 K below that of DMR) has been proposed as a better approach for producing syngas than DMR. The low reaction temperature makes the catalyst less susceptible to deactivation and the process less energy-intensive. In addition, ethane is the second largest component of shale gas with a concentration of 10 vol%, making it a relatively abundant source for syngas production.[15] The most widely investigated catalysts for DER reaction to date include nickel, cobalt, iron, and platinum.[16,17] Chen and co-workers[13] examined the efficacy of $LaFe_{0.9}Ni_{0.1}O_3$ perovskite catalyst for DER and compared it with Ni/La_2O_3 and $NiFe/La_2O_3$. $LaFe_{0.9}Ni_{0.1}O_3$ perovskite catalyst. The authors reported CO_2 and C_2H_6 conversions of 49.7% and 21.4%, respectively for this catalyst. In another investigation, Yan et al.[17] evaluated the activity and stability $PtNi/CeO_2$ bimetallic catalysts for DER reaction and showed that both activity and stability of the bimetallic catalysts were enhanced in comparison to their corresponding monometallic catalysts.

In this investigation, we aimed at developing DFMs that could be used for combined CO_2 capture and conversion to syngas through DER route in one reactor and under isothermal conditions. In particular, several double salts (i.e., K-Ca, Na-Ca, K-Mg, Na-Mg) were used as the adsorbent component of DFMs due to their high adsorption capacity at medium to high temperatures, relative stability, and rapid adsorption-desorption

kinetics.[18–20] Nickel (Ni) was used as the catalyst component owing to its high catalytic activity, abundance, and low cost.[21] Both components were supported on a high surface area γ-Al_2O_3. The properties of the DFMs were characterized by XRD, N_2 physisorption, NH_3-TPD, CO_2-TPD, H_2-TPR, XPS, and gravimetric analysis. The adsorption-desorption behavior of the materials was investigated followed by evaluating their catalytic performance using CO_2 as a co-feed with C_2H_6. In addition, combined capture-reaction was performed by first capturing CO_2 then feeding C_2H_6 into the bed to react with desorbed CO_2 at 650 °C.

2. EXPERIMENTAL SECTION

2.1. DUAL-FUNCTION MATERIALS PREPARATION

γ-Al_2O_3 used as a support for the adsorbent and catalyst components of the DMFs investigated in this study was synthesized according to a sol-gel procedure reported elsewhere.[22] Briefly, 13.75 g of pseudobomite (Catapal B, Sasol) was peptized in a mixture of nitric acid (1.27 g) and distilled water (200 mL). The suspension was sonicated at room temperature for 90 min and then stirred for 17 h at 60 °C. After cooling down to room temperature, the peptized alumina sol was added slowly to a stirred ethanol solution (200 mL) of Pluronic P123 EO_{20}-PO_{70}-EO_{20} triblock copolymer (Sigma-Aldrich, 15.3 g). The mixture was kept under stirring for 24 h at room temperature. Then, the solvent was evaporated after subjected to 60 °C for 60 h in an open beaker. The remaining material was dried at 75 °C for 24 h and calcined in two steps: first at 150 °C for 1 h to remove the remaining water and ethanol with ramp 1 °C /min, and second at 700 °C for 4 h.

Potassium- and sodium-based CaO (K-Ca and Na-Ca), and potassium- and sodium-based MgO (K-Mg and Na-Mg) were all synthesized following the recipes reported in our earlier work or from the literature.[11,19,23] To synthesize DFMs, double salts were first incorporated into the γ-Al_2O_3 using a wet impregnation method. Briefly, desired amounts of double salts were dissolved in distilled water followed by the addition of γ-Al_2O_3. The obtained solution was stirred for 12 h under 400 rpm. In the next step, the obtained paste was dried in an oven at 110 °C for 4 h. Then, the material was calcined for 3 h at 700 °C (for K-Ca/γ-Al_2O_3 and Na-Ca/γ-Al_2O_3) and 500 °C (for K-Mg/γ-Al_2O_3 and Na-Mg/γ-Al_2O_3). To impregnate Ni into the γ-Al_2O_3 – supported double salts, different amounts of $Ni(NO_3)_2.6H_2O$ (Sigma-Aldrich) were dissolved in distilled water followed by the addition of γ-Al_2O_3 – supported double salts and stirring at room temperature for 12 h. The drying and calcination steps were similar to those stated above. The Ni content was varied from 1 to 5, 10, and 20 wt% for each double salt adsorbent.

2.2. DUAL-FUNCTION MATERIALS CHARACTERIZATION

X-ray diffraction (XRD) measurements were performed to evaluate the crystalline structure of the DFMs using a PANalytical X'Pert multipurpose X-ray diffractometer with a scan step size of 0.02 °/step at the rate of 147.4 s/step. The textural properties of the materials were evaluated by N_2 physisorption tests using a volumetric gas analyzer (3Flex, Micrometric). Prior to the measurements, the samples were degassed under vacuum at 300 °C for 6 h. The Brunauer-Emmet-Teller (BET), Horvath and Kawazoe (HK), and non-local density functional theory (NLDFT) methods were used to estimate the surface area, pore volume, and pore size distribution (PSD), respectively. To study the oxidation state of the

DFMs, X-ray photoelectron spectroscopy (XPS) analysis was performed by a Kratos Axis 165 XPS. NH_3-TPD and CO_2-TPD measurements were performed by first degassing the samples under helium flow at 30 mL/min for 2 h at 500 °C with ramping of 10 °C/min. Then, the samples were cooled down to 80 °C followed by NH_3 or CO_2 adsorption for 30 min. After that, He gas was injected for 15 min to remove any physisorbed NH_3 or CO_2 on the sample followed by ramping temperature from 80 to 800 °C at the rate of 10 °C/min. H_2-TPR was also measured by first degassing the materials at 100 °C for 2 h under helium at 50 mL/min followed by injecting H_2 while raising the temperature to 900 °C with the ramp rate of 7.5 °C/min. The amount of coke deposition on the DFMs after DER reaction was quantified using TGA (Q500, TA Instruments). The temperature was varied from 25 to 800 °C at the rate of 20 °C/min.

2.3. CO_2 ADSORPTION-DESORPTION MEASUREMENTS

TGA (Q500, TA Instruments) was used to measure CO_2 adsorption-desorption capacities of the DFMs. The samples were first degassed under nitrogen flow at 650 °C to remove any pre-adsorbed moisture or other gases. The nitrogen gas was then switched to 10% CO_2/N_2 for adsorption to begin at the same temperature. After 30 min, the adsorption was stopped by switching gas back to nitrogen to start desorption step while temperature was kept constant at 650 °C. The desorption step was continued for 30 min and then the test was concluded.

2.4. CATALYTIC TESTS

DER reaction was carried out in a stainless-steel packed-bed reactor with an inner diameter of 0.635 cm and height of 30 cm at 650 °C and 1 bar. The reactor was placed in

an electric furnace with a type K thermocouple that was installed inside the reactor to control the bed temperature. The gas flow rates were controlled using mass flow controllers (MFC, Brooks Instrument). For a typical run, about 0.4 g of the material was outgassed under N_2 for 30 min at 750 °C with flow rate of 30 mL/min followed by catalyst reduction under 5% H_2/He for 1 h at the same temperature and flow rate. The bed was then cooled down to the desired temperature under N_2 to remove any adsorbed H_2 during reduction. For reaction-alone tests, gas mixtures of 10% CO_2/N_2 and 5% C_2H_6/N_2 were co-fed to the reactor with total flow rate 15 mL/min and CO_2:C_2H_6 molar ratio of 1:1. The weight hourly space velocity (WHSV) was 2250 mL/g.h. For adsorption-reaction tests, a gas mixture consisting of 10% CO_2/N_2 was first introduced to the reactor until the bed was saturated, then switched to the co-reactant 5% C_2H_6/N_2 to react with the adsorbed CO_2. The reactor effluent was analyzed online using an SRI 8610C gas chromatograph (GC) equipped with flame ionization detector (FID), FID methanizer, and thermal conductivity detector (TCD). The GC data were used to calculate C_2H_6 and CO_2 conversions and products yield.

3. RESULTS AND DISCUSSION

3.1. CO_2 ADSORPTION-DESORPTION PROFILES

The CO_2 adsorption capacity was used as a metric to optimize the composition of the DFMs. For each class of double salt adsorbents, the CO_2 adsorption capacity of all DFMs

with varied Ni was first measured and the DFM with maximum CO_2 adsorption capacity was chosen for further analysis. The corresponding adsorption uptake curves are shown in Figure S1, Supporting Information. The materials selected from each group for further analysis included $Ni_{10}@(K\text{-}Mg)_{25}/(\gamma\text{-}Al_2O_3)_{75}$, $Ni_{10}@(Na\text{-}Mg)_{50}/(\gamma\text{-}Al_2O_3)_{50}$, $Ni_{20}@(K\text{-}Ca)_{50}/(\gamma\text{-}Al_2O_3)_{50}$, and $Ni_{20}@(Na\text{-}Ca)_{50}/(\gamma\text{-}Al_2O_3)_{50}$ which were denoted as DFM-1, DFM-2, DFM-3, and DFM-4, respectively (see Table 1). As a first step in evaluating the performance of selected DFMs, their CO_2 adsorption-desorption profiles were measured, as presented in Figure 1, and their corresponding capacities were calculated from the profiles, as shown in Table 1. Results in Figure 1 indicated that the candidate materials exhibit a relatively fast CO_2 uptake by reaching 90% of their saturation capacity within the first 2 min. Additionally, investigating the desorption profiles revealed that more than 95% of the adsorbed CO_2 desorbed under N_2 at the same adsorption temperature within the first 5 min of desorption step. Rapid adsorption-desorption is crucial for reducing the cycle time and hence maximizing the throughput of the combined capture-reaction system. It has previously been shown that the mechanism of CO_2 adsorption over double salt adsorbents is through production of double carbonates.[11,19,23] Thus, a similar mechanism to the parent double salts is proposed for the corresponding DFMs.

For 10% CO_2/N_2 and at 650 °C, DFM-3 achieved a maximum CO_2 adsorption capacity of 0.99 mmol/g compared to other DFMs, whereas DFM-4 exhibited lower uptake (c.a. 0.63 mmol/g). The lower adsorption capacity of Mg-based DFMs than that of their Ca-based analogues could be attributed to their narrower operating conditions(i.e., 300-400 °C), as previously shown by other esearchers.[24–27]

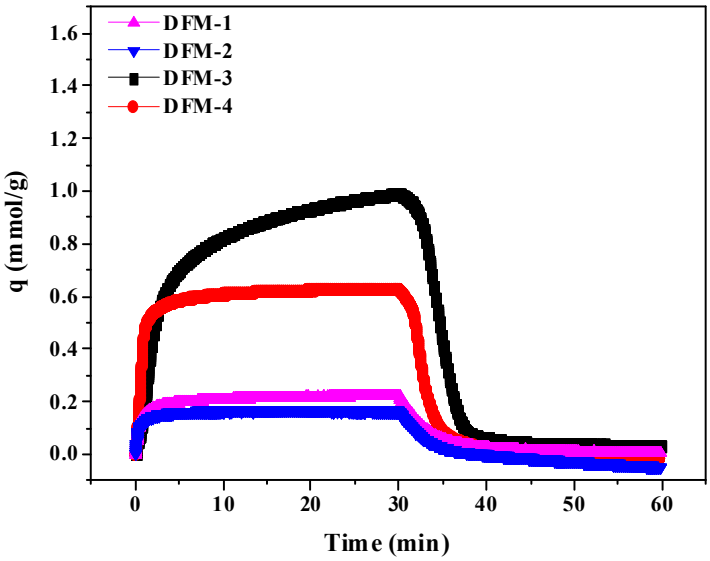

Figure 1. Adsorption-desorption profiles for γ-Al_2O_3-supported DFMs at 650 °C using 10% CO_2/N_2 for adsorption and N_2 for desorption.

Moreover, comparing these uptake capacities with those reported in our previous work,[11] it was evident that the dilution of the double salts with γ-Al_2O_3 support and Ni impregnation both contributed to diminished CO_2 capacity.

Gruene et al.[28] also reported a similar trend and showed that for CaO/Al_2O_3, the efficiency of the uptake per CaO site decreases due to decrease in surface area and pore

Table 1. CO_2 adsorption-desorption capacities for adsorbent-catalyst materials at 650 °C.

Material	Sample code	CO_2 adsorption (mmol/g)	CO_2 desorption (mmol/g)
$Ni_{10}@(K\text{-}Mg)_{25}/(\gamma\text{-}Al_2O_3)_{75}$	DFM-1	0.22	0.22
$Ni_{10}@(Na\text{-}Mg)_{50}/(\gamma\text{-}Al_2O_3)_{50}$	DFM-2	0.16	0.16
$Ni_{20}@(K\text{-}Ca)_{50}/(\gamma\text{-}Al_2O_3)_{50}$	DFM-3	0.99	0.95
$Ni_{20}@(Na\text{-}Ca)_{50}/(\gamma\text{-}Al_2O_3)_{50}$	DFM-4	0.63	0.63

volume, attributed to the pore clogging. Analyzing the CO_2 desorption capacities in Table 1 indicated that while 96% of adsorbed CO_2 desorbed from DFM-3 during desorption step, the other three DFMs exhibited complete regeneration under the same conditions.

3.2. DUAL-FUNCTION MATERIALS CHARACTERIZATION

Figure 2 shows the XRD spectra of the DFMs. The characteristic peaks of γ-Al_2O_3 appeared at angles 37, 46.5, and 66.5° confirmed the successful synthesis of γ-Al_2O_3.[22] The diffraction peaks of MgO and CaO compounds were clear in the spectra of DFMs. For DFM-1, the intensity of the peaks related to the K-Mg were very small as a result of its low amount (25 wt%) in the adsorbent-catalyst material compared to the other adsorbents with 50 wt% double salt loading. The peaks observed at 37, 43, and 63° were correlated to the NiO peaks which further confirmed the successful impregnation of the Ni into the γ-Al_2O_3 – supported double salts. Notably, their intensity increased as the nickel content increased from 10 to 20 wt%. Also, it is noteworthy that in the spectra of CaO-based DFMs, the γ-

Al_2O_3 peaks were less intense which could be correlated to the higher loading of the double salt and impregnated Ni particles.

The N_2 physisorption isotherms and the PSD profiles of the bare γ-Al_2O_3 and the corresponding γ-Al_2O_3-supported DFMs are illustrated in Figure 3. As evident from Figure 3a, the DFMs exhibited type IV isotherm with a type H1 hysteresis loop, having relatively sharp uptakes at $p/p_0 = 0.8$-0.9, indicating that the γ-Al_2O_3-supported DFMs contained

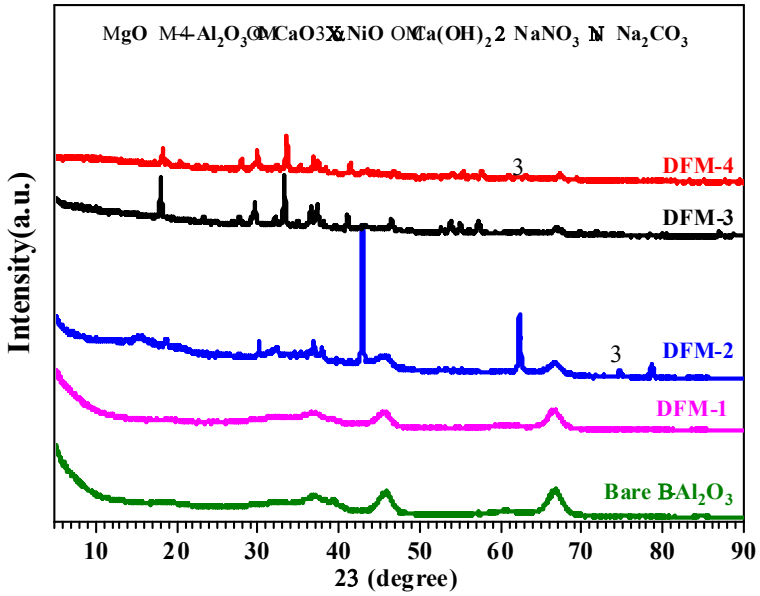

Figure 2. XRD spectra of bare γ-Al_2O_3 and γ-Al_2O_3-supported DFMs.

uniform and well-defined large mesopores. The Mg-based materials displayed higher N_2 uptake than their Ca-based counterparts as a result of their higher porosity. Also, increasing the double salt:alumina weight ratio resulted in lower N_2 uptake, as evident from N_2 isotherms of DFM-1 and DFM-2, mainly because of the less porous nature of double salts relative to the bare alumina. In our earlier study,[11] it was shown that the N_2 uptake is

generally low over double salts as a result of their low porosity. The PSD curves in Figure 3b confirmed the uniform pore distribution for the DFMs in the range of 5 to 15 nm. It was also noticed that there was a shift in the pore size of the DFMs to lower values as compared to that of bare alumina support.

The corresponding textural properties listed in Table 2 highlighted the highest surface area and pore volume for DFM-1 among the DFMs, with values of 176 m^2/g and 0.53 cm^3/g, respectively which were about 70 and 44% of those of bare γ-Al_2O_3. This was

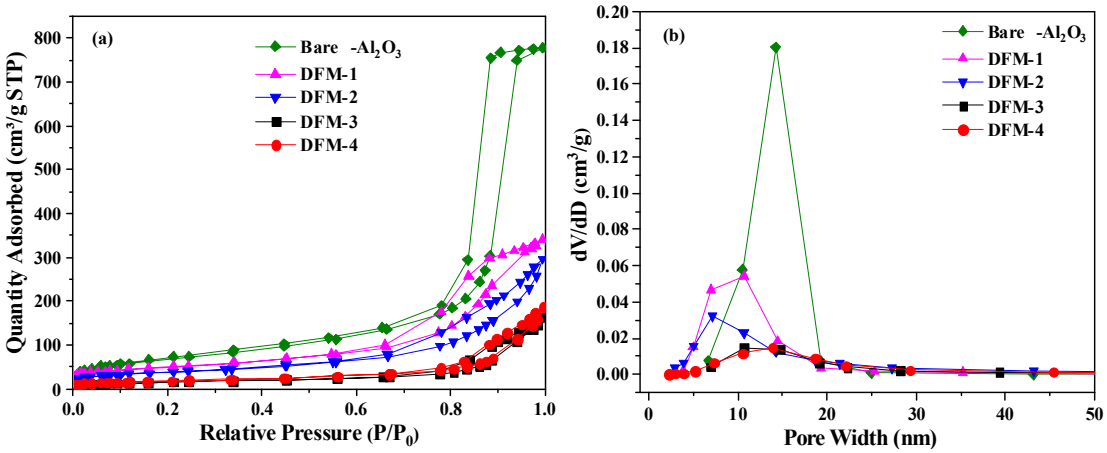

Figure 3. (a) N_2 physisorption isotherms and (b) pore size distribution of γ-Al_2O_3 and γ-Al_2O_3-supported adsorbent-catalyst materials.

expected as the γ-Al_2O_3 in this material with 75 wt% content was less diluted with the double salt. Although the surface area and pore volume decreased dramatically for both K-Ca and Na-Ca DFMs (~74-78%), they were still sufficiently porous to be considered for adsorption and reaction studies. The decrease in surface area and pore volume could be attributed to the filling of the γ-Al_2O_3 mesopores by the double salts and/or Ni particles.

To examine the acidic sites on the DFMs surfaces, NH_3-TPD measurements were carried out and the obtained results are shown in Figure 4a. All of the four samples displayed a relatively sharp peak centered at 175 °C which stemmed from the weak acidic sites.

No additional peak was observed for DFM-1 and DFM-2. However, a broad peak was observed for DFM-3 and DFM-4 in the temperature range of 350-750 °C which was ascribed to either medium or strong acid sites. It is believed that higher Ni loading contributed to higher amount of medium/strong acid sites in these samples. It is also important to note that DFM-3 exhibited lower amount of weak acid sites than DFM-4.

Table 2. Textural properties of the adsorbent-catalyst materials.

Material	S_{BET} [m^2/g]	V_p [cm^3/g]	d_p **[nm]**
Bare γ-Al_2O_3	250	1.21	15
DFM-1	176	0.53	10
DFM-2	135	0.46	12
DFM-3	56	0.26	17
DFM-4	66	0.29	17

To gain insight into the CO_2 adsorption–desorption at different adsorption sites (mainly basic sites) that are present in the DFMs, CO_2-TPD measurements were performed

and the corresponding profiles are shown in Figure 4b. The CO_2 desorption profiles exhibited a clear peak centered at 170 °C which was attributed to the desorption of CO_2 from weak basic sites.[29] Notably, the density of weak basic sites was found to be higher for Ca-based samples than for Mg-based materials, as evident from larger area of the peaks. Another broad peak with smaller intensity was observed at higher temperatures for all materials which could be related to the desorption of CO_2 adsorbed on the medium/strong basic sites. It was noteworthy that the temperature at which the second peak appeared was higher for DFM-3 and DFM-4, which displayed a high intensity peak in the temperature range of 450-600 °C, than for the DFM-1 and DFM-2, which displayed the peak at 350-600 °C. This implies that the interaction of CO_2 with Ca-based DFMs was stronger than that with Mg-based materials. This phenomenon could explain the higher adsorption capacity of Ca-based DFMs (see Table 1) than that of Mg-based DFMs despite their lower surface area (see Table 2).

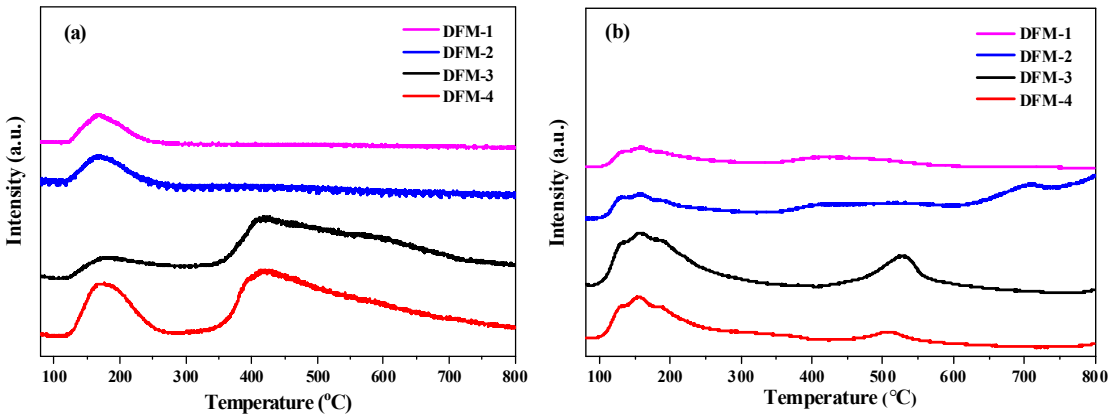

Figure 4. (a) NH_3-TPD and (b) CO_2-TPD profiles of adsorbent-catalyst materials.

The reducibility of the DFMs was examined by H_2-TPR tests. Results in Figure 5 indicated that DFM-3 and DFM-4 samples were easily reducible as noted by the three peaks appeared in their H_2-TPR curves. The first peak observed at 250-500 °C were attributed to the weak interaction of free NiO with the γ-Al_2O_3 support, whereas the second peak in the temperature range of 650-750 °C was assigned to the strong interaction of NiO with the γ-Al_2O_3 support.[30,31] The appearance of another peak centered at 850 °C could be related to the reduction of $NiAl_2O_4$.[32] It was previously reported that the presence of Ca improves the reduction of Ni/α-Al_2O_3 from one peak at 620 °C to three peaks at 400, 690, and 830±20 °C which is in agreement with our results.[30] The authors concluded that the role of CaO is to enhance the interaction between Ni and α-Al_2O_3 thereby limiting Ni sintering and improving its stability. Moreover, the comparison of the reduction profiles of DFM-3 and DFM-4 revealed that the adsorbent component affects the reducibility of the DFMs through impacting the catalyst-support interactions by shifting the reduction temperature. As evident, by changing the double salt from K-Ca to Na-Ca the reduction temperature was shifted from 220 to 350 °C. In the case of Mg-based materials, it was found that unlike Ca-based DFMs, DFM-1 was essentially irreducible when exposed to hydrogen while DFM-2 was partially reducible at high temperatures. It has been shown that in the absence of zero-valent metals on the surface, the reduction with hydrogen is partial and only occur at temperatures greater than 1000 °C.[33] This could be the case for Mg-based samples. For the former sample, no peak was observed at low temperature related to the free NiO, suggesting the strong interaction of NiO with the support which was further verified by the appearance of a peak at 700-800 °C.[29,32]

The XPS spectrum of the Ni-loaded DFMs was investigated to verify the chemical composition and chemical state of the elements that were present in their structures. The survey spectrum in Figure 6a illustrates that the DFMs were primarily composed of Ni, O, K, Mg, Na, Ca, Al, and C elements, and the corresponding binding energies of these surface elements are listed in Table 3. The appearance of C 1s photoelectron peak at binding energy of 284 eV was due to the carbonates (Na_2CO_3 and K_2CO_3) present in the DFM samples. Figure 6b depicts the high-resolution XPS spectra of Ni 2p. The peak located at 854 eV for all the samples was attributed to Ni $2p_{3/2}$ and accompanied by shaking satellite peak at 860

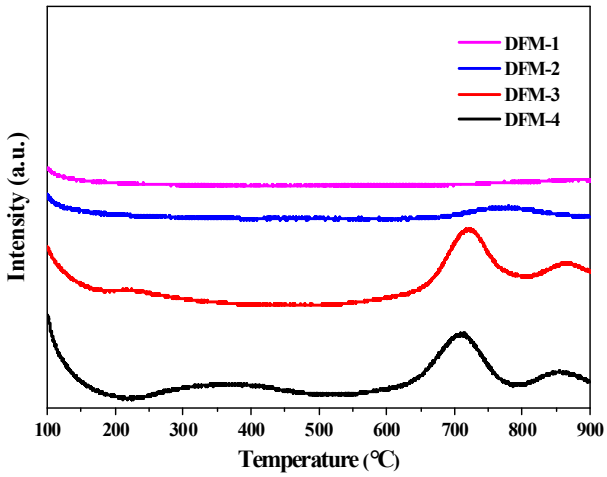

Figure 5. H_2-TPR profiles of adsorbent-catalyst materials.

eV which was related to $NiAl_2O_4$.[34] Moreover, the appearance of another peak at 872 eV was correlated to Ni $2p_{1/2}$. It should be noted that the binding energy of bare NiO is 853.8 eV[30] which suggests that the binding energy of Ni was not affected by the impregnation with the other compounds.

On the basis of these results, it can be concluded that the binding energy of the elements was not affected significantly by other elements and hence, their valence state was maintained. In addition, the XPS analysis confirmed that the DFMs were composed of NiO, double salts, and γ-Al_2O_3.

3.3. REACTION-ALONE RUNS

We first evaluated the performance of the four DFMs under DER reaction-alone conditions upon which CO_2 and C_2H_6 were co-fed into the reactor simultaneously at 650 °C. The obtained CO_2 and C_2H_6 conversions for reaction-alone tests are presented in Figure

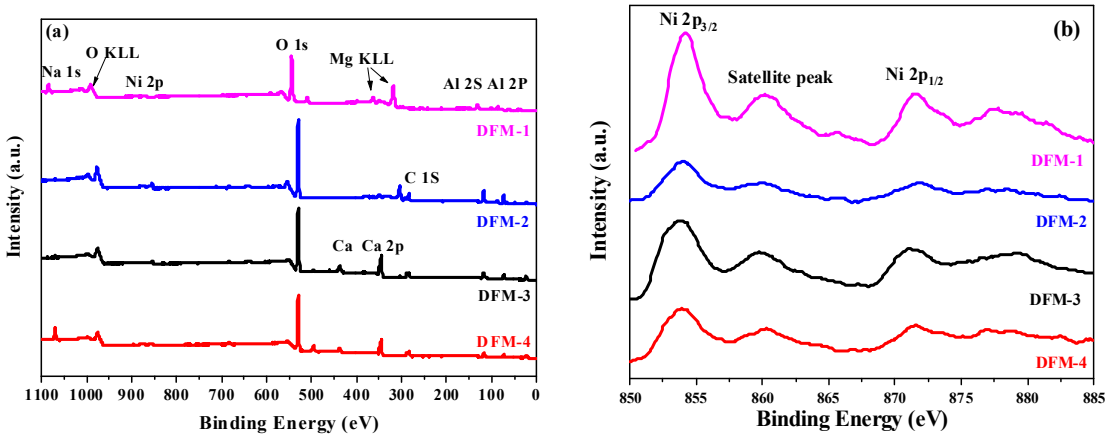

Figure 6. (a) XPS survey spectrum and (b) high-resolution XPS spectra for Ni 2p.

7a. The DFM-3 and DFM-4 exhibited high CO_2 (75 and 65%, respectively) and C_2H_6 (100% for both) conversion, whereas over DFM-1 and DFM-2, the conversions dropped to 14 and 60% for CO_2 and 16 and 47% for C_2H_6, respectively. The dramatic decrease in CO_2

Table 3. Binding energy of Ni, O, K, Na, Mg, Ca, and Al elements obtained by XPS analysis.

Material	Ni 2p	O 1s	K 2p	Na 1s	Mg 2s	Mg 2p	Ca 2p	Al 2p
DFM-1	854	530	292	-	-	49	-	73
DFM-2	854	530.5	-	1071	87.5	-	-	73
DFM-3	854	530	291	-	-	-	345.5	72.5
DFM-4	854	530	-	1070	-	-	345.5	72.5

and C_2H_6 conversions over Mg-based DFMs could be correlated to their lower Ni content which reduced the density of active sites responsible for catalyzing the DER reaction, in agreement with the NH_3-TPD results. Interestingly, the C_2H_6 conversion was significantly affected by lowering Ni content compared to the CO_2 conversion mainly because C_2H_6 is activated at Ni sites while activation of CO_2 occurs at double salt adsorption sites and/or γ-Al_2O_3 support sites.

The possible reaction pathways for CO_2 and C_2H_6 and their heat of reaction values are presented in Supporting Information. These reaction pathways include DER (eq. 1), oxidative dehydrogenation (ODH) to produce ethylene (eq. 2), non-oxidative dehydrogenation (eq. 3), cracking of ethane to methane (eq. 4), reverse water gas shift (RWGS) reaction (eq. 5), Boudouard reaction (eq. 6), ethane decomposition (eq. 7), and methane cracking (eq. 8). Characterizing the reaction products revealed the formation of methane in addition to syngas, albeit with much smaller quantity, implying that DER reaction (eq. 1) was accompanied by ethane cracking (eq. 4) as a side reaction. Coke

formation was also obtained due to the Boudouard reaction (eq. 6) and methane cracking (eq. 8). Zhang et al.[35] carried out dry methane reforming (DMR) over 15%Ni/γ-Al_2O_3 catalyst at 800 °C and reported a CH_4 conversion of 97.3% with 81.5% CO_2 conversion for this catalyst. It should also be pointed out that both ethylene and syngas were obtained over DFM-1 which showed the lowest activity suggesting that this catalyst favored the ODH pathway (eq. 2) with RWGS reaction (eq. 5). The lowest activity of DFM-1 could be related to its irreducible nature under H_2, as shown previously. Ni^0 has been known to be an active catalyst for DER and cracking reactions (eqs. 1 and 8), whereas NiO is an active catalyst for ODH (eq. 2).[36,37] It has also been reported that NiO is not active for DMR which justifies the absence of CH_4 in the product stream in the case of DFM-1.[38] These results are in agreement with the TPR measurements reported earlier. These results demonstrate the effect of adsorbent type on catalytic performance of the DFMs and highlight the importance of identifying a right adsorbent-catalyst material that can selectively cleavage C-C bond to produce syngas or C-H bond to produce ethylene.[39]

Figure 7b displays the H_2/CO ratio for the four adsorbent-catalyst materials obtained at 650 °C. Typically, for the syngas to be used in major chemicals production processes, the stoichiometric H_2/CO ratio should be in the range 1-2.[40] Our catalyst results demonstrated that only DFM-3 and DFM-4 could produce a syngas stream that meets such requirement with the ratios of 1.30 and 1.04, respectively. In contrast, DFM-1 and DFM-2 both exhibited low H_2/CO ratio (c.a. 0.45 and 0.88, respectively). The higher H_2/CO ratio for Ca-based DFMs could be attributed to the higher conversion of C_2H_6 over them which led to production of more H_2 via dry reforming (eq. 1) and other side reactions such as ethane decomposition (eq. 7) and methane cracking (eq. 8).

On the basis of catalytic test results shown above and the CO_2 adsorption capacities (see Figure 1), the DFM-3 was selected for further analyses. Figure 8a displays the effect of temperature on the performance of this DFM. It is clear from this figure that increasing the temperature from 400 to 700 °C resulted in enhanced CO_2 and C_2H_6 conversions over DFM-3 as a result of endothermic nature of the DER reaction (ΔH^0_{25} = 428.1 kJ/mol). In both cases, a sharp increase in conversion was observed by increasing the temperature to 600 °C followed by a monotonic increase from 600 to 700 °C. These results suggest that for CO_2-DER reaction to occur with maximum conversion for both reactants over Ni-loaded K-Ca double salt, the reaction temperature should be maintained at 600-700 °C.

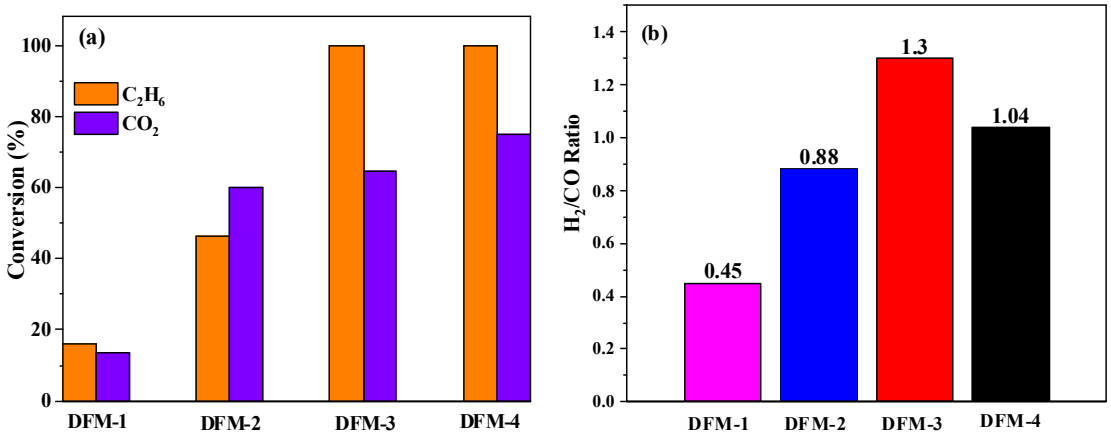

Figure 7. (a) C_2H_6 and CO_2 conversion, and (b) H_2/CO ratio for adsorbent-catalyst materials.

The yield of CO, H_2, and CH_4 were also estimated from the GC data and the results are presented in Figure 8b as a function of temperature. Importantly, the yield of CH_4 experienced a 40% enhancement upon raising temperature from 400 to 600 °C, while beyond 600 °C, it dropped to 11.2%. This trend could be explained by the fact that DFM-

3 favored the ethane decomposition reaction (eq. 7) at temperatures below 600 °C, while beyond that the conversion decreased due to the exothermic nature of this reaction (ΔH^0_{25} = - 66 kJ/mol). Furthermore, the increase in CO yield from 28.6 to 32.5% upon raising temperature from 600 to 550 °C was due to the RWGS reaction which is typically favorable at 550 °C.

To better understand the role of support on catalytic behavior of the DFMs, we performed the CO_2-DER experiments over Ni_{20}@γ-Al_2O_3, Ni_{20}@K-Ca, and Ni_{20}@(K-Ca)$_{50}$(γ-Al_2O_3)$_{50}$ (DFM-3) materials at 650 °C, and the corresponding conversion rates are

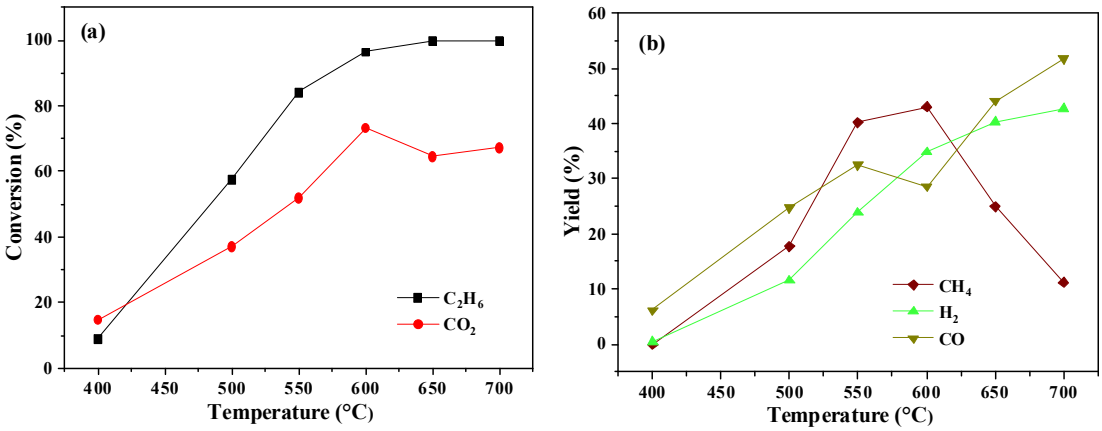

Figure 8. Effect of temperature on (a) C_2H_6 and CO_2 conversion and (b) CO, H_2, and CH_4 yields over DFM-3.

illustrated in Figure S2, Supporting Information. What was noticeable here was the comparable activity of the DFM-3 to that of Ni-loaded γ-Al_2O_3 sample indicating that the presence of double salt did not adversely impact the catalytic behavior of the Ni_{20}@γ-Al_2O_3. While DFM-3 exhibited conversions of 65 and 100% for CO_2 and C_2H_6, respectively, the Ni_{20}@γ-Al_2O_3 and Ni_{20}@K-Ca gave rise to conversions of 68.5 and 84.3%

for CO_2, and 99.8 and 62.6% for C_2H_6, respectively. The enhancement in C_2H_6 conversion over DFM-3 was originated from the cooperation of the adsorbent-support with the catalyst nanoparticles.

The long-term stability of the DFM-3 was also evaluated in DER reaction at 650 °C. Shown in Figure 9 are reactants conversion and products yield as a function of time on stream. The material showed a stable conversion for both CO_2 and C_2H_6 reactants, and yield for H_2 and CO during a 10 h durability run at 650 °C. A slight drop in CO_2 conversion and CO yield (< 5%) was noted after 10 h. Such a stable catalytic performance could be attributed to the low degree of coke deposition during the reaction, as will be verified later.

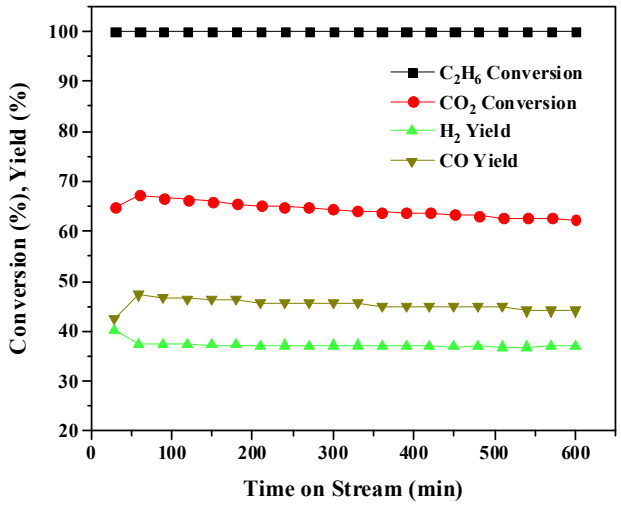

Figure 9. Reactants conversion and products yield over DFM-3 as a function of time on stream obtained at 650 °C.

3.4. COMBINED ADSORPTION-REACTION RUNS

Before performing combined adsorption-reaction runs, the CO_2 desorption in the presence of C_2H_6 from DFMs was evaluated on TGA by first exposing the material to 10% CO_2/N_2 at 650 °C for 30 min and then to 5% C_2H_6/N_2 for another 30 min to mimic the

situation in the packed-bed reactor. The comparison of CO_2 desorption profiles from DFM-3 under pure N_2 and C_2H_6 is depicted in Figure 10. The total amount of adsorbed CO_2 was completely desorbed by C_2H_6 as it was the case for N_2, however with a faster desorption rate. Notably, the additional drop in the weight below initial weight could be ascribed to the catalyst reduction by H_2 gas which was produced from the reaction of CO_2 and C_2H_6 (eq. 1). Moreover, for desorption/reaction under 5% C_2H_6/N_2 atmosphere, subsequent increase in the weight after complete CO_2 desorption could be attributed it to the adsorption of C_2H_6 on the surface of the DFM. These results clearly demonstrate that the material is fully regenerable in the presence of C_2H_6 and that the adsorbed CO_2 completely desorbs for subsequent reaction with C_2H_6 at the same temperature. It should be pointed out that a similar desorption trend was observed for the other three DFMs. For combined CO_2 capture and methanation process over DFMs, Farrauto and co-workers[7,8,41,42] showed that the desorbed CO_2 from adsorption sites spills over to the catalyst sites where the reaction with H_2 takes place. We hypothesize that for our combined CO_2 capture-utilization process over the investigated DFMs, a similar mechanism could be considered by which the spillover of desorbed CO_2 from adsorption sites of double salt to Ni catalyst sites occurs during DER reaction. Proving this hypothesis however requires a detailed molecular investigation which is beyond the scope of this study.

The combined adsorption-reaction results obtained from packed-bed reactor experiments are presented in Figure 11 for the four DFMs. The runs consisted of two steps, namely adsorption and reaction. During the first step, 10% CO_2/N_2 was fed into the reactor until (or close to) the bed saturation. At the beginning of the capture step, there was no or little CO_2 detected at the exit of the reactor. The CO_2 concentration in the effluent gas

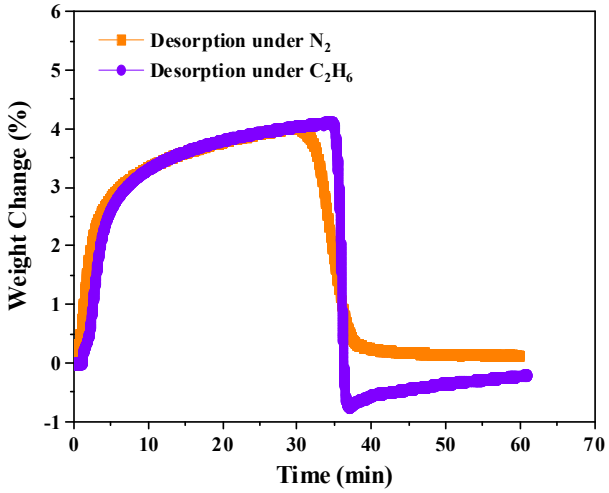

Figure 10. The adsorption-desorption/reaction profiles for DFM-3 under N_2 and C_2H_6/N_2 at 650 °C using TGA.

increased gradually when the bed was saturated which indicated the time for beginning of the second step. Investigation of the effluent gas composition during the first step showed that more CO_2 adsorbed over DFM-3 than over other materials with a breakthrough time of 10 min and with a steeper front, in agreement with the TGA results, discussed previously (see Figure 1).

The reaction step proceeded by switching the 10% CO_2/N_2 to 5% C_2H_6/N_2 during which the pre-adsorbed CO_2 on the surface was reacted with C_2H_6 to produce syngas. The WHSV was maintained at 2250 mL/g.h. Similar to reaction-alone tests, small amount of methane was also obtained in the effluent stream due to the side reactions. Although most of the desorbed CO_2 reacted with C_2H_6, there was negligible amount of unreacted CO_2 detected at the reactor exit as well. For the DFMs with low Ni content (Mg-based materials), the side reactions related to cracking that produced CH_4 were suppressed as compared with the high Ni-impregnated DFMs (Ca-based materials), as shown in Figure 11a and 11b. As with DFM-1, no CH_4 was detected in the product stream, however, small

amount of C_2H_4 was obtained. It is also worth mentioning here that smaller amounts of H_2 and CH_4 were obtained over DFM-1 (Figure 11b). As Ni loading increased from 10 to 20 wt%, the side reactions related to cracking were promoted. In the case of DFM-4 (Figure 11c), the concentration of CH_4 was higher than that of DFM-3, however, the situation was reversed for H_2 concentration. In agreement with the reaction-alone results, no C_2H_6 was detected at the effluent gas during the DER reaction over DFM-3, as demonstrated in Figure 11d. Importantly, the H_2 concentration was enhanced even after CO_2 was consumed, suggesting that this adsorbent-catalyst also favors ethane and methane crackings (eqs. 7 and 8). Moreover, it was found that the amount of CO produced over K-promoted DFMs was higher than that over Na-promoted DFMs mainly due to the increase in CO selectivity of Ni by K which reduces the activation energy of CO formation.[43] It can be concluded that DFM-3 favors methane cracking more than ethane cracking, whereas, DFM-4 favors ethane cracking.

The obtained results suggest that to improve the selectivity toward syngas, it is necessary to optimize the catalyst content in order to inhibit the cracking side reactions that produce methane. Moreover, comparison of the combined capture-reaction results with those of adsorption-, and reaction-alone steps indicated that in a combined-fashion, the adsorptive and catalytic performance of the DFMs are similar to those in uncombined system. In order to verify the low degree of coke formation during DER reaction over DFMs at 650 °C, the spent materials were evaluated by TGA and their weight loss in the temperature range of 25-800 °C was recorded, as shown in Figure 12. The maximum weight loss was obtained for DFM-3 with 9.0 wt% suggesting the highest degree of coke

deposition over this material whereas, DFM-1, DFM-2, and DFM-4 exhibited smaller weight losses (2, 3, and 6 wt%). The higher degree of coke formation over DFM-3 and DFM-4 could be attributed to the higher density of strong acid sites which favor methane cracking[38] and result in deposition of more carbon species on the materials surface, as verified by NH_3-TPD results.

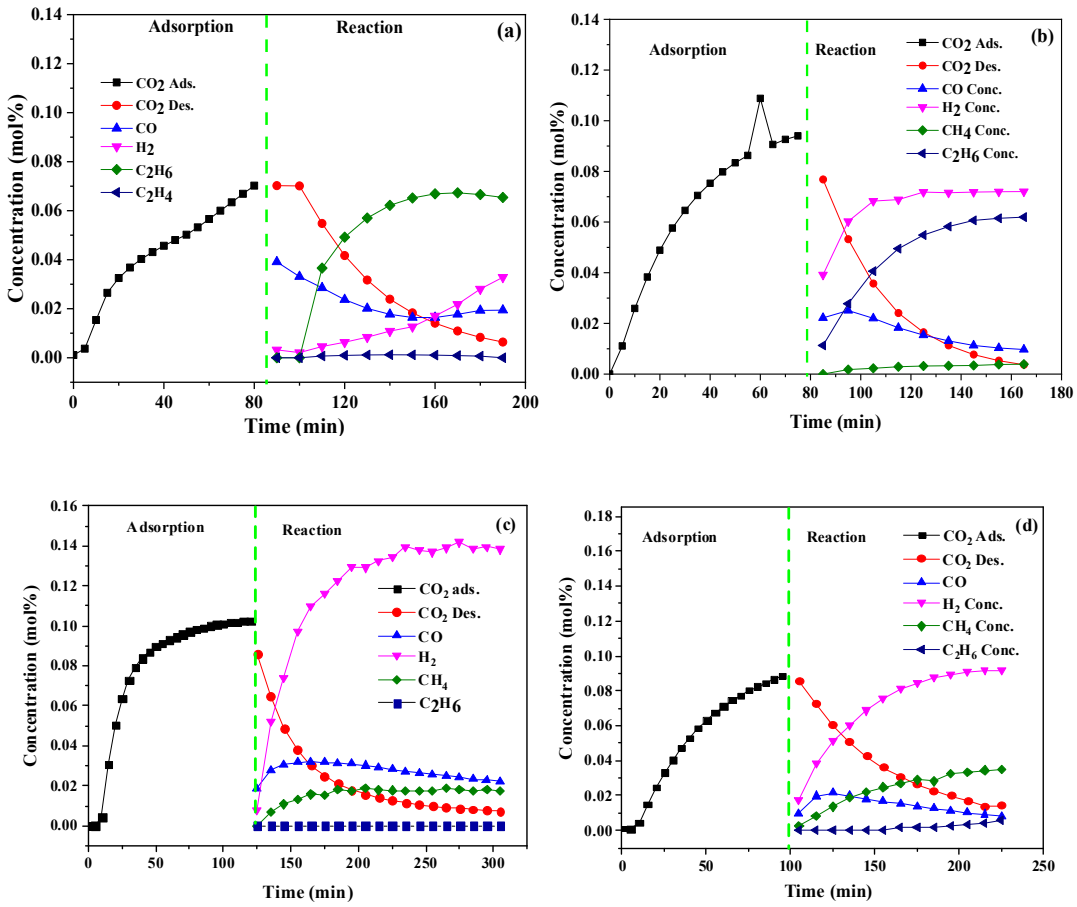

Figure 11. Adsorption-reaction profiles obtained at 650 °C for (a) DFM-1, (b) DFM-2, (c) DFM-3, and (d) DFM-4.

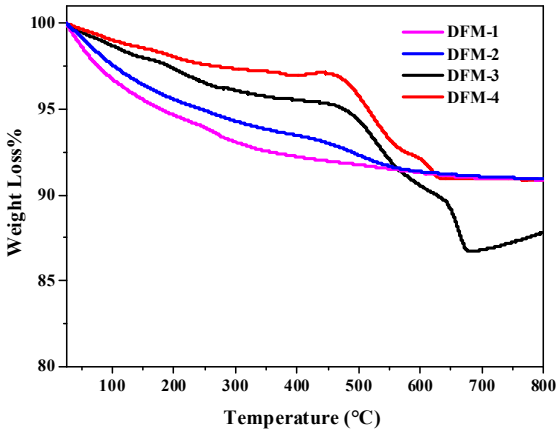

Figure 12. TGA curves for the spent DFMs after DER reaction.

4. CONCLUSIONS

In summary, we report a combined CO_2 capture-utilization process for producing syngas through DER reaction pathway over several Ni-impregnated double salt materials. The adsorption, desorption, and reaction behavior of the DFM materials at 650 °C was systematically investigated and it was demonstrated that Ca-based DFMs not only exhibit higher CO_2 capacity than their Mg-based analogues but also higher catalytic activity. Our results indicated that the best performing DFM, DFM-3 (Ni_{20}@(K-Ca)$_{50}$/(γ-Al_2O_3)$_{50}$), exhibited CO_2 adsorption and desorption capacities of 0.99 and 0.95 mmol/g, respectively, while CO_2 conversion of 65% and C_2H_6 conversion of 100% were achieved over this material. Nevertheless, its relatively high Ni content (20 wt%) led to higher coke formation as a result of cracking side reactions. Despite this, its long-term performance was not severely impacted by coke formation and it showed a relatively stable performance during 600 min time on stream with only 5% drop in activity. Moreover, analysis of the spent DFMs revealed maximum 9 wt% coke deposition during DER reaction. The results

reported in this investigation propose a novel integrated process for capture and utilization of CO_2 in syngas production and highlight the suitability of Ni-impregnated supported double salts in CO_2-DER reaction. To improve their capture/reaction efficiency and to inhibit the side reactions, it is imperative to optimize their chemical and physical properties.

ACKNOWLEDGEMENT

This work was supported by the University of Missouri Research board (UMRB). A. Al-Mamoori would like to acknowledge the Iraq's Ministry of Education for financially supporting his PhD study. The authors also acknowledge the Material Research Center (MRC) at Missouri University of Science and Technology for SEM and XRD.

REFERENCES

(1) U.S. Energy Information Administration. Annual Energy Outlook. *DOE/EIA* **2015**, *0383*, 1–154.

(2) Leung, D. Y. C. C.; Caramanna, G.; Maroto-Valer, M. M. An Overview of Current Status of Carbon Dioxide Capture and Storage Technologies. *Renew. Sustain. Energy Rev.* **2014**, *39*, 426–443.

(3) Boysen, L. R.; Brovkin, V.; Arora, V. K.; Cadule, P.; de Noblet-Ducoudré, N.; Kato, E.; Pongratz, J.; Gayler, V. Global and Regional Effects of Land-Use Change on Climate in 21st Century Simulations with Interactive Carbon Cycle. *Earth Syst. Dyn.* **2014**, *5* (2), 309–319.

(4) Al-Mamoori, A.; Krishnamurthy, A.; Rownaghi, A. A.; Rezaei, F. Carbon Capture and Utilization Update. *Energy Technol.* **2017**, *5* (6), 834–849.

(5) Duyar, M. S.; Farrauto, R. J.; Castaldi, M. J.; Yegulalp, T. M. In Situ CO_2 Capture Using CaO/γ -Al_2O_3 Washcoated Monoliths for Sorption Enhanced Water Gas Shift Reaction. *Ind. Eng. Chem. Res.* **2014**, *53*, 1064–1072.

(6) Duyar, M. S.; Arellano, M. A.; Farrauto, R. J. Dual Function Materials for CO_2 Capture and Conversion Using Renewable H2. *Appl. Catal. B Environ.* **2015**, *168*, 370–376.

(7) Duyar, M. S.; Wang, S.; Arellano-Treviño, M. A.; Farrauto, R. J. CO_2 Utilization with a Novel Dual Function Material (DFM) for Capture and Catalytic Conversion to Synthetic Natural Gas: An Update. *J. CO_2 Util.* **2016**, *15*, 65–71.

(8) Janke, C.; Duyar, M. S.; Hoskins, M.; Farrauto, R. Applied Catalysis B : Environmental Catalytic and Adsorption Studies for the Hydrogenation of CO_2 to Methane. *"Applied Catal. B, Environ.* **2014**, *152–153* (1), 184–191.

(9) Miguel, C. V; Soria, M. A.; Mendes, A.; Madeira, L. M. A Sorptive Reactor for CO_2 Capture and Conversion to Renewable Methane. *Chem. Eng. J.* **2017**, *322*, 590–602.

(10) Bobadilla, L. F.; Riesco-García, J. M.; Penelás-Pérez, G.; Urakawa, A. Enabling Continuous Capture and Catalytic Conversion of Flue Gas CO_2 to Syngas in One Process. *J. CO_2 Util.* **2016**, *14*, 106–111.

(11) Al-Mamoori, A.; Thakkar, H.; Li, X.; Rownaghi, A. A.; Rezaei, F. Development of Potassium- and Sodium-Promoted CaO Adsorbents for CO_2 Capture at High Temperatures. *Ind. Eng. Chem. Res.* **2017**, *56*, 8292−8300.

(12) AlSabban, B.; Falivene, L.; Kozlov, S. M.; Aguilar-Tapia, A.; Ould-Chikh, S.; Hazemann, J. L.; Cavallo, L.; Basset, J. M.; Takanabe, K. In-Operando Elucidation of Bimetallic CoNi Nanoparticles during High-Temperature CH_4/CO_2 reaction. *Appl. Catal. B Environ.* **2017**, *213*, 177–189.

(13) Zhao, B.; Yan, B.; Yao, S.; Xie, Z.; Wu, Q.; Ran, R.; Weng, D.; Zhang, C.; Chen, J. G. $LaFe_{0.9}Ni_{0.1}O_3$ perovskite Catalyst with Enhanced Activity and Coke-Resistance for Dry Reforming of Ethane. *J. Catal.* **2018**, *358*, 168–178.

(14) Pakhare, D.; Spivey, J. A Review of Dry (CO_2) Reforming of Methane over Noble Metal Catalysts. *Chem. Soc. Rev.* **2014**, *43*.

(15) Myint, M. N. Z.; Yan, B.; Wan, J.; Zhao, S.; Chen, J. G. Reforming and Oxidative Dehydrogenation of Ethane with CO_2 as a Soft Oxidant over Bimetallic Catalysts. *J. Catal.* **2016**, *343*, 168–177.

(16) Rodriguez, G.; Roger, A. C.; Bedel, L.; Udron, L.; Carballo, L.; Kiennemann, A. Dry Reforming of Ethane on Tri-Metallic Perovskites ($LaCo_xFe_{1-x}O_3$). Characterisations and Reactivity . *Fuel Chem. Div. Perprints* **2002**, *47* (1), 260–261.

(17) Yan, B.; Yang, X.; Yao, S.; Wan, J.; Myint, M. N. Z.; Gomez, E.; Xie, Z.; Kattel, S.; Xu, W.; Chen, J. G. Dry Reforming of Ethane and Butane with CO_2 over PtNi/CeO_2 Bimetallic Catalysts. *ACS Catal.* **2016**, *6* (11), 7283–7292.

(18) Hyun, C.; Mun, S.; Bong, K. Characteristics of Na – Mg Double Salt for High-Temperature CO_2 Sorption. *Chem. Eng. J.* **2014**, *258*, 367–373.

(19) Hyun, C.; Jae, H.; Chul, H.; Kwon, S.; Goo, S.; Bong, K. Effect of PH-Controlled Synthesis on the Physical Properties and Intermediate-Temperature CO_2 Sorption Behaviors of K – Mg Double Salt-Based Sorbents. *Chem. Eng. J.* **2016**, *294*, 439–446.

(20) Al-Mamoori, A.; Thakkar, H.; Li, X.; Rownaghi, A. A.; Rezaei, F. Development of Potassium- and Sodium-Promoted CaO Adsorbents for CO_2 Capture at High Temperatures. *Ind. Eng. Chem. Res.* **2017**, *56* (29), 8292–8300.

(21) Hassani Rad, S. J.; Haghighi, M.; Alizadeh Eslami, A.; Rahmani, F.; Rahemi, N. Sol-Gel vs. Impregnation Preparation of MgO and CeO_2 doped Ni/Al_2O_3 nanocatalysts Used in Dry Reforming of Methane: Effect of Process Conditions, Synthesis Method and Support Composition. *Int. J. Hydrogen Energy* **2016**, *41* (11), 5335–5350.

(22) Chaikittisilp, W.; Kim, H. J.; Jones, C. W. Mesoporous Alumina-Supported Amines as Potential Steam-Stable Adsorbents for Capturing CO_2 from Simulated Flue Gas and Ambient Air. *Energy and Fuels* **2011**, *25* (11), 5528–5537.

(23) Lee, C. H.; Mun, S.; Lee, K. B.; Hyun, C.; Mun, S.; Bong, K.; Lee, C. H.; Mun, S.; Lee, K. B.; Hyun, C.; et al. Characteristics of Na-Mg Double Salt for High-Temperature CO_2 Sorption. *Chem. Eng. J.* **2014**, *258*, 367–373.

(24) Harada, T.; Simeon, F.; Hamad, E. Z.; Hatton, T. A. Alkali Metal Nitrate-Promoted High-Capacity MgO Adsorbents for Regenerable CO_2 Capture at Moderate Temperatures. *Chem. Mater.* **2015**, *27* (6), 1943–1949.

(25) Qiao, Y.; Wang, J.; Zhang, Y.; Gao, W.; Harada, T.; Huang, L.; Hatton, T. A.; Wang, Q. Alkali Nitrates Molten Salt Modified Commercial MgO for Intermediate-Temperature CO_2 Capture: Optimization of the Li/Na/K Ratio. *Ind. Eng. Chem. Res.* **2017**, *56* (6), 1509–1517.

(26) Harada, T.; Hatton, T. A. Colloidal Nanoclusters of MgO Coated with Alkali Metal Nitrates/Nitrites for Rapid, High Capacity CO_2 Capture at Moderate Temperature. *Chem. Mater.* **2015**, *27* (23), 8153–8161.

(27) Xiao, G.; Singh, R.; Chaffee, A.; Webley, P. Advanced Adsorbents Based on MgO and K2CO3 for Capture of CO2 at Elevated Temperatures. *Int. J. Greenh. Gas Control* **2011**, *5* (4), 634–639.

(28) Gruene, P.; Belova, A. G.; Yegulalp, T. M.; Farrauto, R. J.; Castaldi, M. J. Dispersed Calcium Oxide as a Reversible and Efficient CO_2-Sorbent at Intermediate Temperatures. *Ind. Eng. Chem. Res.* **2011**, *50*, 4042–4049.

(29) Xu, L.; Song, H.; Chou, L. Carbon Dioxide Reforming of Methane over Ordered Mesoporous NiO-MgO-Al_2O_3 composite Oxides. *Appl. Catal. B Environ.* **2011**, *108–109*, 177–190.

(30) Hou, Z.; Yokota, O.; Tanaka, T.; Yashima, T. Characterization of Ca-Promoted Ni/α-Al_2O_3 Catalyst for CH_4 Reforming with CO_2. *Appl. Catal. A Gen.* **2003**, *253* (2), 381–387.

(31) Alipour, Z.; Rezaei, M.; Meshkani, F. Effect of Alkaline Earth Promoters (MgO, CaO, and BaO) on the Activity and Coke Formation of Ni Catalysts Supported on Nanocrystalline Al_2O_3 in Dry Reforming of Methane. *J. Ind. Eng. Chem.* **2014**, *20* (5), 2858–2863.

(32) Roh, H.-S.; Jun, K.-W. Carbon Dioxide Reforming of Methane over Ni Catalysts Supported on Al_2O_3 Modified with La_2O_3, MgO, and CaO. *Catal. Surv. from Asia* **2008**, *12* (4), 239–252.

(33) Taylor, M.; Ndifor, E. N.; Garcia, T.; Solsona, B.; Carley, A. F.; Taylor, S. H. Deep Oxidation of Propane Using Palladium-Titania Catalysts Modified by Niobium. *Appl. Catal. A Gen.* **2008**, *350* (1), 63–70.

(34) Xu, Z.; Zhen, M.; Bi, Y.; Zhen, K. Catalytic Properties of Ni Modified Hexaaluminates $LaNi_yAl_{12-y}O_{19-\delta}$ for CO_2 Reforming of Methane to Synthesis Gas. *Appl. Catal. A Gen.* **2000**, *198*, 267–273.

(35) Zhang, X.; Yang, C.; Zhang, Y.; Xu, Y.; Shang, S.; Yin, Y. Ni-Co Catalyst Derived from Layered Double Hydroxides for Dry Reforming of Methane. *Int. J. Hydrogen Energy* **2015**, *40* (46), 16115–16126.

(36) Heracleous, E.; Lemonidou, A. A. Ni–Nb–O Mixed Oxides as Highly Active and Selective Catalysts for Ethene Production via Ethane Oxidative Dehydrogenation . Part II : Mechanistic Aspects and Kinetic Modeling. *J. Catal.* **2006**, *237*, 175–189.

(37) Deng, S.; Li, H.; Li, S.; Zhang, Y. Activity and Characterization of Modified Cr_2O_3/ZrO_2 nano-Composite Catalysts for Oxidative Dehydrogenation of Ethane to Ethylene with CO_2. *J. Mol. Catal. A Chem.* **2007**, *268* (1–2), 169–175.

(38) Seo, H. Recent Scientific Progress on Developing Supported Ni Catalysts for Dry (CO_2) Reforming of Methane. *Catalysts* **2018**, *8* (3), 110.

(39) Porosoff, M. D.; Myint, M. N. Z.; Kattel, S.; Xie, Z.; Gomez, E.; Liu, P.; Chen, J. G. Identifying Different Types of Catalysts for CO_2 Reduction by Ethane through Dry Reforming and Oxidative Dehydrogenation. *Angew. Chemie - Int. Ed.* **2015**, *54* (51), 15501–15505.

(40) Cao, Y.; Gao, Z.; Jin, J.; Zhou, H.; Cohron, M.; Zhao, H.; Liu, H.; Pan, W. Synthesis Gas Production with an Adjustable H_2/CO Ratio through the Coal Gasification Process: Effects of Coal Ranks And Methane Addition. *Energy & Fuels* **2008**, *22* (3), 1720–1730.

(41) Farrauto, R. J.; Duyar, M. S.; Arellano, M. a. Dual Function Materials for CO_2 Capture and Conversion Using Renewable H2. *Appl. Catal. B Environ.* **2015**, *168*, 370–376.

(42) Zheng, Q.; Farrauto, R.; Chau Nguyen, A. Adsorption and Methanation of Flue Gas CO_2 with Dual Functional Catalytic Materials: A Parametric Study. *Ind. Eng. Chem. Res.* **2016**, *55* (24), 6768–6776.

(43) Hu, L.; Urakawa, A. Continuous CO_2 capture and Reduction in One Process: CO_2 methanation over Unpromoted and Promoted Ni/ZrO_2. *J. CO_2 Util.* **2018**, 25, 323-329.

IV. IMPROVING ADSORPTIVE PERFORMANCE OF CAO FOR HIGH TEMPERATURE CO_2 CAPTURE THROUGH FE AND GA DOPING

Ahmed Al-Mamoori, Shane Lawson, Ali A. Rownaghi, Fateme Rezaei*

Department of Chemical & Biochemical Engineering, Missouri University of Science and Technology, 1101 N State Street, Rolla, MO, 65409, United States

ABSTRACT

Calcium oxide is an efficient adsorbent for high temperature CO_2 capture process, however, it suffers from rapid deactivation and capacity loss after a few cycles as a result of particles sintering. Metal oxide doping is an effective strategy to address the durability issue of CaO. In this investigation, we report development of novel metal oxide-doped CaO adsorbents with high capture capacity, fast kinetics, and long-term stability. In particular, Fe and Ga with varied concentration were used as promoters to improve the adsorption performance of CaO adsorbent. The doped adsorbents comprising of 10% Fe@CaO and 10% Ga@CaO exhibited the highest adsorption capacities of 13.7, and 14.2 mmol/g, respectively at 650 ºC which were at least two folds higher than that of the bare CaO. Moreover, the doped-CaO materials showed reversible performance by desorbing almost all of the adsorbed CO_2 during desorption step at the same temperature. Through *in-situ* XRD measurements, it was shown that the carbonation under CO_2 and desorption under N_2 flow take place, resulting in efficient CO_2 capture and adsorbent regeneration. The cyclic adsorption-desorption runs demonstrated the excellent stability of the materials by retaining 95% of their initial capacity after 10 cycles. Moreover, adsorption temperature was found to have a favorable impact on CO_2 uptake over the doped adsorbents. The

findings of this study highlight the feasibility of metal doping approach for improving the adsorptive performance of CaO adsorbents that could be used for high temperature capture processes.

Keywords: CO_2 capture, Metal-doped CaO, Adsorbent, High temperature, *In-situ* XRD.

1. INTRODUCTION

Utilization of anthropogenic CO_2 emitted from large-point sources has been recently demonstrated to be a sustainable approach for production of global commodity chemicals and fuels from waste sources, while addressing the environmental concerns associated with the consequences of emitted CO_2.[1–3] In this regard, development of processes that can simultaneously capture and convert CO_2 into valuable chemicals appears to be a cost-effective approach from capital and operating costs standpoint.[4–8] Successful implementation of this technology requires bi-functional materials that can act as an adsorbent for efficient capture of CO_2 and as a catalyst for subsequent conversion of adsorbed CO_2 to fuels or chemicals.[9] However, development of such materials is quite challenging owing to the trade-offs between adsorption and reaction processes requirements. Since CO_2 conversion reaction is typically carried out at high temperatures, the adsorption capacity and long-term stability of the adsorbents are compromised at elevated temperatures, thereby rendering such bi-functional materials inefficient for efficient capture and conversion of CO_2 in a single unit operation.[10]

Calcium oxide has been identified as a suitable adsorbent for high temperature CO_2 adsorption applications, in particular, calcium looping process, owing to its high theoretical

capacity, abundant naturally, and low cost.[11–14] Despite these advantages, CaO suffers from rapid deactivation and capacity loses after multiple adsorption/desorption cycles as a result of particle sintering during high temperature carbonation step which is typically above 800 ºC, and the blockage of internal pores which increases the diffusion resistance of CO_2 through the $CaCO_3$ layer.[1516] CaO reacts with CO_2 through carbonation process at sufficiently high temperatures (~ 650 ºC) to achieve high CO_2 equilibrium conversion, as shown in equation 1.[17] However, such operating temperature is higher than the Tamman temperature of $CaCO_3$ (533 ºC), which leads to rapid reduction in surface area and pore volume, and results in agglomeration of small particles, thereby reducing its effectiveness.[18]

$$CaO_{(s)} + CO_{2(g)} \rightarrow CaCO_{3(s)} \qquad \Delta H^0_{25} = -178 \text{ kJ/mol} \qquad (1)$$

The above carbonation reaction proceeds through two sequential steps, namely, surface reaction that produces a layer of $CaCO_3$, and CO_2 diffusion through the $CaCO_3$ layer. While the former step is typically fast, the overall rate of CaO carbonation is controlled by the later step which is a slow process.[19] To continue using CaO adsorbent at high temperatures, it is imperative to address its long-term stability and effectiveness issues. The current body of research has focused primarily on enhancing the efficiency of CaO through various approaches including CaO hydration with ethanol-water solutions, modification with acids, and incorporation of inert supports to overcome the particle aggregation issues.[11,20]

In a study by Hu et al.,[11] various inert refractories such as Al-, Ti-, Mn-, Mg-, Y-, Si-, La, Zr, Ce-, Nd-, Pr- and Yb-based materials were incorporated into CaO as a support aiming at suppressing the particle sintering and it was shown that Al- and Y-based supports

exhibit excellent adsorption/desorption stability than the other materials. On the basis of their obtained results, the authors identified melting point of the support and the surface area of the adsorbent as the two key factors affecting the adsorption performance. In another investigation by Antzara et al.,[17] it was found that the addition of Al_2O_3 and ZrO_2 as promoters enhances the resistivity of CaO toward sintering and results in a stable performance. The authors attributed their improved behavior to the formation of the mixed phases of $Ca_3Al_2O_6$ and $CaZrO_3$. On the contrary, Mg- and La-promoted CaO were found to have lower adsorption capacity and less stability than the parent CaO. Most recently, Guo et al.[21] developed a series of Ce-Mn doped CaO-based adsorbents and examined the synergistic interactions between the doped metals in CO_2 capture at 600 ºC. The authors reported the enhancement in oxygen vacancy generation due to the electrons transfer between Ce and Mn which in turn improved the mobility and diffusion of O^{2-}, thereby increasing the adsorption capacity of the doped adsorbents relative to the bare CaO. It was also shown that the doped metal precluded the particle sintering and hence resulted in stable cyclic performance after 40 cycles of adsorption-desorption. Double salts based on MgO and CaO are another class of adsorbents with potential for high temperature CO_2 capture.[12,22–24] Despite high capacity, their unstable adsorption behavior over multiple cycles compromises their performance and makes them less attractive for this application. In our previous investigation,[12] we developed K_2CO_3 and Na_2CO_3 doped CaO materials and investigated their adsorption behavior. Our K-Ca and Na-Ca adsorbents exhibited relatively high capacity (10.7 and 9.5 mmol/g, respectively) at 650 °C, however, they experienced some degree of capacity loss after 10 cycles of adsorption-desorption. Other non-CaO-based adsorbents have also been developed and investigated for high temperature

CO_2 capture processes.[22,24–27] For example, hydrotalcite adsorbents are commonly used for this process owing to their stable adsorption properties at high temperatures, however, their low capture capacity renders them inefficient for such applications.[28,29]

As discussed above, the incorporation of metals into CaO adsorbent improves its equilibrium capacity and long-term stability. In addition, to impart catalytic functionality to CaO for potential use as an adsorbent-catalyst material with multifunctional properties in combined capture-utilization processes, metal doping appears to be a viable approach. However, the doped metals investigated so far have not resulted in substantial enhancement in both capture capacity and long-term stability of the CaO. Aiming at further enhancing adsorption capacity and kinetics, and stability of CaO adsorbent for CO_2 capture, we selected Fe and Ga to dope CaO and investigated their effects on adsorption behavior of the bare CaO. These metals have previously been shown to be promising candidates for catalytic utilization of CO_2 to chemicals.[30–34] To the best of our knowledge, this is the first investigation of the effect of these metals on adsorptive performance of CaO. More importantly, we aimed at performing both adsorption and desorption steps at the same temperature (650 ºC) as opposed to normal carbonation/calcination process which typically occurs in the temperature range of 700-900 ºC. This was mainly because in practice, the combined capture-utilization process should be performed isothermally to be cost-effective.[4,35–38] Herein, metal-doped CaO adsorbents with varied metal content were prepared and the best performing material in each class was selected for further analysis. The CO_2 adsorption performance of the materials was evaluated through *in-situ* XRD and cyclic adsorption-desorption experiments. The effect of adsorption temperature on adsorption capacity of the materials was also investigated.

2. MATERIALS AND METHODS

2.1. MATERIALS DEVELOPMENT

The CaO used in this investigation was purchased from fisher scientific, whereas iron(III) nitrate nonahydrate and gallium(III) nitrate hydrate were both purchased from Sigma-Aldrich. Ultrahigh purity gases including N_2 and CO_2/N_2 (10:90 by volume) were purchased from Air gas. To synthesize the materials, the commercial CaO was first calcined at 700 ºC for 5 h and then used in a wet impregnation synthesis by which metal-doped adsorbents were prepared. Briefly, various amounts of metal nitrates stated above (1, 5, 10, and 15 wt%) were dissolved in 5 mL distilled water first and the solution was then vigorously stirred using a magnetic stirrer with 400 rpm at room temperature for 12 h. Finally, the obtained materials were dried at 120 ºC for 5 h followed by calcination at 700 ºC for 3 h. The designated samples name was M_x@CaO where M = Fe, Ga, and x = 1, 5, 10, 15.

2.2. MATERIALS CHARACTERIZATION

Metal-doped CaO adsorbents were characterized by powder X-ray diffraction (PXRD) to assess their crystalline structure using a PANalytical X' pert multipurpose X-ray diffractometer with scan size of 0.02 º/step at the rate of 147.4 s/step. X-ray photoelectron spectroscopy (XPS) analysis was performed to determine the chemical composition of the metal-doped materials using Kratos Axis 165 XPS. Surface area and pore volume/size were estimated from nitrogen physisorption isotherms collected at 77 K using a Micromeritics 3Flex instrument. The samples were degassed at 350 ºC under

vacuum for 6 h prior to measurements to remove any preadsorbed gases. The methods used to evaluate specific surface area and pore size distribution were Brunauer−Emmet-Teller (BET) and nonlocal density functional theory (NLDFT) methods, respectively. Field-emission scanning electron microscopy (SEM) (Hitachi, Model S4700) was employed to assess the surface morphology of the obtained powders. The Hitachi model S4700 FE-SEM was also used in combination with Genesis software to collect energy dispersive X-ray spectroscopy (EDS) measurements across the metal-doped adsorbents.

2.3. CO_2 ADSORPTION-DESORPTION MEASUREMENTS

Thermal gravimetric analysis TGA (Q500, TA Instrument) was used to determine the CO_2 adsorption-desorption capacities. Each experiment was preceded by in-*situ* regeneration under N_2 at 650 ºC for 30 min. The gas was then switched to 10% CO_2/N_2 while keeping the temperature constant to start adsorption measurements for 1 h. Subsequent desorption was carried out at the same temperature under N_2 for 30 min. To evaluate the stability of the adsorbents, 10 cycles of adsorption-desorption runs were carried out by switching the inlet feed from 10% CO_2/N_2 during adsorption to N_2 during desorption while keeping the temperature constant at 650 ºC. For these cyclic runs, the adsorption and desorption durations were 1 h and 30 min, respectively.

2.4. *IN-SITU* XRD MEASUREMENTS

To better investigate the change in the chemical structure of the materials upon CO_2 adsorption and desorption at high temperature, *in-situ* X-ray diffraction (XRD) was performed using PANalytical X' pert multipurpose X-ray diffractometer in a similar way

as TGA experiments. The sample degassing was performed at 650 ºC for 30 min before exposing the materials to 10% CO_2/N_2. It should be pointed out here that for these measurements, the gas flow rate of N_2 or CO_2/N_2 was much lower than that for TGA runs (i.e., 10 mL/min versus 60 mL/min) due to limitation of XRD instrument. Following CO_2 adsorption, the desorption runs were carried out under N_2 at the same temperature while recording the XRD data every 5 min.

3. RESULTS AND DISCUSSION

3.1. EFFECT OF METAL CONTENT ON CO_2 ADSORPTION-DESORPTION CAPACITIES

Two sets of metal-doped CaO adsorbents containing various compositions of metals were evaluated in CO_2 adsorption-desorption process at 650 ºC to determine the optimum composition that yields the highest capacity with the best adsorption-desorption kinetics. As shown in Figure 1, the incorporation of Fe resulted in enhanced CO_2 uptake capacity of the bare CaO at all Fe compositions. Whereas the bare CaO exhibited an adsorption capacity of 6.9 mmol/g when exposed to 10%CO_2/N_2, Fe_{10}@CaO achieved the highest CO_2 capacity (13.7 mmol/g) among Fe_1@CaO, Fe_5@CaO, and Fe_{15}@CaO under the same conditions. The promotion of CO_2 uptake by Fe incorporation could be attributed to the role of oxygen ion O^{-2} in enhancing the carbonate formation during the surface reaction step, which promotes the CO_2 capture capacity. Lu et al.[39] investigated the effect of Mn, Ce, Cr, Co, and Cu based CaO adsorbents and found that CO_2 uptake depends significantly upon the onset point (i.e., the transition point from the surface reaction-controlled region to the diffusion-controlled region). Interestingly, the onset point of the

bare CaO was around 4 mmol/g which was much lower than that of the doped ones, especially the Fe_{10}@CaO with the onset point of around 11 mmol/g, which was in agreement with the previous study.[39] The transition from reaction-control to diffusion-control regime usually starts when the thickness of growing carbonate product layer reaches 22 nm.[39] Moreover, the investigation of desorption profiles indicated that the CO_2 adsorption over these materials is reversible and the adsorbed CO_2 completely desorbed from the material under N_2 flow at the same temperature.

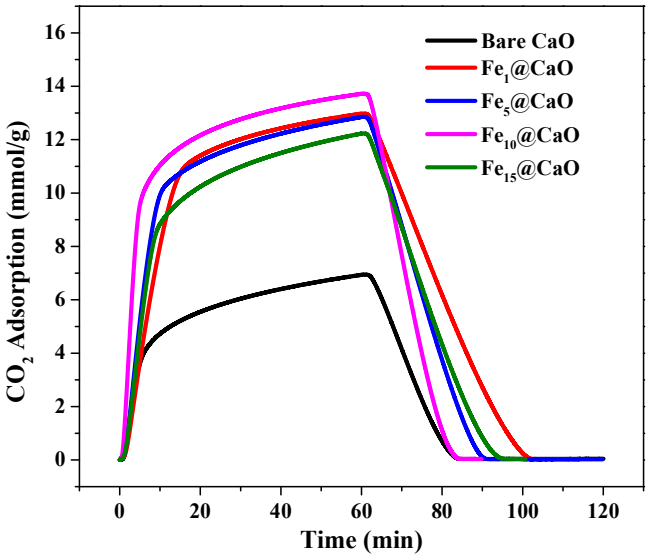

Figure 1. CO_2 adsorption-desorption profiles of Fe-doped CaO adsorbents with different Fe loadings using 10% CO_2/N_2 at 650 ºC.

The corresponding capacities and times to achieve 90% of the capacity are presented in Table 1. Remarkably, the Fe_{10}@CaO not only showed higher adsorption capacity, but also better adsorption-desorption rates relative to the bare CaO, by attaining 90% of its adsorption capacity after 22 min ($t_{ads,90\%}$) in comparison to 34 min for CaO, as

evident from the data in Table 1. Similarly, it took 19 min for this adsorbent to desorb 90% of the adsorbed CO_2 ($t_{des,90\%}$) which was 14 min faster than for the bare material.

Table 1. CO_2 adsorption-desorption capacities of Fe-based CaO adsorbents.

Adsorbent	**CO_2 adsorption capacity (mmol/g)**	**CO_2 desorption capacity (mmol/g)**	**$t_{ads,90\%}$ (min)**	**$t_{des,90\%}$ (min)**
Bare CaO	6.9	6.9	34	33
Fe_1@CaO	13.0	13.0	24	35
Fe_5@CaO	12.8	12.8	25	26
Fe_{10}@CaO	13.7	13.7	22	19
Fe_{15}@CaO	12.2	12.2	30	29

The CO_2 uptake curves in Figure 2 reveal a similar trend for Ga-based adsorbents to their Fe-based materials with Ga_{10}@CaO exhibiting the maximum uptake capacity than Ga_1@CaO, Ga_5@CaO and Ga_{15}@CaO, and with the sharpest adsorption and desorption profiles. We propose that increasing the metal content (Fe, Ga) from 1 to 10 wt% leads to enhancement of the role of O^{-2} and hence formation of more carbonate which will in turn enhance CO_2 uptake, whereas metal contents larger than 10 wt% would result in blockage of active sites on the surface of CaO and hence reduction in CO_2 uptake. Wang et al. [40] reported that as the Ce/Ca ratio increases above 15%, CO_2 capacity drops due to the blockage of CaO with CeO_2. For Ga_{10}@CaO, an adsorption capacity of 14.2 mmol/g was achieved and as was the case for the other two sets, Ga-based materials were able to fully regenerate upon N_2 flow. However, as the adsorption-desorption times in Table 2 indicate,

Ga_{10}@CaO showed much faster CO_2 uptake and release than the best performing material in Fe_x@CaO class (Fe_{10}@CaO) with $t_{90\%}$ of 10 and 17 min for adsorption and desorption of CO_2, respectively. This could be attributed to the higher surface area and pore volume of Ga_{10}@CaO than Fe_{10}@CaO, as will be discussed later and as demonstrated previously in the literature.[39]

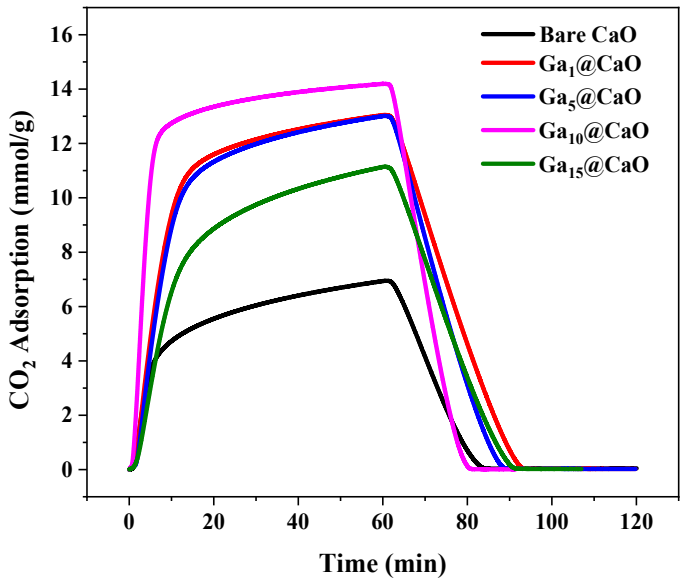

Figure 2. CO_2 adsorption-desorption profiles of Ga-doped CaO adsorbents with different Ga loadings using 10% CO_2/N_2 at 650 ºC.

The enhancement in CO_2 adsorption capacity of metal-doped adsorbents relative to the bare CaO can be attributed to the promoted oxygen mobility and vacancy generation after Fe and Ga incorporation.[21] For example, Gue et al.[21] reported that mobility of O^{2-} is a key to the capture of CO_2 for CaO-based adsorbents and showed that the presence of metals facilitates diffusion and mobility of O^{2-}, thereby enhancing the interaction of oxygen surface atoms with CO_2 molecules and subsequent carbonate (CO_3^{2-}) formation. Moreover,

the well-dispersed metal particles on the CaO surface could also be responsible for improved adsorptive properties, mainly because the CaO crystallite growth and agglomeration could be impeded.[16] Given that Fe and Ga have different oxidation states, it may explain their varied ability in promoting the CO_2 capture behavior of the CaO. Another striking feature of these screening results is that as CO_2 adsorption/desorption capacity increased, the kinetics improved as well, for instance, Ga_{10}@CaO with the highest capacity, exhibited the shortest $t_{ads,90\%}$ and $t_{des,90\%}$. Wang et al.[40] noted a similar effect for CeO_2-doped CaO and reported the fastest carbonation rate for the material with the highest capacity. Similarly, Hu et al.[39] demonstrated that the lower pore volume gives rise to slower kinetic and easier pore blockage than the higher pore volume due to the larger molar volume of $CaCO_3$ (37 cm^3/mol) than that of CaO (17 cm^3/mol). The Fe and Ga metals act as a promoter in preventing the agglomeration of CaO particles while providing oxygen ions for subsequent CO_2 capture. Also, the slightly higher surface area and pore volume of the metal-promoted CaO than those of bare CaO (Table 3) could also have effect in enhancing the adsorbent kinetic as reported previously.[39] The crystallite size of the bare and promoted CaO adsorbents was also estimated using Scherrer equation (S-1) as displayed in the Supporting Information. It was found that the crystallite size of the promoted CaO (31 and 25 nm for Fe_{10}@CaO and Ga_{10}@CaO, respectively) was smaller than that of bare CaO (39 nm). A similar finding was reported by Wang et al.[40] where doping CaO with Ce gave rise to smaller crystallite size. While the doped metal plays a significant role in preventing CaO agglomeration, the smaller crystallite size results in the exposure of more CO_2 molecules to the sorbent active sites.

Table 2. CO_2 adsorption-desorption capacities of Ga-based CaO adsorbents.

Adsorbent	CO_2 adsorption capacity (mmol/g)	CO_2 desorption capacity (mmol/g)	$t_{ads,90\%}$ (min)	$t_{des,90\%}$ (min)
Bare CaO	6.9	6.9	34	33
Ga_1@CaO	13.0	13.0	21	28
Ga_5@CaO	13.0	13.0	25	24
Ga_{10}@CaO	14.2	14.2	10	17
Ga_{15}@CaO	11.1	11.1	34	26

On the basis of the screening results presented above, Fe_{10}@CaO and Ge_{10}@CaO were selected for further analysis, as presented below. It should be pointed out here that the reported capacities for our metal-doped adsorbents are among the highest capacities reported for CaO-based adsorbents so far. Antzara et al.[17] reported sorption capacities higher than 9 mmol/g for Al- and Zr-promoted CaO at 650 °C. Additionally, a capacity of 13.9 mmol/g was reported for (Ce-Mn)-doped CaO adsorbents at 600 °C.[21]

3.2. PHYSICAL AND CHEMICAL CHARACTERISTICS OF SELECTED ADSORBENTS

Characterization of the textural properties of candidate adsorbents by N_2 physisorption at 77 K was carried out to determine their BET surface area and pore volume. As Figure 3a illustrates, typical type IV isotherms with narrow hysteresis loops were obtained for Fe_{10}@CaO and Ga_{10}@CaO, similar to their parent CaO. Interestingly, the N_2 uptake was found to be slightly higher over the metal-doped materials than over bare CaO.

The PSD profiles (Figure 3b) revealed relatively uniform mesopores with a diameter centered at approximately 4.0 nm for the three materials.

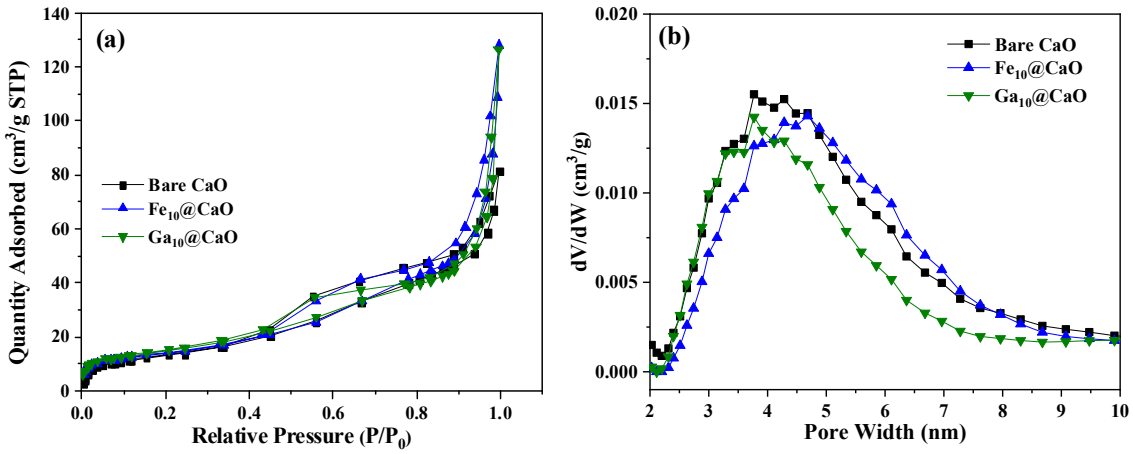

Figure 3. (a) N_2 physisorption isotherms and (b) pore size distribution profile of bare CaO and metal-doped CaO adsorbents.

From the corresponding data presented in Table 3, Fe_{10}@CaO and Ga_{10}@CaO exhibited BET surface areas of 49 and 53 m^2/g, respectively which were slightly higher than that of the bare CaO with 47 m^2/g. Pore volume of the adsorbents were also improved, albeit marginally, from 0.11 cm^3/g for the bare CaO to 0.15 and 0.16 cm^3/g for Fe_{10}@CaO and Ga_{10}@CaO. The slightly higher surface area and porosity of the metal-doped adsorbents could be attributed to the porous nature of metal oxides added to the bare CaO. Similar trends were reported by Guo et al.[21] for Ce-doped CaO materials. To determine the oxidation states and binding energy of the metal oxides, XPS analysis was performed and the binding energy curves for Ca2p, O1s, Fe2p, and Ga2p are depicted in Figure 4. As Figure 4a reveals, the doublet peaks of Ca2p1/2 and Ca2p3/2 with a separation of ~3.5 eV were observed, which are representative of Ca^{2+}.

Table 3. Textural properties of CaO and metal-based CaO adsorbents.

Adsorbents	BET surface area (m^2/g)	Pore volume (cm^3/g)	Pore width (nm)
Bare CaO	47	0.11	3.7
Fe_{10}@CaO	49	0.15	4.6
Ga_{10}@CaO	53	0.16	3.7

Compared to the bare CaO, a clear shift in the position of these peaks to the higher binding energies was observed for the metal-doped materials, indicating the improvement in electron transfer ability of Ca to the surface oxygen atoms that transfer oxygen to CO_2 during adsorption process.[21] Considering the O1s spectrum shown in Figure 4b, the peak at 530 eV is assigned to the oxygen in CaO and doped metal oxide. It was observed that the peak location was shifted to the higher binding energies for the metal-doped adsorbents, implying the enhancement in oxygen mobility of these materials. It was also noted that the intensity of the O1s peak was reduced indicating the relative content of oxygen species on the adsorbents was reduced due to the oxygen vacancy generation after incorporation of the metals. As evident from Figure 4c, the presence of Fe was confirmed by Fe2p peak appearing at 711 eV and a satellite peak at 724 eV which are related to Fe_2O_3.[414243] Similarly, as depicted in Figure 4d**,** Ga2p peak appeared at 1119 along with a satellite peak 1143 eV which are assigned to Ga_2O_3.[44]

To determine the composition of the metal-doped adsorbents, elemental mapping was performed on the SEM images taken from the selected samples. The EDS spectra shown in Figure 5, confirm the presence of elements used for doping. In addition to the

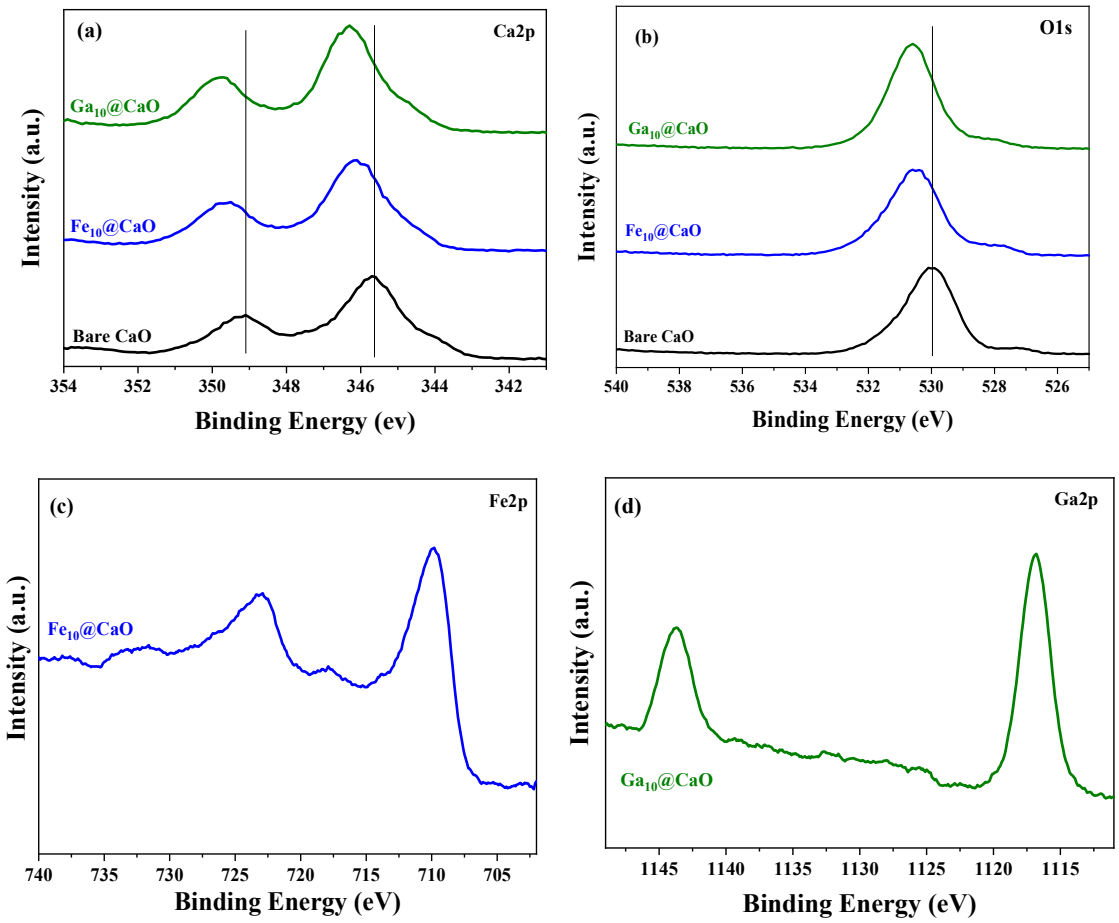

Figure 4. High resolution XPS spectra of (a) Ca2p, (b) O1s, (c) Fe2p, and (d) Ga2p for CaO and metal-doped CaO adsorbents.

doped metals, other elements such as Ca, O, and C were also detected with Ca and O being the most predominant elements, as expected. It should be noted here that the presence of C stems partly from the $CaCO_3$ compound that is present in the fresh CaO, as also shown by other researchers [45] and partly from carbon tape used for sample coating. Moreover, the SEM images show different surface morphology for two types of adsorbents investigated here. The elemental mapping of the promoted CaO was also obtained from EDS analysis

for Fe and Ga. It is evident that the metals dispersed uniformly within the adsorbent which further confirmed the successful impregnation of the metals in the CaO.

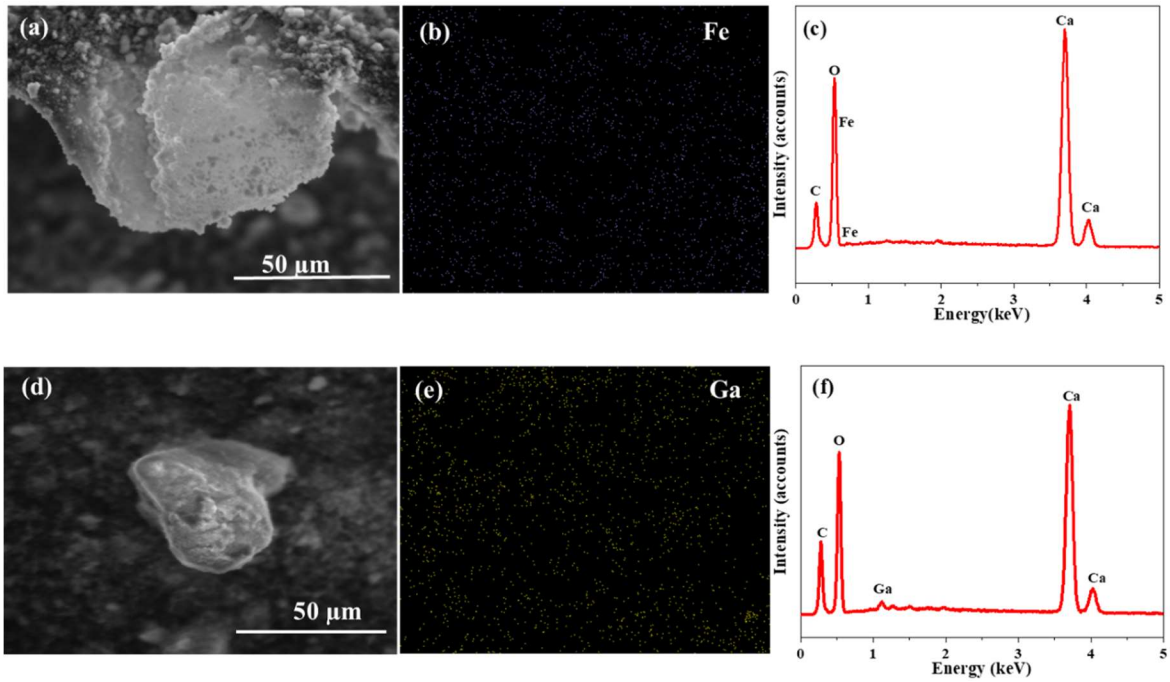

Figure 5. SEM images, elemental mapping and EDS measurements of (a-c) Fe_{10}@CaO and (d-f) Ga_{10}@CaO adsorbents.

3.3. CO_2 ADSORPTIVE BEHAVIOR OF SELECTED ADSORBENTS

The *in-situ* XRD experiments were conducted to better investigate the variation in the crystalline structure of the selected adsorbents during CO_2 adsorption-desorption. The analysis of XRD patterns of Fe_{10}@CaO in Figure 6 revealed that the characteristics peaks of the material were retained during both adsorption and desorption steps, however, the intensity of CaO and $CaCO_3$ peaks changed under CO_2 and N_2 flows. As clear from Figure 6a, the CaO peaks at 32º, 37º, and 54º decreased in intensity upon CO_2 adsorption, whereas the intensity of $CaCO_3$ peaks at 29º, 36º, 43º, 47º, and 48º increased after 25 min of

adsorption. On the other hand, we observed an opposite trend upon CO_2 desorption under N_2, as shown in Figure 6b wherein the CaO peaks became stronger while the $CaCO_3$ experienced reduction in intensity. Nevertheless, the original positions of the peaks remained unchanged. Notably, the crystalline structure of the Fe_{10}@CaO after complete desorption (at t = 25 min) was found to be almost identical to that of fresh sample, indicating a stable crystalline structure.

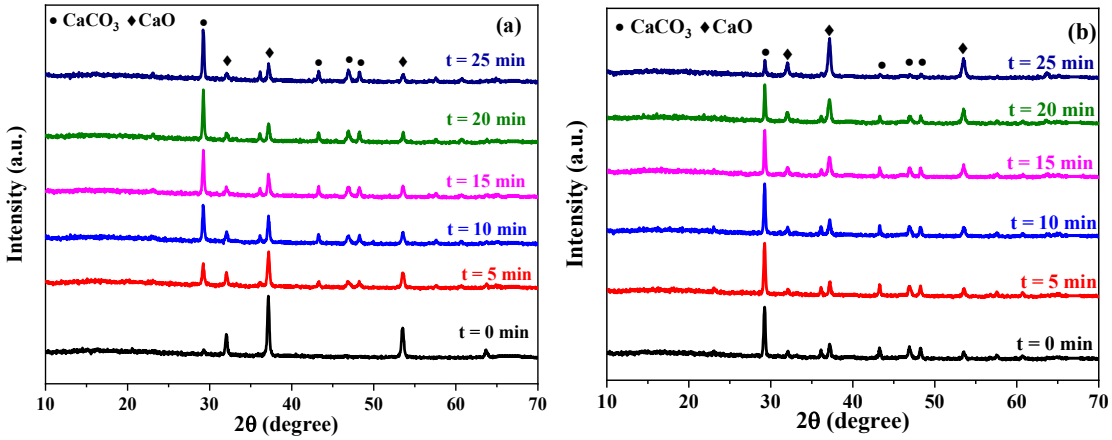

Figure 6. *In-situ* XRD spectra of Fe_{10}@CaO under (a) CO_2 and (b) N_2 at 650 ºC.

Similar *in-situ* XRD adsorption-desorption experiments were carried out over Ga_{10}@CaO. The *in-situ* XRD patterns of Ga_{10}@CaO during adsorption under CO_2 and desorption under N_2 are illustrated in Figure 7. The reversible formation of $CaCO_3$ upon CO_2 capture and release was confirmed by the change in the intensity of XRD peaks associated with CaO and $CaCO_3$ during adsorption and desorption. As it was the case for Fe_{10}@CaO, the intensity of the prominent peaks associated with CaO (32º, 37º, 54º) was reduced as a result of reaction with CO_2 and subsequent conversion to $CaCO_3$, evident from increased intensity of the $CaCO_3$ peaks (in particular, 29º, 36º, 43º) as the adsorption

progressed over time (Figure 7a). Similarly, the structural changes of the material during regeneration under N_2 flow (Figure 7b) were exactly the opposite of those during adsorption.

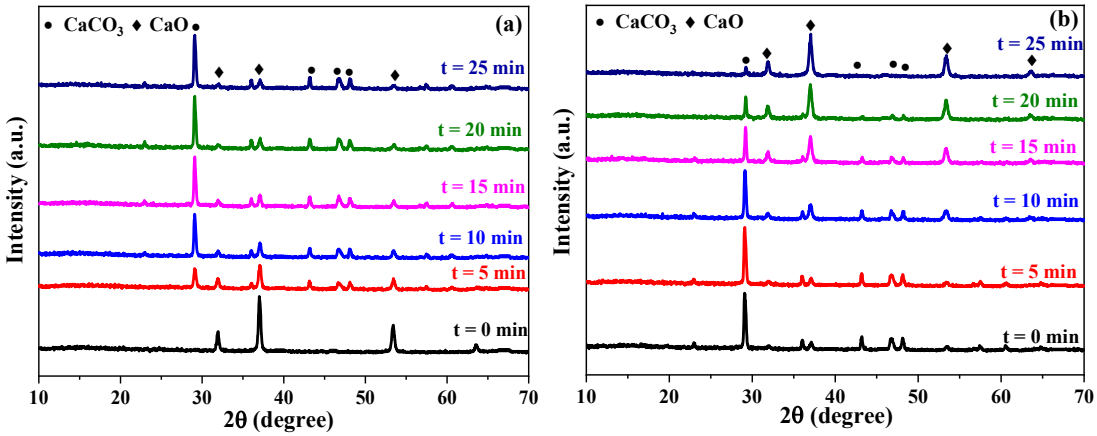

Figure 7. *In-situ* XRD spectrum of Ga_{10}@CaO under (a) CO_2 and (b) N_2 at 650 ºC.

The mechanism of CO_2 adsorption on the surface of CaO (equation 1) could be realized from the pathways steps shown in equations 2-4. First, gaseous CO_2 molecule adsorb on the adsorbent surface (equation 2), then the CO_2 combines with surface oxygen ion (O^{2-}) to form CO_3^{2-} (equation 3). Finally, CO_3^{2-} ion combines with CaO to produce $CaCO_3$ (equation 4).

$$CO_{2(g)} \rightarrow CO_{2(ads)} \quad (2)$$

$$CO_{2(ads)} + O^{2-} \rightarrow CO_3^{2-} \quad (3)$$

$$CO_3^{2-} + CaO_{(s)} \rightarrow CaCO_{3(s)} + O^{2-} \quad (4)$$

The diffusion of CO_2 through the carbonate layer ($CaCO_3$) and the mobility of O^{2-} are the key factors for enhancing CO_2 capture capacity and rate in the beginning of the

diffusion-controlled reaction.[2116] The role of the doped metals is in promoting the rate of carbonate ion production (equation 3) through providing more oxygen ions, as discussed before, which in turn translates into the formation of more calcium carbonate. On the basis of these results, it appears that the CO_2 capture on the metal-doped CaO adsorbents followed the standard carbonation (during adsorption) and calcination (during desorption) reactions, shown in equation 1,[17] with the distinct difference that unlike conventional calcination step, the temperature remains the same as the carbonation step. It should be pointed out here that no diffraction peaks related to the metal oxides were detected by XRD which could be attributed to their amorphous nature in the doped samples.

To study the kinetics of CO_2 capture on the bare and promoted CaO adsorbent the double exponential model (equation 5) was used to fit the experimental uptake profiles.

$$y = A\mathrm{e}^{-k_1 t} + B\mathrm{e}^{-k_2 t} + C \tag{5}$$

In this equation, y represents CO_2 adsorption capacity, t is the adsorption time, k_1 and k_2 are the exponential rate constants for CO_2 capture when the kinetic reactions are controlled by the surface reaction and diffusion processes, respectively, A and B are corresponding constants for each process that controls the whole CO_2 capture process, and C is the y value when time approaches infinity (i.e., the maximum CO_2 capture capacity). The experimental and predicted CO_2 capture profiles for bare CaO, Fe_{10}@CaO and Ga_{10}@CaO are illustrated in Figure 8 and the corresponding fitted kinetic parameters are listed in Table 4. It is evident that for all three materials, the model was fitted the experimental trends with the R^2 values ranging between 0.980-0.996. From Table 4, the value of k_1 for the bare CaO was estimated to be ~16 times greater than k_2 implying that the CO_2 capture process was controlled mainly by the CO_2 diffusion through the $CaCO_3$ layer.

Table 4. The double exponential model parameters for bare CaO and metals-promoted CaO.

Adsorbents	k_1 **(min^{-1})**	k_2 **(min^{-1})**	***A***	***B***	***C***	R^2
Bare CaO	0.279	0.017	-5.606	-3.821	8.293	0.996
Fe_{10}@CaO	0.019	0.334	-4.245	-13.227	15.151	0.996
Ga_{10}@CaO	0.006	0.313	-3.54	-16.219	16.7	0.980

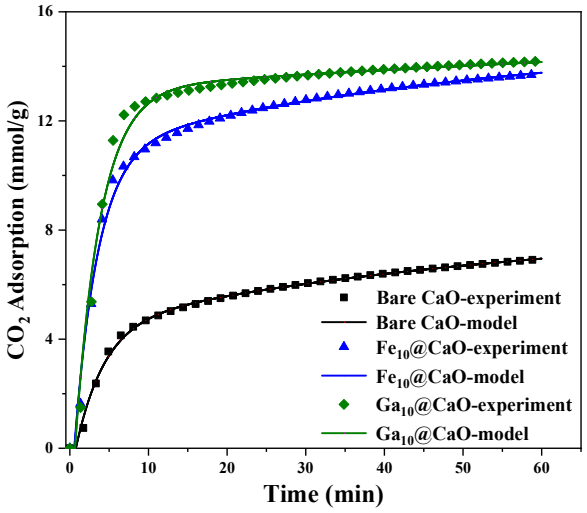

Figure 8. Experimental and model-predicted CO_2 adsorption profiles for bare CaO, Fe_{10}@CaO and Ga_{10}@CaO adsorbents at 650 ºC.

On the contrary, for Fe_{10}@CaO and Ga_{10}@CaO samples, k_2 was 52 and 18 times greater than k_1 for Ga_{10}@CaO and Fe_{10}@CaO, respectively, indicating that the surface reaction controls the reaction rate. On the basis of these results, it can be concluded that the oxygen ion transfer in the metal-promoted CaO not only enhances the CO_2 capture

capacity but also improves the CO_2 capture kinetics. The effect of temperature on adsorptive performance of selected adsorbents was evaluated by conducting CO_2 uptake measurements at three different temperatures (450, 550, and 650 ºC) while keeping other parameters constant. As evident from Figure 9, for both adsorbents, decreasing the temperature from 650 to 550 and 450 ºC resulted in lower CO_2 uptake capacity. However, the effect of temperature was noticeable for Fe_{10}@CaO and Ga_{10}@CaO with 69.6 and 60.5% drop in capacity from 650 to 450 ºC, respectively. Despite reduced uptake, the obtained capacities are still high, implying the efficacy of the materials for CO_2 adsorption in the temperature range of 450-650 ºC. Furthermore, it could be noticed that while the adsorption uptake curve became sharper at lower temperatures during the first few minutes of exposure, the overall time to reach 90% of the adsorption capacity decreased with temperature, suggesting the positive effect of temperature on adsorption kinetics. We suggest that the enhanced CO_2 adsorption capacity and kinetics exhibited by metal-doped CaO adsorbents with temperature can be considered as a result of improved Knudsen diffusion through $CaCO_3$ layer which relates to the square root of temperature.[46]

In the next step, we evaluated the cyclic performance of the candidate adsorbents through 10 consecutive adsorption-desorption runs at 650 ºC. The corresponding cyclic results are presented in Figure 10. It is evident that overall, the metal-doped CaO adsorbents retained most of their capacity. More specifically, the adsorption capacity of Fe_{10}@CaO and Ga_{10}@CaO experienced 10 and 14% drop in their initial capacity, respectively after 10 cycles of adsorption-desorption, as shown in Figure 10a and 10b. The capacity loss for these samples was much smaller than that of bare CaO under the same

testing conditions. These results demonstrate the role of doped metals in precluding the particle sintering effects and promoting the durability of CaO-based adsorbents.

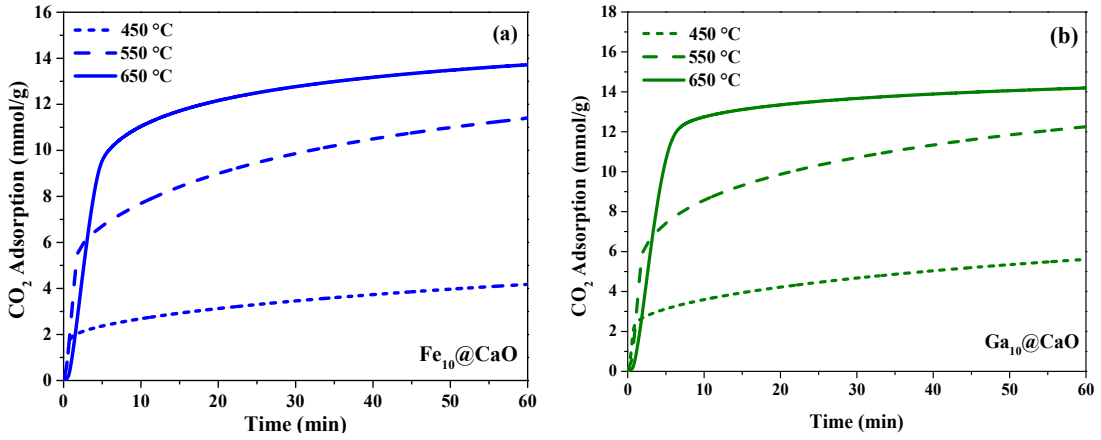

Figure 9. CO_2 adsorption capacity for (a) Fe_{10}@CaO and (b) Ga_{10}@CaO at 450, 550, and 650 ºC.

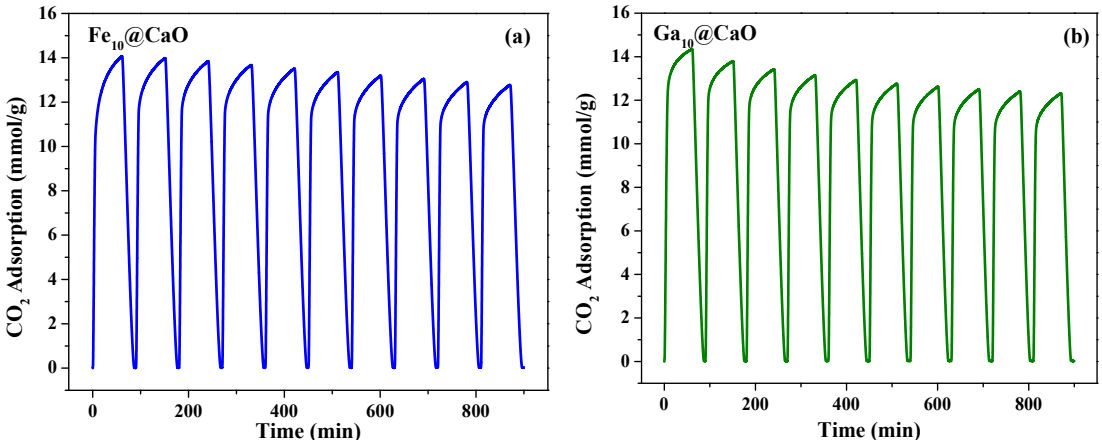

Figure 10. Cyclic CO_2 adsorption-desorption profiles for (a) Fe_{10}@CaO and (b) Ga_{10}@CaO at 650 ºC.

.

4. CONCLUSIONS

In this study, the high temperature CO_2 capture over Fe- and Ga-doped CaO adsorbents has been investigated in detail. We found that in both cases, the incorporation of metal oxide promotes capture capacity of the bare CaO. However, the extent of improvement varied significantly with the type of metal and also its content. Among the materials investigated herein, Ga_{10}@CaO exhibited the highest adsorption capacity of 14.2 mmol/g at 650 ºC with fastest adsorption rate. Moreover, the regeneration of the materials under N_2 flow at the same temperature revealed the reversible nature of CO_2 interactions with the doped materials. The *in-situ* XRD analysis further confirmed the excellent regenerability of the adsorbents and determined the mechanism of CO_2 capture over these adsorbents. The stability measurement results revealed that the degree of CaO capacity loss due to particles sintering could be lowered in the presence of doped metals. This investigation demonstrates the efficacy of metal oxide doping in addressing the stability issue of CaO-based adsorbents and highlights the suitability of Fe@CaO and Ga@CaO materials for efficient capture of CO_2 at high temperatures.

ACKNOWLEDGEMENT

This work was supported by the University of Missouri Research board (UMRB). A. Al-M. would like to acknowledge the Iraq's Ministry of Higher Education and Scientific Research/Al-Nahrain University for financially supporting his PhD study. The authors also

acknowledge Dr. Eric Bohannan of Material Research Center (MRC) for helping with *in-situ* XRD measurements.

REFERENCES

(1) Al-Mamoori, A.; Krishnamurthy, A.; Rownaghi, A. A.; Rezaei, F. Carbon Capture and Utilization Update. *Energy Technol.* **2017**, *5* (6), 834–849.

(2) Leung, D. Y. C. C.; Caramanna, G.; Maroto-Valer, M. M. An Overview of Current Status of Carbon Dioxide Capture and Storage Technologies. *Renew. Sustain. Energy Rev.* **2014**, *39*, 426–443.

(3) Atanga, M. A.; Rezaei, F.; Jawad, A.; Fitch, M.; Rownaghi, A. A. Oxidative Dehydrogenation of Propane to Propylene with Carbon Dioxide. *Appl. Catal. B Environ.* **2017**, *220*, 429–445.

(4) Farrauto, R. J.; Duyar, M. S.; Arellano, M. a. Dual Function Materials for CO_2 Capture and Conversion Using Renewable H_2. *Appl. Catal. B Environ.* **2015**, *168*, 370–376.

(5) Duyar, M. S.; Wang, S.; Arellano-Treviño, M. A.; Farrauto, R. J. CO_2 Utilization with a Novel Dual Function Material (DFM) for Capture and Catalytic Conversion to Synthetic Natural Gas: An Update. *J. CO_2 Util.* **2016**, *15*, 65–71.

(6) Miguel, C. V; Soria, M. A.; Mendes, A.; Madeira, L. M. A Sorptive Reactor for CO_2 Capture and Conversion to Renewable Methane. *Chem. Eng. J.* **2017**, *322*, 590–602.

(7) Hu, L.; Urakawa, A. Continuous CO_2 Capture and Reduction in One Process: CO_2 Methanation over Unpromoted and Promoted Ni/ZrO_2. *J. CO_2 Util.* **2018**, *25*, 323–329.

(8) Bobadilla, L. F.; Riesco-García, J. M.; Penelás-Pérez, G.; Urakawa, A. Enabling Continuous Capture and Catalytic Conversion of Flue Gas CO_2 to Syngas in One Process. *J. CO_2 Util.* **2016**, *14*, 106–111.

(9) Al-Mamoori, A.; Rownaghi, A. A.; Rezaei, F. Combined Capture and Utilization of CO2for Syngas Production over Dual-Function Materials. *ACS Sustain. Chem. Eng.* **2018**, *6* (10), 13551–13561.

(10) Blamey, J.; Anthony, E. J.; Wang, J.; Fennell, P. S. The Calcium Looping Cycle for Large-Scale CO_2 Capture. *Prog. Energy Combust. Sci.* **2010**, *36* (2), 260–279.

(11) Hu, Y.; Liu, W.; Chen, H.; Zhou, Z.; Wang, W.; Sun, J.; Yang, X.; Li, X.; Xu, M. Screening of Inert Solid Supports for CaO-Based Sorbents for High Temperature CO_2 Capture. *Fuel* **2016**, *181*, 199–206.

(12) Al-Mamoori, A.; Thakkar, H.; Li, X.; Rownaghi, A. A.; Rezaei, F. Development of Potassium- and Sodium-Promoted CaO Adsorbents for CO_2 Capture at High Temperatures. *Ind. Eng. Chem. Res.* **2017**, *56*, 8292−8300.

(13) Valverde, J. M. Ca-Based Synthetic Materials with Enhanced CO_2 Capture Efficiency. *J. Mater. Chem. A* **2013**, *1* (3), 447–468.

(14) Valverde, J. M.; Perejon, A.; Perez-Maqueda, L. A. Enhancement of Fast CO_2 Capture by a Nano-SiO_2/CaO Composite at Ca-Looping Conditions. *Environ. Sci. Technol.* **2012**, *46* (11), 6401–6408.

(15) Gruene, P.; Belova, A. G.; Yegulalp, T. M.; Farrauto, R. J.; Castaldi, M. J. Dispersed Calcium Oxide as a Reversible and Efficient CO_2-Sorbent at Intermediate Temperatures. *Ind. Eng. Chem. Res.* **2011**, *50*, 4042–4049.

(16) Guo, H.; Feng, J.; Zhao, Y.; Wang, S.; Ma, X. Effect of Micro-Structure and Oxygen Vacancy on the Stability of (Zr-Ce)-Additive CaO-Based Sorbent in CO_2 Adsorption. *J. CO_2 Util.* **2017**, *19*, 165–176.

(17) Antzara, A.; Heracleous, E.; Lemonidou, A. A. Improving the Stability of Synthetic CaO-Based CO_2 sorbents by Structural Promoters. *Appl. Energy* **2015**, *156*, 331–343.

(18) Hu, Y.; Liu, W.; Sun, J.; Li, M.; Yang, X.; Zhang, Y.; Liu, X.; Xu, M. Structurally Improved CaO-Based Sorbent by Organic Acids for High Temperature CO_2 Capture. *Fuel* **2016**, *167*, 17–24.

(19) Han, R.; Gao, J.; Wei, S.; Su, Y.; Qin, Y. Development of Highly Effective CaO@Al_2O_3 with Hierarchical Architecture CO_2 Sorbents via a Scalable Limited-Space Chemical Vapor Deposition Technique. *J. Mater. Chem. A* **2018**, *6* (8), 3462–3470.

(20) Li, Y.; Zhao, C.; Chen, H.; Liang, C.; Duan, L.; Zhou, W. Modified CaO-Based Sorbent Looping Cycle for CO_2 Mitigation. *Fuel* **2009**, *88* (4), 697–704.

(21) Guo, H.; Kou, X.; Zhao, Y.; Wang, S.; Sun, Q.; Ma, X. Effect of Synergistic Interaction between Ce and Mn on the CO_2 Capture of Calcium-Based Sorbent: Textural Properties, Electron Donation, and Oxygen Vacancy. *Chem. Eng. J.* **2018**, *334*, 237–246.

(22) Zhang, K.; Li, X. S.; Chen, H.; Singh, P.; King, D. L. Molten Salt Promoting Effect in Double Salt CO_2 Absorbents. *J. Phys. Chem. C* **2016**, *120* (2), 1089–1096.

(23) Lee, C. H.; Mun, S.; Lee, K. B.; Hyun, C.; Mun, S.; Bong, K.; Lee, C. H.; Mun, S.; Lee, K. B.; Hyun, C.; et al. Characteristics of Na-Mg Double Salt for High-Temperature CO_2 Sorption. *Chem. Eng. J.* **2014**, *258*, 367–373.

(24) Vu, A. T.; Ho, K.; Jin, S.; Lee, C. H. Double Sodium Salt-Promoted Mesoporous MgO Sorbent with High CO_2 Sorption Capacity at Intermediate Temperatures under Dry and Wet Conditions. *Chem. Eng. J.* **2016**, *291*, 161–173.

(25) Ma, S.; Huang, L.; Ma, L.; Shim, Y.; Islam, S. M.; Wang, P.; Zhao, L. D.; Wang, S.; Sun, G.; Yang, X.; et al. Efficient Uranium Capture by Polysulfide/Layered Double Hydroxide Composites. *J. Am. Chem. Soc.* **2015**, *137* (10), 3670–3677.

(26) Liang Huang, Yu Zhang, Wanlin Gao, Takuya Harada, Qingqing Qin, Qianwen Zheng, Alan Hatton, and Q. W. Alkali Carbonate Molten Salt-Coated CaO with Highly Improved CO_2 Capture Capacity. *Energy Technol.* **2017**, *5*, 1–10.

(27) Wang, Q.; Wu, Z.; Tay, H. H.; Chen, L.; Liu, Y.; Chang, J.; Zhong, Z.; Luo, J.; Borgna, A. High Temperature Adsorption of CO_2 on Mg-Al Hydrotalcite: Effect of the Charge Compensating Anions and the Synthesis PH. *Catal. Today* **2011**, *164* (1), 198–203.

(28) Aschenbrenner, O.; McGuire, P.; Alsamaq, S.; Wang, J.; Supasitmongkol, S.; Al-Duri, B.; Styring, P.; Wood, J. Adsorption of Carbon Dioxide on Hydrotalcite-like Compounds of Different Compositions. *Chem. Eng. Res. Des.* **2011**, *89* (9), 1711–1721.

(29) Yong, Z.; Mata, V.; Rodrigues, a. Adsorption of Carbon Dioxide at High Temperature—a Review. *Sep. Purif. Technol.* **2002**, *26* (2–3), 195–205.

(30) Wei, J.; Ge, Q.; Yao, R.; Wen, Z.; Fang, C.; Guo, L.; Xu, H.; Sun, J. Directly Converting CO_2 into a Gasoline Fuel. *Nat. Commun.* **2017**, *8*, 1–8.

(31) Michorczyk, P.; Ku, P.; Kolak, A. Ordered Mesoporous Ga_2O_3 and $Ga_2O_3 – Al_2O_3$ Prepared by Nanocasting as Effective Catalysts for Propane Dehydrogenation in the Presence of CO_2. *Catal. Commun.* **2013**, *35*, 95–100.

(32) Myint, M. N. Z.; Yan, B.; Wan, J.; Zhao, S.; Chen, J. G. Reforming and Oxidative Dehydrogenation of Ethane with CO_2 as a Soft Oxidant over Bimetallic Catalysts. *J. Catal.* **2016**, *343*, 168–177.

(33) Ramesh, Y.; Thirumala Bai, P.; Hari Babu, B.; Lingaiah, N.; Rama Rao, K. S.; Prasad, P. S. S. Oxidative Dehydrogenation of Ethane to Ethylene on Cr_2O_3/Al_2O_3–ZrO_2 Catalysts: The Influence of Oxidizing Agent on Ethylene Selectivity. *Appl. Petrochemical Res.* **2014**, *4* (3), 247–252.

(34) Asghari, E.; Haghighi, M.; Rahmani, F. CO_2-Oxidative Dehydrogenation of Ethane to Ethylene over Cr/MCM-41 Nanocatalyst Synthesized via Hydrothermal/Impregnation Methods: Influence of Chromium Content on Catalytic Properties and Performance. *J. Mol. Catal. A Chem.* **2016**, *418–419*, 115–124.

(35) Janke, C.; Duyar, M. S.; Hoskins, M.; Farrauto, R. Applied Catalysis B: Environmental Catalytic and Adsorption Studies for the Hydrogenation of CO_2 to Methane. *Appl. Catal. B, Environ.* **2014**, *152–153* (1), 184–191.

(36) Duyar, M. S.; Farrauto, R. J.; Castaldi, M. J.; Yegulalp, T. M. In Situ CO_2 Capture Using CaO/γ-Al_2O_3 Washcoated Monoliths for Sorption Enhanced Water Gas Shift Reaction. *Ind. Eng. Chem. Res.* **2014**, *53*, 1064–1072.

(37) Zheng, Q.; Farrauto, R.; Chau Nguyen, A. Adsorption and Methanation of Flue Gas CO_2 with Dual Functional Catalytic Materials: A Parametric Study. *Ind. Eng. Chem. Res.* **2016**, *55* (24), 6768–6776.

(38) Gruene, P.; Belova, A. G.; Yegulalp, T. M.; Farrauto, R. J.; Castaldi, M. J. Dispersed Calcium Oxide as a Reversible and Efficient CO_2-Sorbent at Intermediate Temperatures. *Ind. Eng. Chem. Res.* **2011**, *50*, 4042–4049.

(39) Lu, H.; Smirniotis, P. G. Calcium Oxide Doped Sorbents for CO_2 Uptake in the Presence of SO_2 at High Temperatures. *Ind. Eng. Chem. Res.* **2009**, *48*, 5454–5459.

(40) Wang, S.; Fan, S.; Fan, L.; Zhao, Y.; Ma, X. Effect of Cerium Oxide Doping on the Performance of CaO-Based Sorbents during Calcium Looping Cycles. *Environ. Sci. Technol.* **2015**, *49* (8), 5021–5027.

(41) Deng, S.; Li, S.; Li, H.; Zhang, Y. Oxidative Dehydrogenation of Ethane to Ethylene with CO_2 over Fe-Cr/ZrO_2 Catalysts. *Am. Chem. Soc.* **2009**, *48* (16), 7561–7566.

(42) C.C. Kuivila, J.B. Butt, P. C. S. Characterization of Surface Species on Iron Synthesis Catalysts by X-Ray Photoelectron Spectroscopy. *Appl. Surf. Sci.* **1988**, *32*, 99–121.

(43) Sun, Y. nan; Tao, L.; You, T.; Li, C.; Shan, H. Effect of Sulfation on the Performance of Fe_2O_3/Al_2O_3 Catalyst in Catalytic Dehydrogenation of Propane to Propylene. *Chem. Eng. J.* **2014**, *244*, 145–151.

(44) Serykh, A. I.; Amiridis, M. D. In Situ X-Ray Photoelectron Spectroscopy Study of Gallium-Modified MFI Zeolite. *Surf. Sci.* **2009**, *603* (13), 2037–2041.

(45) Yoon, H. J.; Lee, K. B. Introduction of Chemically Bonded Zirconium Oxide in CaO-Based High-Temperature CO_2 Sorbents for Enhanced Cyclic Sorption. *Chem. Eng. J.* **2019**, *355*, 850–857.

(46) Shokrollahi Yancheshmeh, M.; Radfarnia, H. R.; Iliuta, M. C. High Temperature CO_2 Sorbents and Their Application for Hydrogen Production by Sorption Enhanced Steam Reforming Process. *Chem. Eng. J.* **2016**, *283*, 420–444.

V. DIRECT PRODUCTION OF ETHYLENE FROM CO_2 FLUE GAS USING AN INTEGRATED CAPTURE-CONVERSION PROCESS

Ahmed Al-Mamoori, Shane Lawson, Ali A. Rownaghi, Fateme Rezaei*

Department of Chemical & Biochemical Engineering, Missouri University of Science and Technology, 1101 N State Street, Rolla, MO, 65409, United States

ABSTRACT

Finding cost-effective approaches to capture and utilize the emitted CO_2 could open new avenues to the sustainable creation of energy with less environmental footprint. Combined capture-utilization approach offers a promising route to use waste CO_2 as a feedstock for producing valuable commodity chemicals and fuels. In this investigation, we report *in-situ* capture and utilization of CO_2 in ethylene production through oxidative dehydrogenation of ethane over adsorbent-catalyst materials consisting of CaO, double salts K-Ca and Na-Ca as adsorbents, Cr nanoparticles as catalyst, and H-ZSM-5 as a catalyst support. The structural and physiochemical characteristics of the materials were assessed by N_2 physisorption, XRD, XPS, SEM, NH_3-TPD, and H_2-TPR. The adsorption step was conducted at 600 ºC using a feed gas mixture of 10%CO_2/Ar followed by the reaction step at 700 ºC using C_2H_6/Ar. The K-Ca double salt exhibited a higher CO_2 capacity (5.2 mmol/g), thus was chosen for the capture-conversion tests. The effects of Cr content, CO_2/C_2H_6 mole ratio, and weight hourly space velocity (WHSV) were investigated to determine the optimum process conditions for this combined process. The $(K\text{-}Ca)_{50}/(Cr_{10}@HZSM\text{-}5)_{50}$ material was found to exhibit the highest ethane conversion (25%) with ethylene selectivity of 88% at 5000 mL/g.hr and 0.4 CO_2/C_2H_6 mole ratio.

Overall, this study demonstrates a proof-of-concept for novel hybrid materials which are capable of combined capture and utilization of CO_2 in ethylene production. Through proper optimization, we anticipate that the materials reported herein could be used to mitigate CO_2 emissions and produce valuable chemical commodities.

Keywords: CO_2 capture, Oxidative dehydrogenation, Adsorbent-catalyst, Ethylene

1. INTRODUCTION

In the petrochemical industry, ethylene has been considered as one of the most important building blocks in chemical industry for production of a wide variety of chemicals such as polyethylene, ethylene oxide, ethylbenzene, etc.[1][2] This important chemical feedstock is industrially produced through steam cracking of natural gas or heavy naphtha which is extremely energy intensive[3]. Oxidative dehydrogenation of ethane (ODHE) with a mild oxidant (e.g., CO_2) has been suggested as a promising route to produce ethylene as it provides an opportunity to use underutilized ethane from shale gas (with a volume fraction of ~16%). Moreover, as the ODHE occurs at lower temperatures than the steam cracking reaction, the heat and energy required would be lower. Most importantly, utilization of waste CO_2 from process streams in light olefins production offers an efficient means to alleviate excessive CO_2 emissions to the atmosphere, while producing value-added chemicals from a renewable feedstock. According to International Energy Agency (IEA), carbon capture, utilization, and sequestration accounts for 7% of the cumulative emissions reductions needed globally by 2040 to keep the average temperature rise below 2 ºC [4].

Recently, combined CO_2 capture and utilization processes by which CO_2 is first captured and then converted to a chemical commodity or fuel have attracted a great deal of interest among researchers. Such integrated systems could provide a solution to both energy and environmental problems currently encountered worldwide. From economic point of view, such hybrid systems would be better than the two separate steps since they require less capital investment (i.e., one unit). Moreover, CO_2 capture and ODHE reaction steps could be implemented at the same temperature so that the need for a high temperature swing could be avoided. In this way, cycle time can be significantly shortened by eliminating the long cooling step that is typically required in temperature swing processes. Furthermore, the high cost of the transportation and infrastructure for carbon capture and sequestration could boost the carbon capture and utilization demanding[5][6][7][8][9].

A primary concern with combined capture and utilization beds has been material selection, as the bi-functional material should exhibit a sizable CO_2 capture capacity as well as favorable catalytic properties (multiple oxidation states, high number of acidic sites, etc.). Moreover, the material should be thermally stable up to 750 °C [10] so as to not degrade during activation and should be inexpensive to minimize material costs for scale-up. Farrauto and his group developed a series of different dual function materials (DFMs) for combined CO_2 capture and methanation through Sabatier reaction. Their efforts focused on improving CH_4 productivity utilizing different adsorbents (CaO, K_2CO_3, Na_2CO_3, and MgO) and catalysts (Ru, Rh, Pt, Pd, Ni, Co, Ru-Ni, and Ru-Pt) supported on γ-Al_2O_3[11–16]. Kim et al.[17] reported a combined capture-utilization process for syngas production directly from flue gas through dry methane reforming. Their process that utilized CaO as an adsorbent and Ni-based hydrotalcite (HTC) as a catalyst, achieved almost full

conversion of CO_2 and CH_4 with trace amount of CO_2 (0.08%) and CH_4 (0.06%) were detected in the off-gas stream. In another investigation, Sun et al.[18] proposed a new DFM consisting of Ca/Ni/Ce with molar ratio of 1:0.1:0.03 to capture CO_2 and then convert it to CO through reverse water gas shift reaction (RWGS). The material exhibited 100% CO selectivity and 51.8% CO_2 conversion. In our previous investigation [19], we demonstrated syngas production through a combined CO_2 capture-utilization process using various DFMs composing of double salt adsorbent (K-Ca, Na-Ca, K-Mg, and Na-Mg), catalyst (Ni), and a support (γ-Al_2O_3). In this process, CO_2 first captured on the adsorbent surface followed by its subsequent reaction with C_2H_6 on the catalyst surface to produce syngas. Maximum C_2H_6 and CO_2 conversions of 100% and 75%, respectively were obtained over our DFMs. [20]. Creation of novel *in-situ* capture-conversion technologies requires advancements in both materials science and process engineering.

While ODHE reaction with CO_2 has been extensively studied before, to the best of our knowledge, the use of combined CO_2 capture-utilization process for ethylene production through ODHE has not been reported before. Herein, we performed a proof-of-concept study on ethylene production through ODHE directly from CO_2 flue gas in a hybrid bed of adsorbent and catalyst materials that are physically mixed. Various adsorbents including K-Ca, Na-Ca, and CaO were chosen for this study owing to their high CO_2 uptake capacity and fast kinetics, abundant, and low cost[9][21][22][23]. Chromium (Cr) was used as a catalyst on the basis of its catalytic activity and redox properties [24][20]. H-ZSM-5 was used as a support for Cr nanoparticles due to its high surface area, three-dimensional microporous structure, controllable acidity, and thermal and mechanical stability[25][26][27]. Using characterization tools like XRD, N_2-physisorption, NH_3-TPD,

H_2-TPR, and XPS, the properties of the materials were thoroughly assessed prior to use. The capture-conversion experiments were carried out under semi-isothermal conditions where step 1 (capture) was performed at 600 ºC and step 2 (reaction) at 700 ºC. The isothermal condition was not achieved because of thermodynamically unfavorable CO_2 adsorption at ≥ 700 ºC. Combined capture-conversion tests were carried out under various conditions and with various materials to systematically evaluate the effects of adsorbent type, chromium composition, CO_2/C_2H_6 mole ratio, and weight hourly space velocity (WHSV) on ethane conversion and ethylene yield.

2. EXPERIMENTAL SECTION

2.1. MATERIALS SYNTHESIS

Potassium- and sodium-based calcium oxide double salts (K-Ca and Na-Ca) were synthesized following a procedure described in our previous work [9]. Commercially purchased CaO (Fischer Scientific) was calcined at 700 ºC for 5 h before use, while ammonium ZSM-5 (Si/Al ratio = 50) was calcined at 650 ºC for 6 h to obtain H-ZSM-5. Chromium nitrate nonahydrate ($Cr(NO_3)_3.9H_2O$, Sigma-Aldrich) was used as chromium precursor. To incorporate Cr onto the H-ZSM-5 material, wet impregnation method was used by which proper amounts of $Cr(NO_3)_3.9H_2O$ (5,10,15 wt. %) were dissolved in distilled water and then the solution was added to the H-ZSM-5 powder and kept under stirring (400 rpm) for 1 h at room temperature. Next, the slurry was dried at 120 ºC for 4 h and the obtained powder was calcined at 650 ºC for 6 h to obtain the designated catalyst. The adsorbents and HZSM-5 supported Cr catalysts were physically mixed at a weight

ratio of 0.5:0.5 and the obtained materials were designated as $(K\text{-}Ca)_{50}/(Cr_x@HZSM\text{-}5)_{50}$, $(Na\text{-}Ca)_{50}/(Cr_x@HZSM\text{-}5)_{50}$, and $(CaO)_{50}/(Cr_x@HZSM\text{-}5)_{50}$, where x represents the weight ratio of $Cr(NO_3)_3.9H_2O$ to HZSM-5 powder.

2.2. MATERIALS CHARACTERIZATION

The characterization measurements in this research focused solely on catalysts mainly because the properties of the adsorbents (CaO, K-Ca, and Na-Ca) were discussed in our previous works[8][9]. The crystallinity of the materials $Cr_x@HZSM\text{-}5$ were assessed by X-ray diffraction (XRD) analysis using a PANalatical X' pert multipurpose X-ray diffractometer with a scan size of 0.02º /step at a rate of 147.4 s/step. To study the textural properties of $Cr_x@HZSM\text{-}5$ materials, nitrogen physisorption isotherms were measured and the corresponding surface area, pore volume, and pore size distribution (PSD) were estimated using Brunauer-Emmmet-Teller (BET), Horvath and Kawazoe (HK), and non-local density functional theory (NLDFT) methods, respectively. Prior to the experiments, the materials were degassed under vacuum at 300 ºC for 6 h. X-ray photoelectron spectroscopy (XPS) was performed on a Kratos Axis 165 XPS to determine the composition of the catalysts. Scanning electron microscopy (SEM) was performed on a Zeiss Merlin Gemini field emission microscope (FE-SEM) to study the materials morphology. High resolution transition electron microscopy (HR-TEM) images were obtained on a JEOL JEM-2100 operated at 200 kv. Prior to taking images, the samples were dispersed in isopropanol and then collected using copper grids covered with carbon film. Energy dispersive spectroscopy (EDS) analysis was also performed to obtain elemental mapping of the materials. the acidity of the $Cr_x@HZSM\text{-}5$ catalysts was

investigated by NH_3-TPD analysis. In these tests, the sample was first degassed at 400 ºC for 1 h followed by cooling down to 80 ºC under He flow, after which 5% NH_3/He was introduced to the sample with a flow rate of 40 mL/min for 30 min. Subsequently, He was fed to the sample cell to remove any physiosorbed NH_3 for 30 min followed by ramping the temperature from 80 to 800 ºC at the rate of 10 ºC/min. H_2-TPR was also performed to study the reducibility of the catalysts. In these tests, the sample was first degassed at 400 ºC for 1 h and then cooled down to 100 ºC under He, followed by ramping the temperature from 100 to 700 ºC at the rate of 10 ºC/min under H_2 flow (5% H_2/He).

2.3. COMBINED CAPTURE-REACTION TEST

The experimental set-up is shown schematically in Figure 1. A stainless-steel packed bed reactor with dimensions of 0.635 × 30 cm was placed inside an electric furnace and its temperature was controlled using a K-type thermocouple and an omega benchtop controller. During each experiment, 0.4 g of the hybrid material (0.2 g adsorbent and 0.2 g catalyst) was placed in the reactor. Before placing the sample into the reactor, it was placed between two layers of quartz wool to prevent scattering from the gas stream. Ultra-pure carrier (UPC) Ar UPC (99.9993), 10% CO_2/Ar, and 10% C_2H_6/Ar (Airgas) gases were fed into the reactor using mass flow controllers (MFC, Brooks). The effluent gas composition was analyzed using Mass Spectrometer Cirrus 2 (MKS). Argon was used as a zero gas to remove the MKS background. Each gas was calibrated with Ar to obtain the sensitivity factors. The atomic mass unit (amu) of gases were selected as the following: Ar (40), CO_2 (44), C_2H_6(30), C_2H_4(25), H_2O (18), CH_4(16), CO (14), and H_2 (2). Peaks 40 and 44 were selected for Ar and CO_2, respectively [28]. 28 amu is an overlap peak among C_2H_6, C_2H_4,

CO_2, and CO, as reported by NIST chemistry database [28], therefore, peak 28 was not selected for any gases.

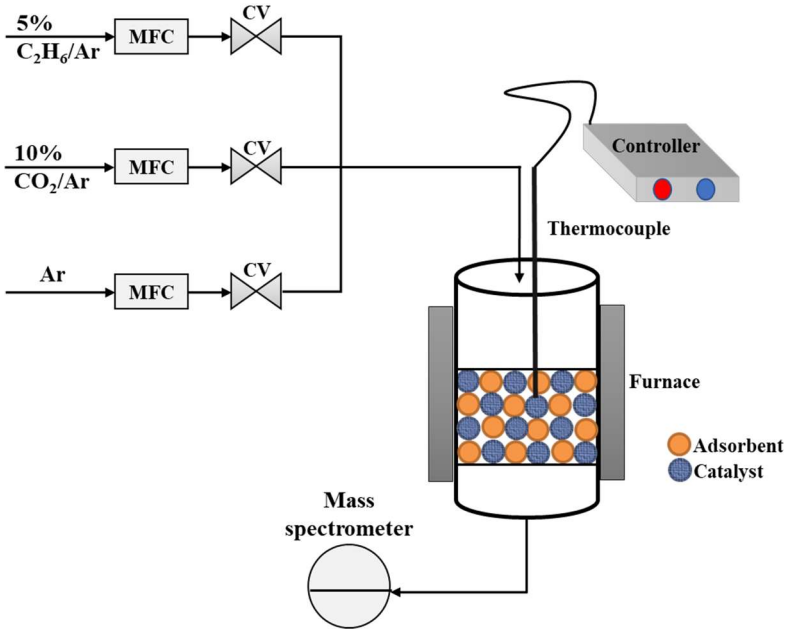

Figure 1. Schematic representation of the experimental set-up.

The hybrid adsorbent-catalysts performance in the combined CO_2 capture-utilization process was assessed by the process shown in Figure 2. In step one, the sample was degassed under 35 mL/min of Ar flow at 700 ºC for 1 h at a heating rate of 20 ºC/min. In step two, Ar flow was continued into the reactor and the system was allowed to cool down at the rate of ~3 °C/min until its temperature reached 600 °C. In step three, 35 mL/min of 10% CO_2/Ar was flown into the reactor at 600 °C until full saturation was observed on the mass spectrometer. Finally, in step four, the reactor was heated to 700 °C at 30 °C/min and simultaneously 10% CO_2/Ar was shut off and 35 mL/min of 5% C_2H_6/Ar was flown into the reactor. The reaction was allowed to progress until the CO_2

concentration in the effluent gas was observed to be zero. From these experiments, the quantities of CO_2 adsorbed, desorbed, and reacted were calculated using Eqns. S1-S4, in Supporting Information while the molar quantities of effluent gas, C_2H_6 conversion, C_2H_4 selectivity, and C_2H_4 yield were calculated by Eqns. S5-S8, in Supporting Information. Carbon balance was also carried out for the adsorption-reaction process as shown in Eqn. S9 in Supporting Information. Here, it should also be noted that, although adsorption and reaction occurred in one bed over a dual functional material, it was not possible to obtain complete isothermality because CO_2 adsorption was found to be unfavorable when the temperature was greater than or equal to 700 °C.

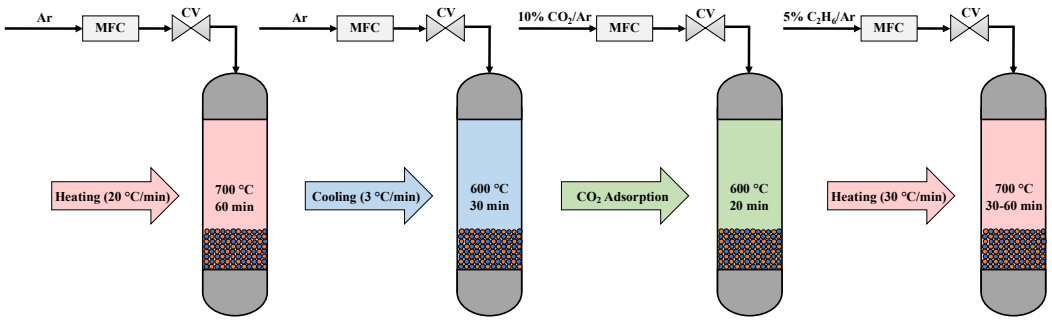

Figure 2. Steps of the combined capture-reaction process.

3. RESULTS AND DISCUSSIONS

3.1. MATERIALS PROPERTIES

The N_2 physisorption isotherms and PSD profiles of Cr_x@H-ZSM-5 catalysts are presented in Figure 3 while the corresponding textural properties are summarized in Table 1. From the N_2 physisorption isotherms (Figure 3a), all of the materials exhibited Type IV physisorption profiles with a H3 hysteresis loop, consistent with mesoporous materials

[29][30]. As expected, the zeolite experienced a ~32-38.5% reduction in N_2 uptake of all the samples following Cr incorporation. As presented in Table 1**,** the surface area and pore volume dropped from 470 m^2/g and 0.47 cm^3/g for bare H-ZSM-5 to 380 m^2/g and 0.29 cm^3/g for Cr_5@HZSM-5, 368 m^2/g and 0.27cm^3/g for Cr_{10}@HZSM-5, and 391 m^2/g and 0.28 cm^3/g for Cr_{15}@HZSM-5 on account of the metal oxide filling within the zeolite pores, which blocks some of the available surface area and pore volume. This was further supported by the PSD profiles (Figure 3b), where a sizable reduction in pore volume was observed in the Cr samples compared to the pristine zeolite. As is apparent from these PSD curves, however, the chromium loaded in both the zeolitic meso- and micropores, as a reduction in pore volume was observed across every diameter and not just in one regime. Also, it is evident from Table 1 that the zeolite support has both micro- and meso- pores in its structure and that most of the pores are of mesopore size. Overall, the dataset shown in Figure 3 agrees with literature for metal oxide doped-HZSM-5[26][27].

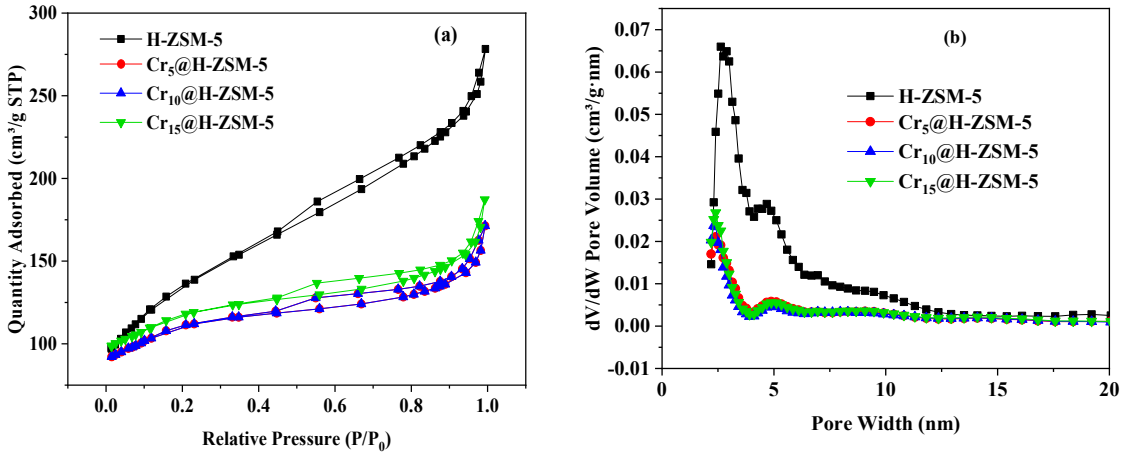

Figure 3. (a) N_2 physisorption isotherms and (b) pore size distributions of Cr_x@H-ZSM-5 catalysts.

Table 1. Textural properties of the Cr_x@H-ZSM-5 catalysts.

Materials	S_{BET} (m^2/g)	V_{total} (cm^3/g)	V_{micro}(cm^3/g)	V_{meso}(cm^3/g)	d_p (nm)
HZSM-5	470	0.43	0.04	0.39	1.2, 3.0, 4.8
Cr_5@HZSM-5	380	0.29	0.09	0.2	1.1, 3.1, 4.9
Cr_{10}@HZSM-5	368	0.27	0.09	0.18	1.2, 3.0, 4.8
Cr_{15}@HZSM-5	391	0.28	0.1	0.18	1.2, 3.0, 4.9

The comparison of XRD and XPS spectra for the materials examined in this study are displayed in Figure 4. From the XRD (Figure 4a), the most dominant diffractive indices were those consistent with H-ZSM-5, which were observed at $2\theta = 8^o$, 8.9^o , 23.1^o, and 24^o, and corresponded to the (101), (200), (501), and (303) planes [31,32]. Importantly, because all of these planes were of similar intensity and shape across the different samples, it could be concluded that the Cr incorporation did not significantly alter the zeolite structure. The XPS analysis was also performed for the bare and Cr incorporated H-ZSM-5 materials as presented in Figure 4b and Table 2. As evident, the data illustrate the presence of Si, Al, O, and C in addition to Cr for the incorporated Cr_x@HZSM-5 samples. It is also clear from Table 2 that the amount of atomic chromium enhanced from 0.13 to 0.57% as the chromium incorporated ratio increased from 5 to 15 wt. %.

The samples' surface topographies were assessed by SEM, as shown in Figure 5. In the pristine H-ZSM-5 (Figure 5a), the particles of irregular shape with sizes on the order of ~300 nm in diameter were observed, which agrees with literature [33]. At 5 wt.% Cr loading (Figure 5b), the particles maintained their overall shape and little to no

agglomeration was observed. This was to be expected at low loadings because the Cr nanoparticles were solely contained within the micropores and should not have produced any intraparticle binding during their calcination. At 10 wt.% loading, however, (Figure 5c), conglomerates of H-ZSM-5 particles started to form because the elevated loading

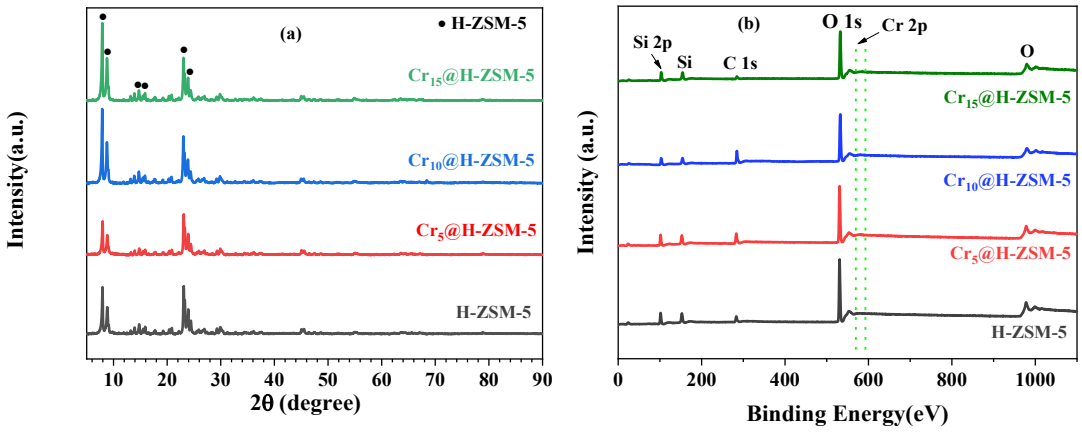

Figure 4. (a) XRD spectra and (b) XPS survey spectrum of the bare H-ZSM-5 and Cr_x@H-ZSM-5 materials.

Table 2. Elemental composition (atomic %) obtained by XPS.

Materials	O 1s	C 1s	Si 2p	Al 2p	Cr 2p
H-ZSM-5	58.53	16.56	23.63	1.27	-
Cr_5@H-ZSM-5	49.88	28.19	20.99	0.8	0.13
Cr_{10}@H-ZSM-5	46.64	36.8	15.83	0.38	0.35
Cr_{15}@H-ZSM-5	61.6	11.8	25.12	0.9	0.57

began to adhere the particles to one another. This effect was further observed at 15 wt.% Cr loading (Figure 5d) where agglomeration was increasingly prevalent and it was difficult to distinguish individual zeolite particles. This being stated, these effects were to be expected from literature, which has repeatedly shown increasing oxide nanoparticle loadings on zeolites gives rise to adhesion in between individual particles [34].

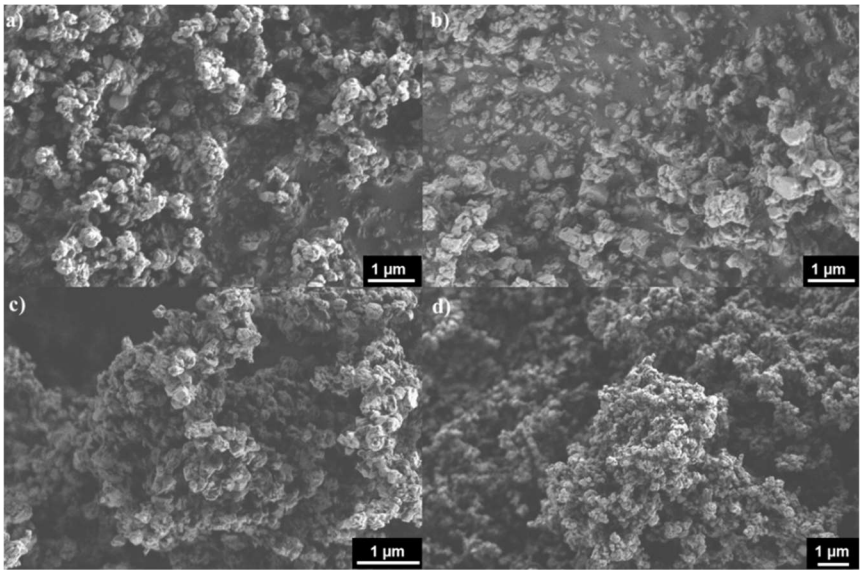

Figure 5. SEM micrographs for (a) bare H-ZSM-5, (b) Cr_5@H-ZSM-5, (c) Cr_{10}@H-ZSM-5, and (d) Cr_{15}@H-ZSM-5.

To qualitatively assess the Cr species dispersion on the H-ZSM-5 zeolite, TEM and elemental mapping images were obtained, as shown in Figure 6a-i. The black dots in the TEM images are related to Cr species as reported in the literature for the Cr-incorporated H-ZSM-5 material[27] [35]. Analysis of these TEM images revealed that Cr particles in Cr_5@H-ZSM-5 and Cr_{10}@H-ZSM-5 have irregular shape with sizes around 100 nm, whereas in Cr_{15}@H-ZSM-5, particle size became larger (~ 250 nm) due to particles agglomeration. EDS elemental mapping from TEM analysis present the chromium species

dispersion on the H-ZSM-5 samples. As can be seen, Cr_5@H-ZSM-5 and Cr_{10}@H-ZSM-5 samples show very well dispersed chromium species. For further increasing in the chromium content to Cr_{15}@H-ZSM-5, the sample illustrates clustered Cr particles, in agreement with TEM images, and H_2-TPR results.

NH_3-TPD and H_2-TPR experiments were performed on the bare H-ZSM-5 and the Cr incorporated H-ZSM-5 samples and the results are illustrated in Figure 7. From the NH_3-TPD experiments (Figure 7a), it was found that the bare H-ZSM-5 contained weak (Brønsted and /or Lewis sites) and strong acid sites (Brønsted sites), as evidenced by the two desorption peaks at 188 and 364 ºC, respectively. In the Cr_5@H-ZSM-5, there was a small shift in the acid site density, as indicated by the change in peak temperature from 364 ºC to ~350 ºC and from 188 to ~175 ºC. This effect was more pronounced in the Cr_{10}@H-ZSM-5 and Cr_{15}@H-ZSM-5, as further increase in the Cr loading caused the peak to shift to 330 ºC for the strong acid sites, whereas for 10 wt.% sample, the weak acid sites peak was shifted to lower temperature (114 ºC) and for 15 wt.% to 140 ºC, in agreement with literature [36], this indicated that Cr played a crucial role in reducing the H-ZSM-5 surface acidity and made the acid sites more active at lower temperature.

Moving on to the H_2-TPR profiles (Figure 7b), the bare H-ZSM-5 sample gave rise to no noticeable peaks which could be attributed to the reduction of oxygen in the H-ZSM-5 framework. The 5 wt.% Cr sample exhibited a small peak in the temperature range of 180-450 ºC which was attributed to the reduction of Cr^{6+} (CrO_3) to the Cr^{3+} (Cr_2O_3). When the Cr loading was increased to 10 wt.%, the peak was shifted to lower temperature between 150-450 ºC with higher amount of H_2-consumption, because of the reduction of

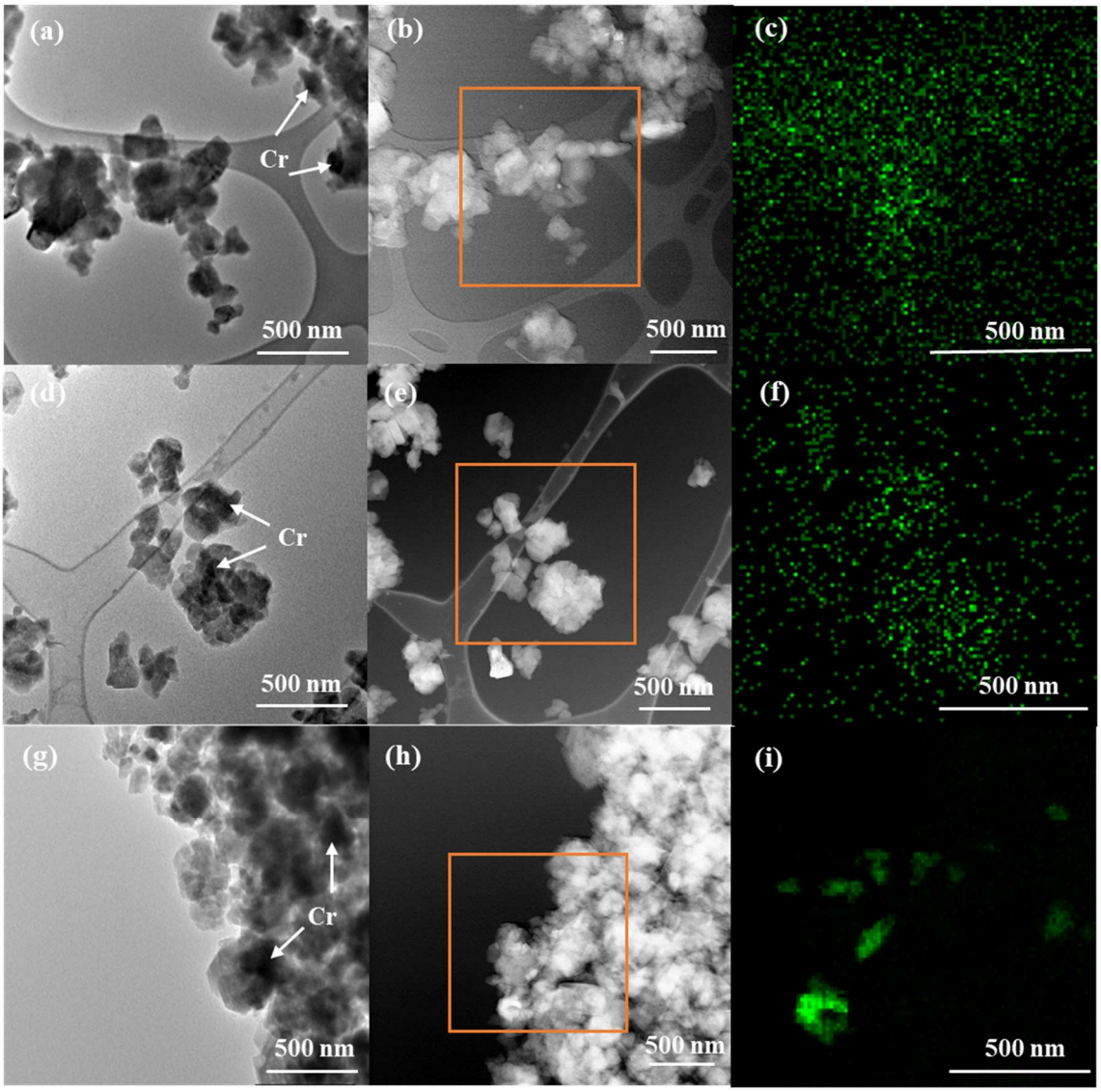

Figure 6. TEM images and corresponding EDS Cr maps for (a-c) Cr_5@H-ZSM-5, (d-f), Cr_{10}@H-ZSM-5, and (g-i) Cr_{15}@H-ZSM-5.

Cr^{6+} to the Cr^{3+}. In Cr_{15}@H-ZSM-5, both of the peaks which were observed in the lower loadings were observed, however, a new shoulder was also developed from 450-700 ºC, on account of the formation of α-Cr_2O_3, which are inactive species for ethane dehydrogenation [37]. Here, it is also important to note that the amount of hydrogen consumed increased steadily as the Cr concentration increased from 5 to 10% wt. % but

upon further increase to 15 wt. % Cr, the amount of H_2-consumption decreased, which could be due to the particles agglomerations, as noted in TEM images, or to the formation of new phase α-Cr_2O_3. Namely, increasing the Cr concentration from 5 to 10 wt.% increased the H_2 consumption from 0.332 mmol/g to 0.502 mmol/g, while increasing the Cr concentration from 10 to 15 wt.% gave rise to 0.305 mmol/g H_2 consumption.

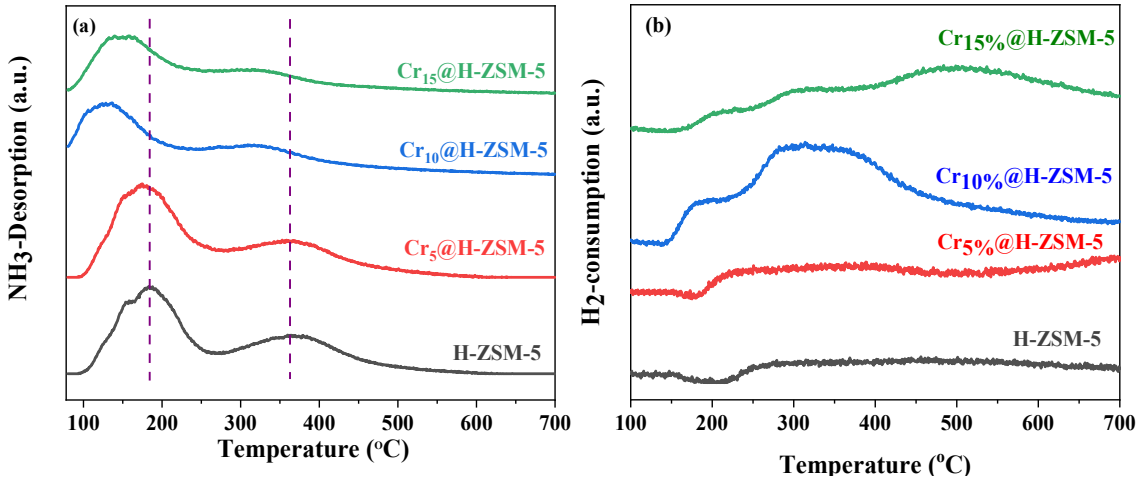

Figure 7. (a) NH_3-TPD of the bare H-ZSM-5 and Cr_x@H-ZSM-5 and (b) H_2-TPR of Cr_x@H-ZSM-5.

3.2. ADSORPTION-REACTION TEST RESULTS

Three materials – $(CaO)_{50}/(Cr_{10}@H\text{-}ZSM\text{-}5)_{50}$, $(Na\text{-}Ca)_{50}/(Cr_{10}@H\text{-}ZSM\text{-}5)_{50}$ and $(K\text{-}Ca)_{50}/(Cr_{10}@H\text{-}ZSM\text{-}5)_{50}$ – were selected for testing in our adsorption-reaction setup to examine the effect of adsorbent material on overall CO_2 capture, C_2H_6 conversion, and C_2H_4 selectivity. The experiments were performed at 10500 mg/L.h WHSV with 5% C_2H_6/Ar and the results are illustrated in Figure 8. From the initial adsorption step, CO_2 adsorption capacities of 5.2, 3.2, and 0.8 mmol/g were observed for $(K\text{-}Ca)_{50}/(Cr_{10}@H\text{-}ZSM\text{-}5)_{50}$, $(Na\text{-}Ca)_{50}/(Cr_{10}@H\text{-}ZSM\text{-}5)_{50}$, and $(CaO)_{50}/(Cr_{10}@H\text{-}ZSM\text{-}5)_{50}$, respectively.

The enhanced CO_2 capacities in $(K\text{-}Ca)_{50}/(Cr_{10}@H\text{-}ZSM\text{-}5)_{50}$ and $(Na\text{-}Ca)_{50}/(Cr_{10}@H\text{-}ZSM\text{-}5)_{50}$ was attributed to the formation of $K_2Ca(CO_3)_2$ and $Na_2Ca(CO_3)_2$ double carbonates, and were in agreement with our previous work [9]. Moving on to the reaction step, C_2H_6 conversions of 28.1%, 18.3%, and 18.1%, as well as CO_2 conversions of 24.2%, 23.9%, and 19.8%, were observed for $(CaO)_{50}/(Cr_{10}@H\text{-}ZSM\text{-}5)_{50}$, $(Na\text{-}Ca)_{50}/(Cr_{10}@H\text{-}ZSM\text{-}5)_{50}$ and $(K\text{-}Ca)_{50}/(Cr_{10}@H\text{-}ZSM\text{-}5)_{50}$, respectively. It is also worth noting here that a small amount of CO and H_2O were detected as well, on account of their formation during the ODHE reaction. It is clear also from Figure 7 a-c at the beginning of the reaction step ethane composition reached plateau and then decreased mainly because while it reached the plateau the temperature was still ramping from 600-700 ºC and then it declined due to the reaction enhancement as it reached 700 ºC. Also, there was H_2O and a little CO detected at the beginning of the reaction step and this could be attributed to the RWGS that is favored at lower temperature.

The reaction mechanisms are summarized in Table 3. CO_2 reacts with C_2H_6 through oxidative dehydrogenation of ethane to produce C_2H_4, CO, and H_2O (eqn. 1**)**. Ethylene can also be produced through other side reaction (ethane dehydrogenation), as shown in eqn. 2. The role of CO_2 has been is to either re-oxidize the Cr (III) to Cr (VI) species[38] or eliminate the hydrogen produced by ethane dehydrogenation through RWGS reaction (eqn. 3) [39]. Interestingly, the amount of ethylene produced is almost equal to the amount of hydrogen and water which means that ethylene was produced simultaneously through the oxidative dehydrogenation of ethane (eqn. 1) and ethane dehydrogenation (eqn. 3). However, the amount of CO produced was a little higher than the amount of water implying that CO can also be produced by another side reaction (reverse Boudouard reaction) that

can eliminate or reduce the coke formation (eqn. 4). By the time CO_2 exhausted, the amount of ethylene decreased but hydrogen and CO increased. The decreasing of ethylene production was because no more CO_2 was available to re-oxidize the Cr (III) to Cr (VI) and it is well known that Cr (III) has lower activity for dehydrogenation of light alkanes [40]. Notably, the amount of hydrogen was very high, as a result of ethane cracking reaction (eqn. 5). The presence of CO could be attributed to the coke formation by ethane cracking with the oxygen from the catalyst lattice. The total amount of ethylene produced was calculated for the three sets of the materials are depicted in Figure 7d. It was found that as the amount of CO_2 capture increased, the amount of ethylene capacity enhanced and the highest CO_2 uptake of 1.04 mmol and C_2H_6 capacity of 0.46 mmol were obtained for $(K\text{-}Ca)_{50}/(Cr_{10}@H\text{-}ZSM\text{-}5)_{50}$, therefore, this material was selected for further investigation due to the higher CO_2 capture capacity and higher ethylene productivity.

As shown in Figure 9, the effect of Cr concentration on catalytic activity was investigated by performing adsorption-reaction experiments on K-Ca adsorbent physically mixed with the 5, 10, and 15 wt.% Cr@ZSM-5 (at the adsorbent: catalyst weight fraction of 0.5:0.5), which are denoted as, $(K\text{-}Ca)_{50}/(Cr_5@H\text{-}ZSM\text{-}5)_{50}$, $(K\text{-}Ca)_{50}/(Cr_{10}@H\text{-}ZSM\text{-}5)_{50}$, and $(K\text{-}Ca)_{50}/(Cr_{15}@H\text{-}ZSM\text{-}5)_{50}$, respectively. As can be seen, increasing the Cr concentration from 0 – 5 wt.% nearly doubled the C_2H_6 conversion and increased the CO_2 conversion by 25%. At 10% Cr, the highest C_2H_6 and CO_2 conversions were observed, indicating that this loading was optimal for combined capture-conversion experiments. Meanwhile, at 15% Cr, the catalytic activity decreased, on account of $\alpha\text{-}Cr_2O_3$ formation, which limited the selectivity towards C_2H_6 [37], as noted earlier. These results were in agreement with the H_2-TPR in Figure 7b, which indicated that the catalytic activity was

increased from 5 to 10 wt.% Cr but was reduced at 15 wt.%. Cr surface density (the number of Cr atoms per unit surface area) was estimated for the Cr_x@H-ZSM-5 samples using Eqn. S10 in supporting information and the results are shown in Table 4. Cr surface density is an indicator of the degree of chromium dispersion on the surface, and its lower value typically implies a better dispersion [41–43]. The Cr surface density results revealed that $Cr_{5\%}$@H-ZSM-5 and $Cr_{10\%}$@H-ZSM-5 have better Cr dispersion than $Cr_{15\%}$@H-ZSM-5 sample, in agreement with the TEM images. Michorczyk et al. [42] reported that when surface density exceeds 0.54 Cr atom/nm^2, agglomeration of Cr^{3+} species on SBA-15 takes place. Here we believe that agglomeration of Cr species at 15 wt.% led to reduction in the Cr dispersion and enhancement of the 3D bulk oxide species formation, which in turn resulted in limited catalytic activity.It should also be noted here that a control experiment was performed with $(K\text{-}Ca)_{50}$/$(H\text{-}ZSM\text{-}5)_{50}$ (0 Cr loading) under the same conditions and the results were compared with those of other catalysts, as shown in Figure 9.

Table 3. Possible reaction pathways for conversion of ethane to ethylene by ODHE.

Reaction possible pathways	**Equation**
$C_2H_6 + CO_2 \rightarrow C_2H_4 + CO + H_2O$	**eqn. 1**
$C_2H_6 \rightarrow C_2H_4 + H_2$	**eqn. 2**
$CO_2 + H_2 \rightarrow CO + H_2O$	**eqn. 3**
$CO_2 + C \rightarrow 2CO$	**eqn. 4**
$C_2H_6 \rightarrow 2C + 3H_2$	**eqn. 5**
$3C_2H_6 + 2CrO_3 \rightarrow 3C_2H_4 + Cr_2O_3 + 3H_2O$	**eqn. 6**

As clearly evident, a negligible ethylene yield was obtained over this material with an C_2H_6 conversion of <5% and CO_2 conversion of <10%. Bugrova et al. [24] reported an ethane conversion and ethylene selectivity of 20% and 80%, respectively over CrO_X/ZrO_2, and 20% and 90% over CrO_x/Al_2O_3, respectively at 700 ºC. In the next step, we investigated the effect of CO_2/C_2H_6 mole ratio on catalytic performance of $(K\text{-}Ca)_{50\%}/(Cr_{10\%}@H\text{-}ZSM\text{-}5)_{50\%}$ by varying C_2H_6 feed concentration from 1 to 2.5 and 5 vol% (balanced with Ar) while keeping the WHSV constant at 10500 mL/g.h. The results from these experiments are presented in Figure 10a.

As evident, the C_2H_4 selectivity experienced a considerable reduction at lower C_2H_6 concentrations. Specifically, using a 5% C_2H_6 feed produced 18.3% C_2H_6 conversion, 19.7% CO_2 conversion, and 96.7% C_2H_4 selectivity, however, decreasing the C_2H_6 feed concentration to 2.5% slightly enhanced the C_2H_6 conversion but at the expense of C_2H_4 selectivity which was reduced from 96.7% to 73%.

Further reducing the C_2H_6 concentration exacerbated these effects, as the 1% C_2H_6 feed further enhanced the overall conversion (50%), but also reduced the C_2H_4 selectivity to ~50%. Such enhanced C_2H_4 yield to 18.8% and 22.7% at 2.5% and 1% C_2H_6 feed respectively but accompanied with CO_2 conversion reduced could be related to the enhanced RWGS (eqn. 3**)** which eliminated H_2 and promoted ethylene production. Similar effects have been reported in the literature [31,44].

The effect of weight hourly space velocity (WHSV) on catalyst performance is demonstrated in Figure 10b. For this figure, there was no clear correlation between WHSV and CO_2 conversion, however, C_2H_6 conversion decreased steadily at higher WHSV

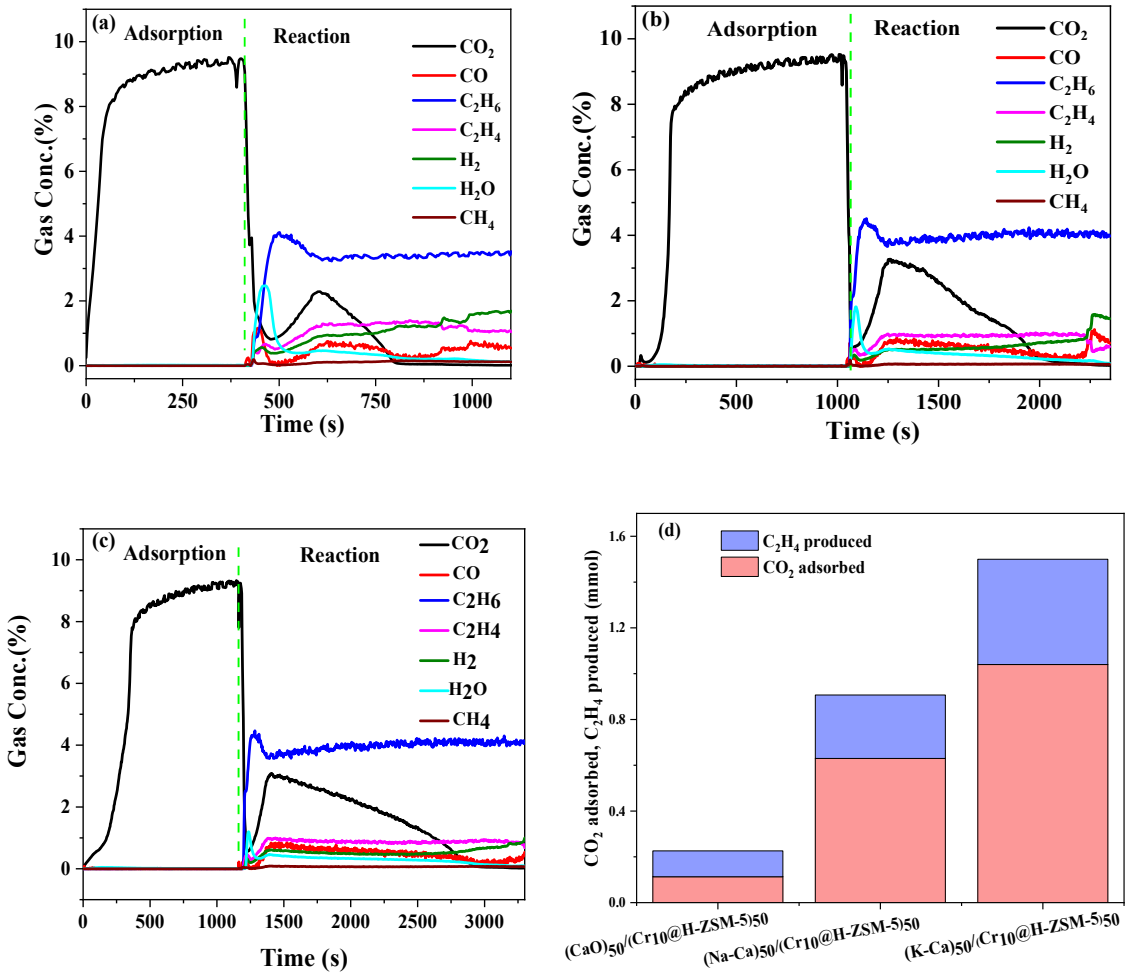

Figure 8. Adsorption-reaction profiles for (a) $(CaO)_{50}/(Cr_{10}@H\text{-}ZSM\text{-}5)_{50}$, (b) $(Na\text{-}Ca)_{50}/(Cr_{10}@H\text{-}ZSM\text{-}5)_{50}$, and (c) $(K\text{-}Ca)_{50}/(Cr_{10}@H\text{-}ZSM\text{-}5)_{50}$, and (d) comparison of the amount CO_2 uptake and C_2H_4 production for different materials.

Table 4. Chromium surface density of the Cr_x@H-ZSM-5 materials.

Catalyst	**Cr surface density(atom/nm^2)**
$Cr_{5\%}$@H-ZSM-5	0.198
$Cr_{10\%}$@H-ZSM-5	0.41
$Cr_{15\%}$@H-ZSM-5	0.58

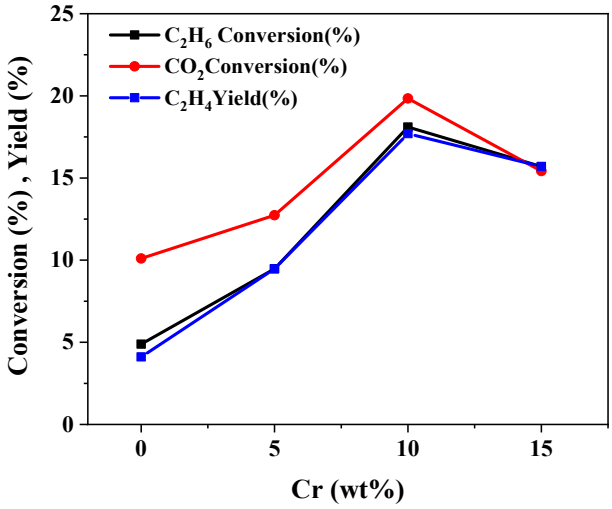

Figure 9. Effect of Cr loading on C_2H_6 conversion, C_2H_4 yield, and CO_2 conversion for $(K\text{-}Ca)_{50}/(H\text{-}ZSM\text{-}5)_{50}$, $(K\text{-}Ca)_{50}/(Cr_5@H\text{-}ZSM\text{-}5)_{50}$, $(K\text{-}Ca)_{50}/(Cr_{10}@H\text{-}ZSM\text{-}5)_{50}$, and $(K\text{-}Ca)_{50}/(Cr_{15}@H\text{-}ZSM\text{-}5)_{50}$ materials.

values. The best C_2H_6 yield achieved was 22% at 5000 mL/g. h. The latter effect was attributed to a decreased C_2H_6 residence time, which decreased the amount of contact time between the gas molecules and catalyst surface, and did not allow sufficient interaction

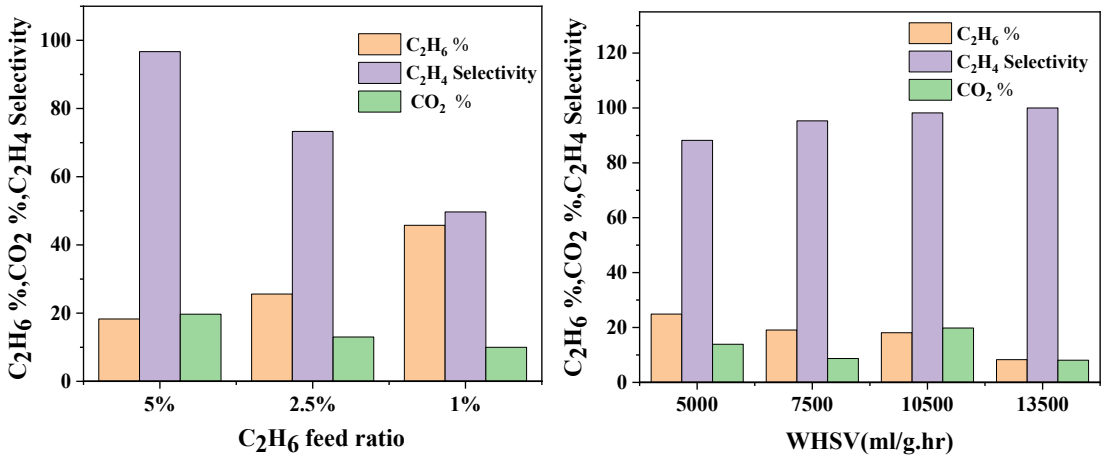

Figure 10. Effect of (a) C_2H_6 feed ratio and (b) WHSV on C_2H_6 conversion, CO_2 conversion and C_2H_4 selectivity.

between the two species. A similar effect has also been reported by Rahmani et. al [25], who studied the effect of gas hourly space velocity (GHSV), and reported decreased C_2H_6 conversion at higher GHSV values.

Thermalgravimetric analysis (TGA) was performed on the K-Ca)$_{50}$/(Cr$_{10}$@H-ZSM-5)$_{50}$ to determine the amount of coke formed during the ODHE reaction, as shown in Figure 11. For the fresh sample (Figure 11a), a small peak was observed at 400 °C while a large peak was observed at 700 °C. The former was assigned to the decomposition of $Ca(OH)_2$ [45], while the latter was attributed to the decomposition of $CaCO_3$ [46]. Both of these compounds were expected, as they are known to form during cooling after calcination. for the used sample after combined adsorption-reaction (Figure 11b), the $Ca(OH)_2$ and $CaCO_3$ peaks were retained, however, a new peak appeared at ~600 °C, which was related to the carbon formation. Coke analysis of the same sample after adsorption-reaction test (Figure 11b) revealed however, the amount of coke formed on this sample was low as 0.7 wt.% indicated the importance of the role of CO_2 during ODHE reaction in enhancing the catalyst stability and ethylene productivity through reverse Boudouard (eqn. 4) and RWGS reaction (eqn. 3), respectively.

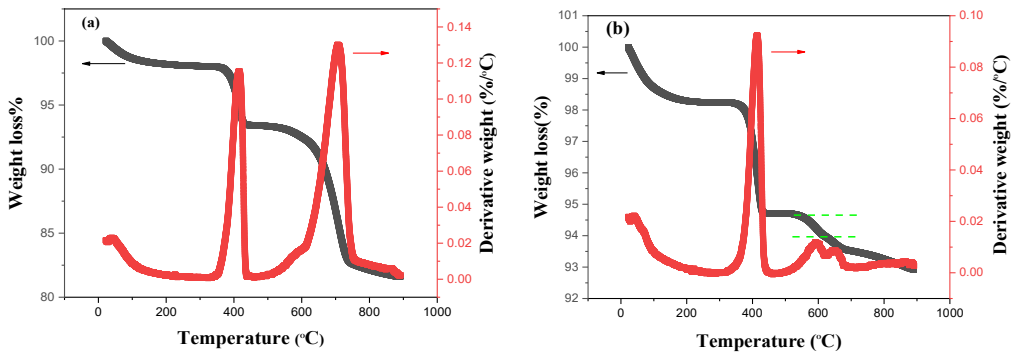

Figure 11. Thermal gravimetric analysis of (a) fresh and (b) spent (K-Ca)$_{50}$/(Cr$_{10}$@H-ZSM-5)$_{50}$.

4. CONCLUSIONS

In this work, a combined CO_2 capture-utilization system was studied over a hybrid bed consisting of adsorbent and catalyst materials, for conversion of ethane to ethylene through oxidative dehydrogenation reaction. Overall, the integrated system was found to be effective for both CO_2 adsorption and C_2H_6 conversion. Between the three materials examined here, $(K\text{-}Ca)_{50}/(Cr_{10}@HZSM\text{-}5)_{50}$, was found to exhibit the best performance, as the combination of double carbonate formation as well as availability of Cr sites led to 1.04 mmol CO_2 adsorption capacity as well as 0.46 mmol C_2H_4 productivity. The effect of C_2H_6 feed concentration was also examined here, and C_2H_4 selectivity was found to decrease at lower C_2H_6 concentrations but in general C_2H_4 yield was enhanced, as result of the reverse water gas shift reaction. Therefore, it was concluded that the C_2H_6 feed composition should be held at 5% in order to maximize the C_2H_4 selectivity and CO_2 conversion. Lastly, the best results shown for $(K\text{-}Ca)_{50}/(Cr_{10}@HZSM\text{-}5)_{50}$ material with CO_2 capacity 5.2 mmol/g at 600 °C and the catalytic activity at 700 °C with highest ethane conversion 25%, ethylene selectivity and yield of 88% and 22%, and CO_2 conversions 14% conversion at 5000 mL/g.hr and 0.4 CO_2/C_2H_6 mole ratio. Also, coke formation analysis demonstrated small amount of coke (ca. 0.7 wt.%) formed on the spent material's surface. Overall, this study demonstrated the utility of a combined capture-utilization process for producing light olefins directly from waste CO_2. Assuming that the materials are further optimized, they could be soon utilized as a novel route for CO_2 utilization, greenhouse gas production, and manufacturing of value-added commodities.

ACKNOWLEDGEMENTS

The authors acknowledge Oak Ridge National Labs (ORNL) for allowing us to use their SEM and EDS equipment. The authors also acknowledge Materials Research Center (MRC) at Missouri University of Science and Technology for TEM and EDS. A.Al-Mamoori would like to acknowledge Al-Nahrain university/Iraq and HCED/Iraq for their financial support.

REFERENCES

[1] R. Koirala, R. Buechel, S.E. Pratsinis, A. Baiker, Silica is preferred over various single and mixed oxides as support for CO_2-assisted cobalt-catalyzed oxidative dehydrogenation of ethane, Appl. Catal. A Gen. 527 (2016) 96–108. https://doi.org/10.1016/j.apcata.2016.08.032.

[2] C.A. Gärtner, A.C. Van Veen, J.A. Lercher, Oxidative Dehydrogenation of Ethane : Common Principles and Mechanistic Aspects, (2013) 3196–3217. https://doi.org/10.1002/cctc.201200966.

[3] A.S. Al-awadi, A.M. El-toni, S.M. Al-zahrani, A.E. Abasaeed, M. Alhoshan, A. Khan, J.P. Labis, A. Al-fatesh, Role of TiO2 nanoparticle modification of Cr/MCM41 catalyst to enhance Cr-support interaction for oxidative dehydrogenation of ethane with carbon dioxide, Appl. Catal. A, Gen. 584 (2019) 117114. https://doi.org/10.1016/j.apcata.2019.117114.

[4] IEA, Carbon capture, utilisation and storage, (n.d.). https://www.iea.org/topics/carbon-capture-and-storage/.

[5] A. Al-Mamoori, A. Krishnamurthy, A.A. Rownaghi, F. Razeai, Carbon Capture and Utilization Update, Energy Technol. (2017) DOI: 10.1002/ente.201600747. https://doi.org/10.1002/ente.201600747.

[6] C. V Miguel, M.A. Soria, A. Mendes, L.M. Madeira, A sorptive reactor for CO_2 capture and conversion to renewable methane, Chem. Eng. J. 322 (2017) 590–602. https://doi.org/10.1016/j.cej.2017.04.024.

[7] A. Al-Mamoori, A.A. Rownaghi, F. Rezaei, Combined Capture and Utilization of CO_2 for Syngas Production over Dual-Function Materials, ACS Sustain. Chem. Eng. 2 (2018) 1–18. https://doi.org/10.1021/acssuschemeng.8b03769.

[8] A. Al-mamoori, S. Lawson, A.A. Rownaghi, F. Rezaei, Improving Adsorptive Performance of CaO for High-Temperature CO_2 Capture through Fe and Ga Doping, (2019). https://doi.org/10.1021/acs.energyfuels.8b03996.

[9] A. Al-Mamoori, H. Thakkar, X. Li, A.A. Rownaghi, F. Rezaei, Development of Potassium- and Sodium-Promoted CaO Adsorbents for CO2Capture at High Temperatures, Ind. Eng. Chem. Res. 56 (2017) 8292–8300. https://doi.org/10.1021/acs.iecr.7b01587.

[10] N. Mimura, M. Okamoto, H. Yamashita, S. Ted Oyama, K. Murata, Oxidative dehydrogenation of ethane over Cr/ZSM-5 catalysts using CO_2 as an oxidant, J. Phys. Chem. B. 110 (2006) 21764–21770. https://doi.org/10.1021/jp061966l.

[11] R.J. Farrauto, M.S. Duyar, M. a Arellano, Dual function materials for CO_2 capture and conversion using renewable H_2, Appl. Catal. B Environ. 168 (2015) 370–376. https://doi.org/10.1016/j.apcatb.2014.12.025.

[12] M.S. Duyar, S. Wang, M.A. Arellano-Treviño, R.J. Farrauto, CO_2 utilization with a novel dual function material (DFM) for capture and catalytic conversion to synthetic natural gas: An update, J. CO_2 Util. 15 (2016) 65–71. https://doi.org/10.1016/j.jcou.2016.05.003.

[13] S. Wang, E.T. Schrunk, H. Mahajan, R.J. Farrauto, The Role of Ruthenium in CO_2 Capture and Catalytic Conversion to Fuel by Dual Function Materials (DFM), Catalysts, (2017) *7*(3), 88. https://doi.org/10.3390/catal7030088.

[14] S. Wang, R.J. Farrauto, S. Karp, J. Ho, E.T. Schrunk, Parametric , cyclic aging and characterization studies for CO_2 capture from fl ue gas and catalytic conversion to synthetic natural gas using a dual functional material (DFM), J. CO_2 Util. 27 (2018) 390–397. https://doi.org/10.1016/j.jcou.2018.08.012.

[15] M.A. Arellano-treviño, Z. He, M.C. Libby, R.J. Farrauto, Catalysts and adsorbents for CO_2 capture and conversion with dual function materials : Limitations of Ni-containing DFMs for flue gas applications, J. CO_2 Util. 31 (2019) 143–151. https://doi.org/10.1016/j.jcou.2019.03.009.

[16] M.A. Arellano-treviño, N. Kanani, C.W. Jeong-potter, R.J. Farrauto, Bimetallic catalysts for CO_2 capture and hydrogenation at simulated flue gas conditions, Chem. Eng. J. 375 (2019) 121953. https://doi.org/10.1016/j.cej.2019.121953.

[17] S.M. Kim, P.M. Abdala, M. Broda, D. Hosseini, C. Cope, C. Mu, Integrated CO_2 Capture and Conversion as an Efficient Process for Fuels from Greenhouse Gases, ACS Catal. 8, (2018) 2815–2823. https://doi.org/10.1021/acscatal.7b03063.

[18] H. Sun, J. Wang, J. Zhao, B. Shen, J. Huang, Dual functional catalytic materials of Ni over Ce-modi fi ed CaO sorbents for integrated CO_2 capture and conversion, Appl. Catal. B Environ. 244 (2019) 63–75. https://doi.org/10.1016/j.apcatb.2018.11.040.

[19] A. Al-Mamoori, A.A. Rownaghi, F. Rezaei, Combined Capture and Utilization of CO_2 for Syngas Production over Dual-Function Materials, ACS Sustain. Chem. Eng. 6 (2018). https://doi.org/10.1021/acssuschemeng.8b03769.

[20] X. Li, S. Liu, H. Chen, S. Luo, F. Jing, W. Chu, Improved Catalytic Performance of Ethane Dehydrogenation in the Presence of CO_2 over Zr-Promoted Cr/SiO_2, *ACS Omega,* 27 (2019), 22562-22573. https://doi.org/10.1021/acsomega.9b03301.

[21] Y. Chang, Y. Chen, P. Chang, S. Chen, Synthesis, Characterization, and CO_2 Adsorptive Behavior of Mesoporous AlOOH-Supported Layered Hydroxides, 300 (2012) 1249–1257. https://doi.org/10.1002/cssc.201100617.

[22] and Q.W. Liang Huang, Yu Zhang, Wanlin Gao, Takuya Harada, Qingqing Qin, Qianwen Zheng, Alan Hatton, Alkali carbonate molten salt-coated CaO with highly improved CO_2 capture capacity, Energy Technol. (2017) DOI: 10.1002/ente.201600628.

[23] P. Gruene, A.G. Belova, T.M. Yegulalp, R.J. Farrauto, M.J. Castaldi, Dispersed Calcium Oxide as a Reversible and Efficient CO_2-Sorbent at Intermediate Temperatures, Ind. Eng. Chem. Res. 50 (2011) 4042–4049. https://doi.org/10.1021/ie102475d.

[24] T.A. Bugrova, V. V Dutov, V.A. Svetlichnyi, V. Cortés, Oxidative dehydrogenation of ethane with CO_2 over CrO_x catalysts supported on Al_2O_3, ZrO_2,CeO_2,and $CexZr_{1-X}O_2$, (2018). https://doi.org/10.1016/j.cattod.2018.04.047.

[25] F. Rahmani, M. Haghighi, One-pot hydrothermal synthesis of ZSM-5–CeO_2 composite as a support for Cr-based nanocatalysts: influence of ceria loading and process conditions on CO_2-enhanced dehydrogenation of ethane, RSC Adv. 6 (2016) 89551–89563. https://doi.org/10.1039/C6RA15787D.

[26] Y. Cheng, C. Miao, W. Hua, Y. Yue, Z. Gao, Cr/ZSM-5 for ethane dehydrogenation: Enhanced catalytic activity through surface silanol, Appl. Catal. A Gen. 532 (2017) 111–119. https://doi.org/10.1016/j.apcata.2016.12.025.

[27] F. Rahmani, M. Haghighi, B. Mohammadkhani, Enhanced dispersion of Cr nanoparticles over nanostructured ZrO_2-doped ZSM-5 used in CO_2-oxydehydrogenation of ethane, Microporous Mesoporous Mater. 242 (2017) 34–49. https://doi.org/10.1016/j.micromeso.2017.01.012.

[28] National institute of Standad and Technology, NIST Chemistry WebBOOK,SRD 69, (n.d.). https://webbook.nist.gov/chemistry/.

[29] M. Thommes, K. Kaneko, A. V. Neimark, J.P. Olivier, F. Rodriguez-Reinoso, J. Rouquerol, K.S.W. Sing, Physisorption of gases, with special reference to the evaluation of surface area and pore size distribution (IUPAC Technical Report), Pure Appl. Chem. 87 (2015). https://doi.org/10.1515/pac-2014-1117.

[30] A.A. Rownaghi, F. Rezaei, J. Hedlund, Yield of gasoline-range hydrocarbons as a function of uniform ZSM-5 crystal size, CATCOM. 14 (2011) 37–41. https://doi.org/10.1016/j.catcom.2011.07.015.

[31] Y. Cheng, F. Zhang, Y. Zhang, C. Miao, W. Hua, Y. Yue, Z. Gao, Oxidative dehydrogenation of ethane with CO_2 over Cr supported on submicron ZSM-5 zeolite, Chinese J. Catal. 36 (2015) 1242–1248. https://doi.org/10.1016/S1872-2067(15)60893-2.

[32] X. Li, F. Rezaei, D.K. Ludlow, A.A. Rownaghi, Synthesis of SAPO-34 @ ZSM - 5 and SAPO-34@Silicalite -1 Core − Shell Zeolite Composites for Ethanol Dehydration, (2018) 1–8. https://doi.org/10.1021/acs.iecr.7b05075.

[33] S. Lai, D. Meng, W. Zhan, Y. Guo, Y. Guo, Z. Zhang, G. Lu, The promotional role of Ce in Cu/ZSM-5 and in situ surface reaction for selective catalytic reduction of NO_x with NH_3, RSC Adv. 5 (2015) 90235–90244. https://doi.org/10.1039/c5ra12505g.

[34] F. Zhang, R. Wu, Y. Yue, W. Yang, S. Gu, C. Miao, W. Hua, Z. Gao, Chromium oxide supported on ZSM-5 as a novel efficient catalyst for dehydrogenation of propane with CO_2, Microporous Mesoporous Mater. 145 (2011) 194–199. https://doi.org/10.1016/j.micromeso.2011.05.021.

[35] F. Rahmani, M. Haghighi, M. Amini, The beneficial utilization of natural zeolite in preparation of Cr/clinoptilolite nanocatalyst used in CO_2 -oxidative dehydrogenation of ethane to ethylene, J. Ind. Eng. Chem. 31 (2015) 142–155. https://doi.org/10.1016/j.jiec.2015.06.018.

[36] F. Magzoub, X. Li, J. Al-darwish, F. Rezaei, A.A. Rownaghi, Environmental 3D-printed ZSM-5 monoliths with metal dopants for methanol conversion in the presence and absence of carbon dioxide, Appl. Catal. B Environ. 245 (2019) 486–495. https://doi.org/10.1016/j.apcatb.2019.01.008.

[37] P. Michorczyk, J. Ogonowski, P. Kus, Chromium oxide supported on MCM-41 as a highly active and selective catalyst for dehydrogenation of propane with CO_2, Appl. Catal. A Gen. 349 (2008) 62–69. https://doi.org/10.1016/j.apcata.2008.07.008.

[38] M.K.H.T.H.S.S.K. Wang S., Dehydrogenation of ethane with carbon dioxide over supported chromium oxide catalysts, Appl. Catal. A Gen. 196 (2000) 1–8. http://www.scopus.com/inward/record.url?eid=2-s2.0-0034719651&partnerID=40&md5=35a1979e779d30e362b5b8c26ca49d5b.

[39] I. Ascoop, V. V. Galvita, K. Alexopoulos, M.F. Reyniers, P. Van Der Voort, V. Bliznuk, G.B. Marin, The role of CO_2 in the dehydrogenation of propane over WO_x-VO_x/SiO_2, J. Catal. 335 (2016) 1–10. https://doi.org/10.1016/j.jcat.2015.12.015.

[40] J.F.S. de Oliveira, D.P. Volanti, J.M.C. Bueno, A.P. Ferreira, Effect of CO2 in the oxidative dehydrogenation reaction of propane over Cr/ZrO_2 catalysts, Appl. Catal. A Gen. 558 (2018) 55–66. https://doi.org/https://doi.org/10.1016/j.apcata.2018.03.020.

[41] Z. Shen, J. Liu, H. Xu, Y. Yue, W. Hua, W. Shen, Dehydrogenation of ethane to ethylene over a highly efficient Ga2O3/HZSM-5 catalyst in the presence of CO_2, Appl. Catal. A Gen. 356 (2009) 148–153. https://doi.org/10.1016/j.apcata.2008.12.038.

[42] A.S. Al-awadi, S.M. Al-zahrani, A.M. El-toni, Dehydrogenation of Ethane to Ethylene by CO_2 over Highly Dispersed Cr on Large-Pore Mesoporous, (2020).

[43] C.C. Yang, P.W. Chen, C.Y. Wu, Synthesis of calcium zincate powders by a chemical co-precipitation method and their electrochemical performances, J. Nanosci. Nanotechnol. 10 (2010) 4586–4591. https://doi.org/10.1166/jnn.2010.1692.

[44] J.P. Fernandes Ramos, Effect of Calcium Oxide Microstructure on the Diffusion of Isotopes (Efeito da Microestrutura do Óxido de Cálcio na Difusão de Isótopos), (2012) 101.

[45] C.C. Yang, P.W. Chen, C.Y. Wu, Synthesis of calcium zincate powders by a chemical co-precipitation method and their electrochemical performances, J. Nanosci. Nanotechnol. 10 (2010) 4586–4591. doi:10.1166/jnn.2010.1692.

[46] J.P. Fernandes Ramos, Effect of Calcium Oxide Microstructure on the Diffusion of Isotopes (Efeito da Microestrutura do Óxido de Cálcio na Difusão de Isótopos), (2012) 101.

SECTION

2. CONCLUSIONS AND RECOMMENDATIONS

2.1. CONCLUSIONS

In this investigation, novel materials and processes related to integrated CO_2 capture and utilization have been developed and performed.to produce chemicals and fuel. First, double salts based CaO (K-Ca and Na-Ca) and metal based CaO (Fe_x@CaO and Ga_x@CaO) adsorbents have been developed at high temperature. Superior CO_2 uptake were achieved for 10 wt% Fe @CaO and 10 wt% Ga @CaO 13.7 and 14.2 mmol/g at 650 ^oC.

Second, Combined CO_2 capture and utilization system has been implemented for syngas and ethylene production through dry reforming of ethane. (DRE) and oxidative dehydrogenation of ethane (ODHE) respectively. Specifically, dual function materials (DFMs) have been employed for syngas production with high conversion of ethane 100% For ethylene production, the material $(K\text{-}Ca)_{50\%}/(Cr_{10}@HZSM\text{-}5)_{50\%}$ exhibited 25% ethane conversion and 88% ethylene selectivity.

2.2. RECOMMENDATIONS

The following recommendations can be considered as future work to improve the performance of DFMs:

1. Enhancing the catalytic activity for ethylene production by either using bimetallic catalysts or developing more efficicient supports.

2. Developing novel materials that can capture and utilize CO_2 into ethylene in isothermal manner.
3. Developing novel materials for integrated CO_2 capture and utilization into valuable-added chemicals and fuels such as methane, methanol, propelene, and DME.
4. Performing density functional theory (DFT) computations to understand the adsorption and reaction mechanisms on the dual functional materials.

APPENDIX A.

TABLE OF CONTENTS GRAPHIC AND SUPPORTING INFORMATION OF PAPER II

TABLE OF CONTENTS GRAPHIC

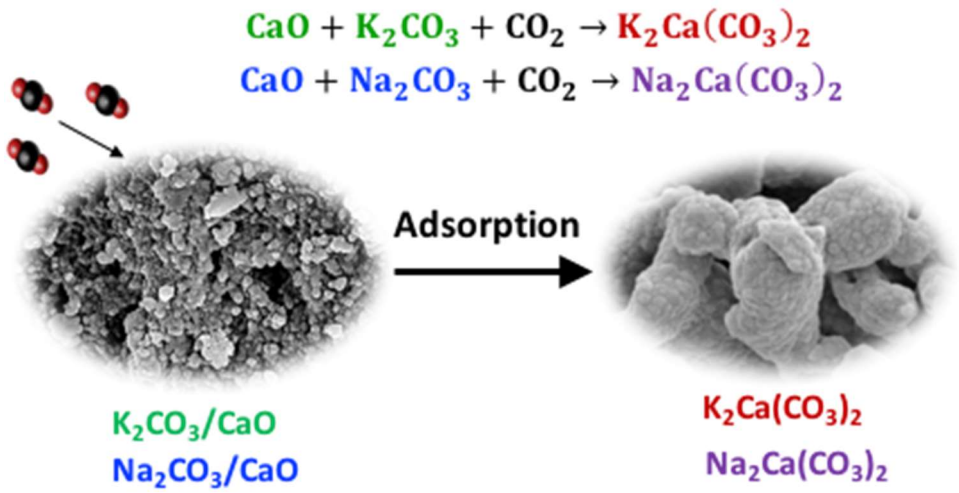

SUPPORTING INFORMATION FOR DEVELOPMENT OF POTASSIUM- AND SODIUM- PROMOTED CAO ADSORBENTS FOR CO_2 CAPTURE AT HIGH TEMPERATURES

Ahmed Al-Mamoori, Harshul Thakkar, Xin Li, Ali A. Rownaghi, Fateme Rezaei*

Department of Chemical & Biochemical Engineering, Missouri University of Science and Technology, 1101 N State Street, Rolla, MO, 65409, United States

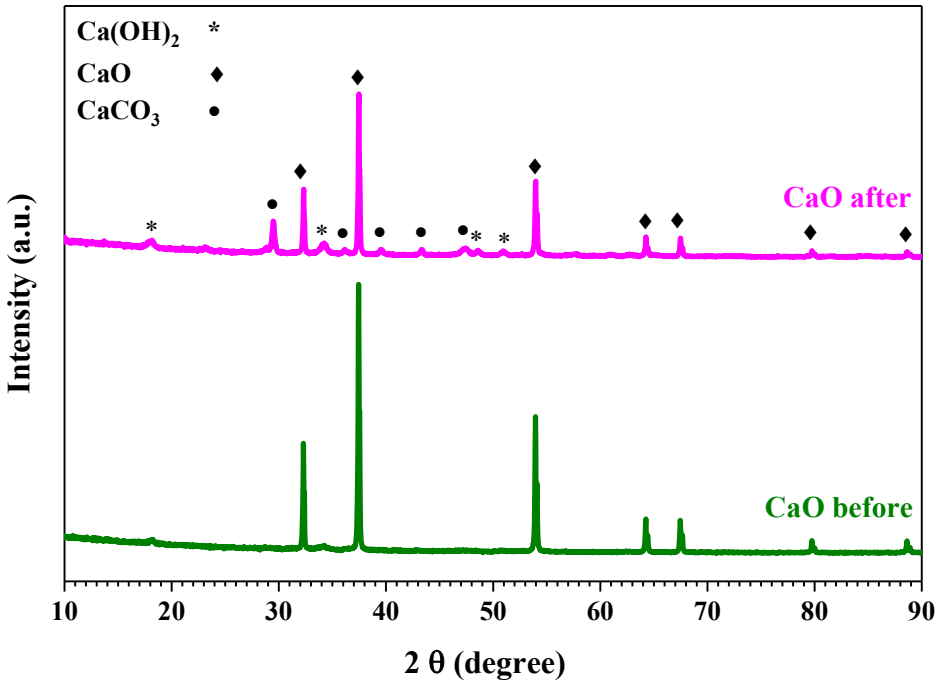

Figure S1. XRD spectra of bare CaO before and after CO_2 adsorption at 375 °C.

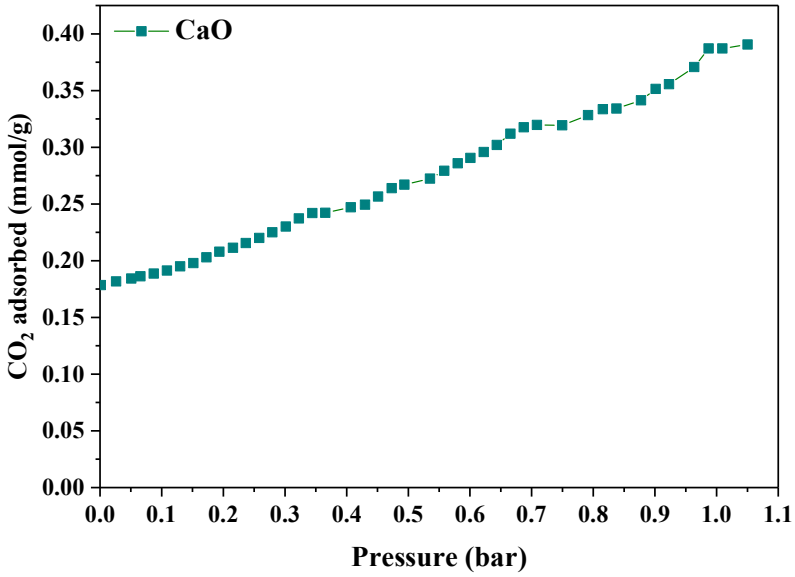

Figure S2. Adsorption isotherm of bare CaO at 375 °C.

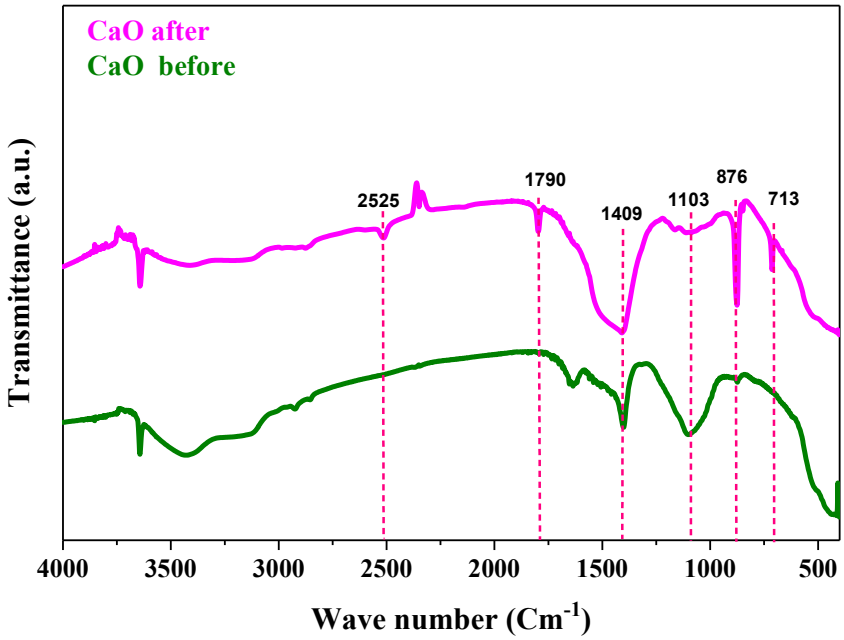

Figure S3. FT-IR spectra of bare CaO before and after CO_2 adsorption at 375 °C.

APPENDIX B.

TABLE OF CONTENTS GRAPHIC AND SUPPORTING INFORMATION OF PAPER III

TABLE OF CONTENTS GRAPHIC

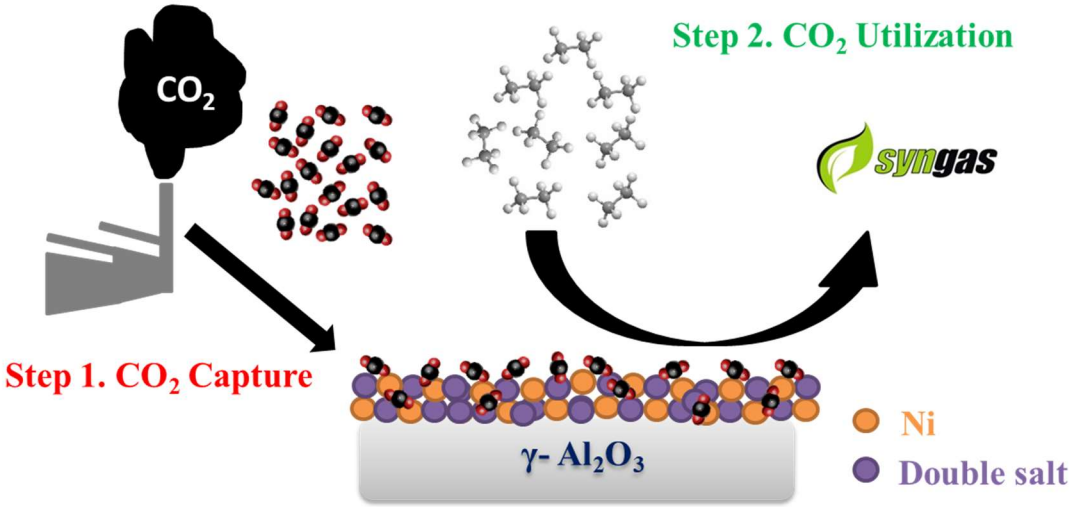

SUPPORTING INFORMATION FOR COMBINED CAPTURE AND UTILIZATION OF CO_2 FOR SYNGAS PRODUCTION OVER DUAL-FUNCTION MATERIALS

Ahmed Al-Mamoori, Ali A. Rownaghi, Fateme Rezaei*

Department of Chemical & Biochemical Engineering, Missouri University of Science and Technology, 1101 N State Street, Rolla, MO, 65409, United States

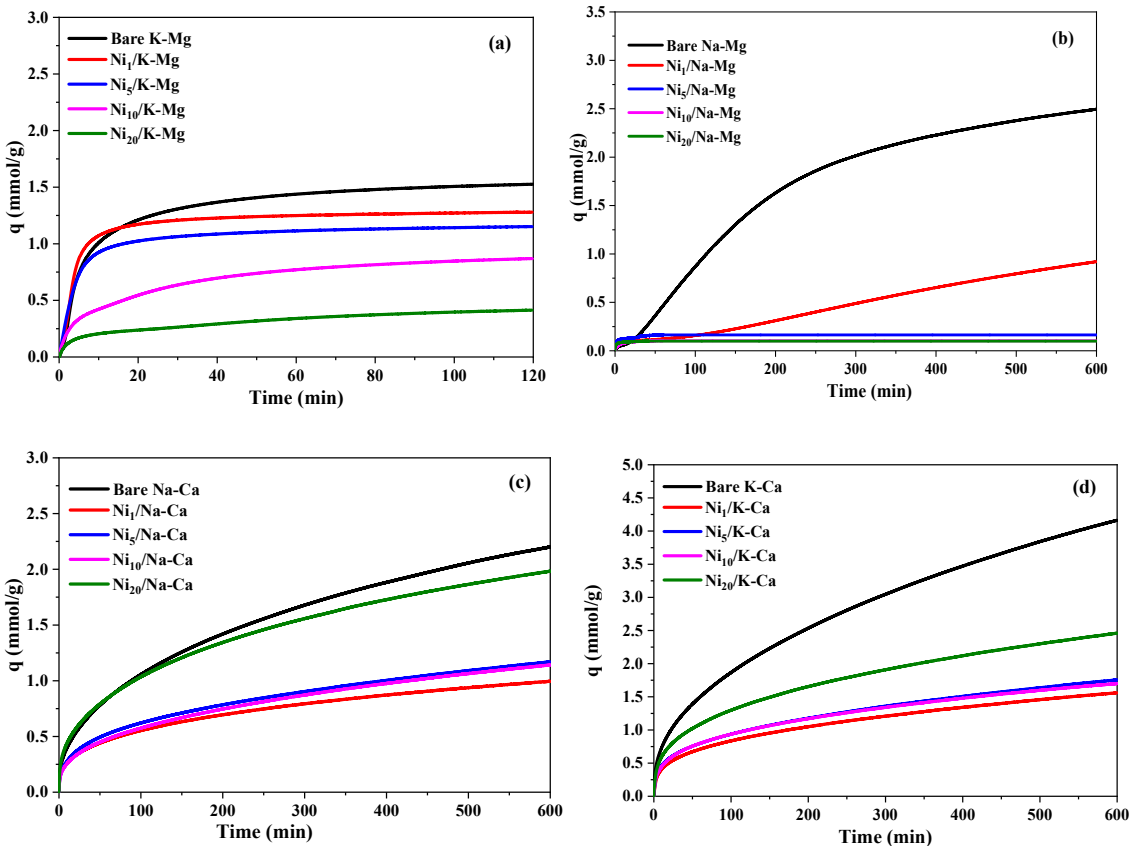

Figure S1. CO_2 capacity of (a) Ni@K-Mg, (b) Ni@Na-Mg, (c) Ni@Na-Ca, and (d) Ni@K-Ca with different Ni weight ratios at 375 °C and 1 bar.

Reaction Pathways

$C_2H_6 + 2CO_2 \rightarrow 4CO + 3H_2$ $\Delta H^0_{25} = 428.1$ kJ/mol (1)

$C_2H_6 + CO_2 \rightarrow C_2H_4 + CO + H_2O$ $\Delta H^0_{25} = 134$ kJ/mol (2)

$C_2H_6 \rightarrow C_2H_4 + H_2$ $\Delta H^0_{25} = 137$ kJ/mol (3)

$C_2H_6 + 2CO_2 \rightarrow CH_4 + 3CO + H_2O$ $\Delta H^0_{25} = 180$ kJ/mol (4)

$CO_2 + H_2 \rightarrow CO + H_2O$ $\Delta H^0_{25} = 28$ kJ/mol (5)

$2CO \rightarrow CO_2 + C$ $\Delta H^0_{25} = -172$ kJ/mol (6)

$C_2H_6 + H_2 \rightarrow 2CH_4$ $\Delta H^0_{25} = -66$ kJ/mol (7)

$CH_4 \rightarrow C + 2H_2$ $\Delta H^0_{25} = 75$ kJ/mol (8)

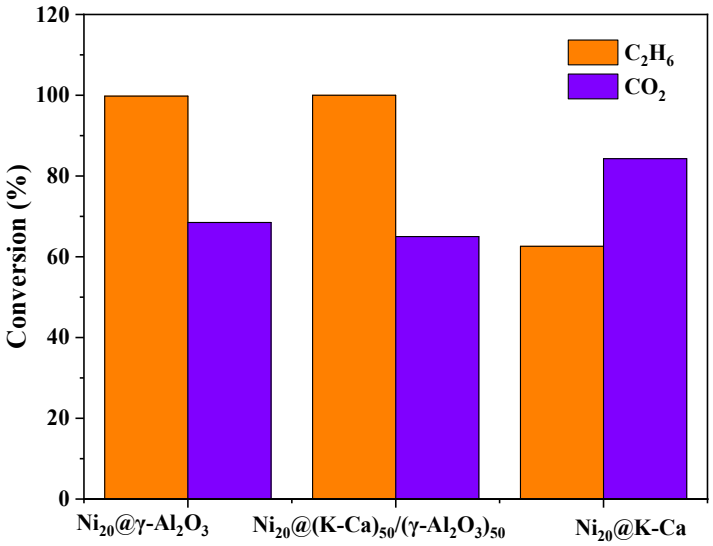

Figure S2. Effect of support on CO_2 and C_2H_2 conversion at 650 °C.

APPENDIX C.

TABLE OF CONTENTS GRAPHIC AND SUPPORTING INFORMATION OF PAPER IV

TABLE OF CONTENTS GRAPHIC

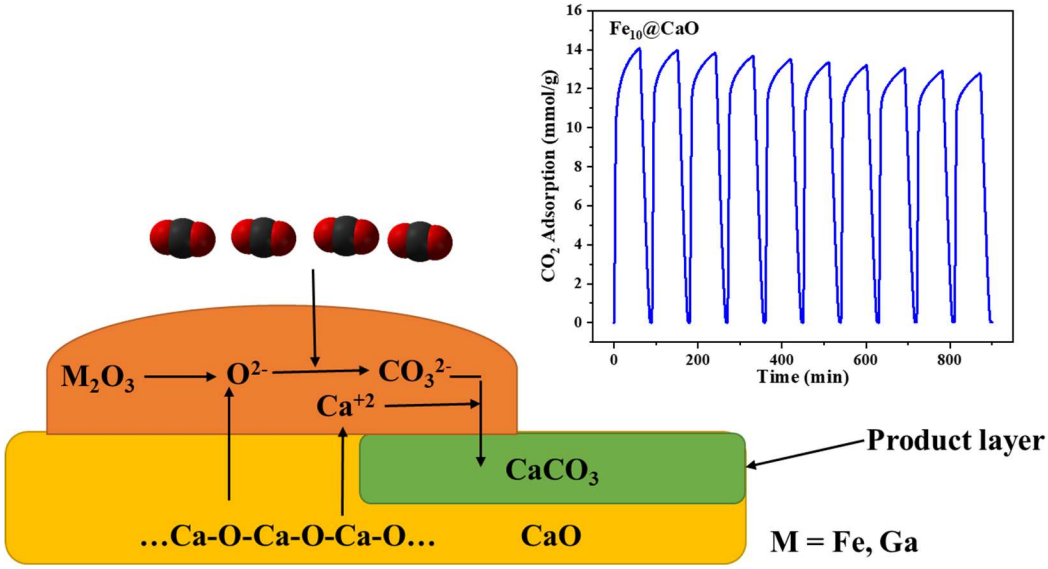

SUPPORTING INFORMATION FOR IMPROVING ADSORPTIVE PERFORMANCE OF CAO FOR HIGH TEMPERATURE CO_2 CAPTURE THROUGH FE AND GA DOPING

Ahmed Al-Mamoori, Shane Lawson, Ali A. Rownaghi, Fateme Rezaei*

Department of Chemical & Biochemical Engineering, Missouri University of Science and Technology, Rolla, MO 65409-1230, United States

CRYSTALLITE SIZE CALCULATION

The crystallite size of the bare CaO, Fe_{10}@CaO, and Ga_{10}@CaO were obtained using Scherrer equation:

$$\tau = \frac{K\,\lambda}{\beta\,cos\theta} \quad (1)$$

where

τ : size of crystallite size

K : shape factor = 0.94

λ : copper wavelength = 0.154 nm,

β : full width half maximum intensity (FWHM) of CaO,

θ : Bragg angle

Table S-1. Crystallite size of the bare and promoted CaO adsorbents.

Adsorbent	Crystallite size (nm)
Bare CaO	39
Fe_{10}@CaO	31
Ga_{10}@CaO	25

APPENDIX D.

TABLE OF CONTENTS GRAPHIC AND SUPPORTING INFORMATION OF PAPER V

TABLE OF CONTENTS GRAPHIC

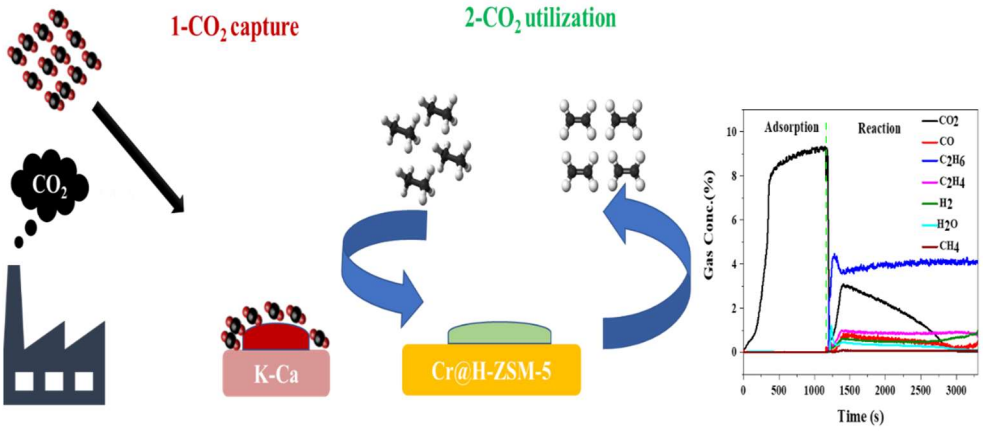

SUPPORTING INFORMATION FOR INTEGRATED CAPTURE AND UTILIZATION OF CO_2 IN ETHYLENE PRODUCTION OVER COMBINED ADSORBENT-CATALYST MATERIALS

Ahmed Al-Mamoori, Shane Lawson, Ali A. Rownaghi, Fateme Rezaei*

Department of Chemical & Biochemical Engineering, Missouri University of Science and *Technology, 1101 N State Street, Rolla, MO, 65409, United States*

GAS AMOUNT CALCULATIONS

CO_2 adsorption capacity (q, mmol/g) was determined as follows:

$$q\left(mmol/g\right) = \frac{F_{CO_2 in}\int_0^{t_a}\left(1-\frac{y_{CO_2 out}}{y_{CO_2 in}}\right)dt}{m_{ads}} \quad (1)$$

where F_{CO2in} is the CO_2 molar flow rate at the column inlet in mmol/s, $y_{co2\ in}$ and $y_{co2\ out}$ are CO_2 mole fractions at the inlet and outlet streams respectively. m_{ads} stands for the adsorbent mass in g and t_a is the adsorption time in s. The amount of CO_2 adsorbed and desorbed were calculated as follows:

$$n_{CO_2 ads.} = F_{CO_2 in}\int_0^{t_a}\left(1-\frac{y_{CO_2 out}}{y_{CO_2 in}}\right)dt \quad (2)$$

$$n_{CO_2 des.} = \int_0^{t_d}(F_{outlet\ total}\times y_{CO_2 out})\,dt \quad (3)$$

where t_d: is the desorption time. CO_2 Conversion was obtained as follows:

$$X_{CO_2} = \frac{CO_{2\ ads.} - CO_{2\ des.}}{CO_{2\ ads.}}\times 100\% \quad (4)$$

The moles of gases at the outlet can be calculated

$$n_{i\ outlet} = \int_0^{t_r}(F_{outlet\ total}\times y_i)\,dt \quad (5)$$

where $n_{i\ outlet}$ is the gas mole at the outlet, t_r is the reaction time, and y_i is the gas mole fraction. The C_2H_6 conversion, C_2H_4 selectivity, and C_2H_4 yield were obtained as the following:

$$X_{C_2H_6}\% = \frac{C_2H_6 molar\ flow\ in - C_2H_6 molar\ flow\ out}{C_2H_6 molar\ flow\ in} \times 100\% \quad (6)$$

$$S_{C_2H_4}\% = \frac{C_2H_4 molar\ flow\ out}{C_2H_6 molar\ flow\ in - C_2H_6 molar\ flow\ out} \times 100\% \quad (7)$$

$$Y_{C_2H_4}\% = \frac{C_2H_4 molar\ flow\ out}{C_2H_6 molar\ flow\ in} \times 100\% \quad (8)$$

Carbon balance was calculated for all the samples as shown in the following eqn.:

$$carbon\ balance\% = \frac{\sum_{i=1}^{n} total\ moles\ of\ gas_i\ at\ the\ outlet * no.of\ C\ atom\ in\ the\ gas_i}{\sum_{i=1}^{n} total\ moles\ of\ gas_i\ at\ the\ inlet * no.of\ C\ atom\ in\ the\ gas_i} * 100\% \quad (9)$$

Table S-1. Carbon balance of the adsorption-reaction tests.

Materials	**WHSV (ml/g.h)**	**C_2H_6 feed ratio**	**Carbon balance (%)**
$(CaO)_{50\%}/(Cr_{10\%}@H\text{-}ZSM\text{-}5)_{50\%}$	10500	5%	101
$(Na\text{-}Ca)_{50\%}/(Cr_{10\%}@H\text{-}ZSM\text{-}5)_{50\%}$	10500	5%	97
$(K\text{-}Ca)_{50\%}/(Cr_{10\%}@H\text{-}ZSM\text{-}5)_{50\%}$	10500	5%	101
$(K\text{-}Ca)_{50\%}/(Cr_{5\%}@H\text{-}ZSM\text{-}5)_{50\%}$	10500	5%	101
$(K\text{-}Ca)_{50\%}/(Cr_{10\%}@H\text{-}ZSM\text{-}5)_{50\%}$	10500	1%	90.9
$(K\text{-}Ca)_{50\%}/(Cr_{10\%}@H\text{-}ZSM\text{-}5)_{50\%}$	10500	2.5%	96.8
$(K\text{-}Ca)_{50\%}/(Cr_{10\%}@H\text{-}ZSM\text{-}5)_{50\%}$	7500	5%	103
$(K\text{-}Ca)_{50\%}/(Cr_{10\%}@H\text{-}ZSM\text{-}5)_{50\%}$	13500	5%	107
$(K\text{-}Ca)_{40\%}/(Cr_{10\%}@H\text{-}ZSM\text{-}5)_{60\%}$	5000	5%	101

VITA

Ahmed Adnan Atshan Al-mamoori was born in January 1985 in Baghdad /Iraq., He earned his BSc. and MSc. in Chemical Engineering from Al-nahrain University in 2005 and 2009 respectively. He joined Missouri University of Science and Technology in 2015 as a PhD student. He worked during his PhD study under supervision of Dr. Rezaei. His research area was focusing on developing novel materials and processes for CO_2 capture and utilization. Ahmed earned his PhD in Chemical Engineering from Missouri University of Science and Technology in May 2020.